CFD ANALYSIS
OF
PRINTED CIRCUIT HEAT EXCHANGER

A THESIS SUBMITTED IN PARTIAL FULFILLMENT OF THE
REQUIREMENTS FOR THE DEGREE OF

Master of Technology

in

Mechanical Engineering

By

SATYA PRAKASH KAR

Department of Mechanical Engineering
National Institute of Technology
Rourkela
2007

CFD ANALYSIS
OF
PRINTED CIRCUIT HEAT EXCHANGER

A THESIS SUBMITTED IN PARTIAL FULFILLMENT OF THE
REQUIREMENTS FOR THE DEGREE OF

Master of Technology

in

Mechanical Engineering

By

SATYA PRAKASH KAR

Under the guidance of

Prof. SUNIL KUMAR SARANGI

Department of Mechanical Engineering
National Institute of Technology
Rourkela
2007

National Institute of Technology

Rourkela

CERTIFICATE

This is to certify that the thesis entitled, **"Cfd Analysis Of Printed Circuit Heat Exchanger"** submitted by **Sri Satya Prakash Kar** in partial fulfillment of the requirements for the award of MASTER of Technology Degree in **Mechanical Engineering** with specialization in **"Thermal Engineering"** at the National Institute of Technology, Rourkela (Deemed University) is an authentic work carried out by him/her under my/our supervision and guidance.

To the best of my knowledge, the matter embodied in the thesis has not been submitted to any other University/ Institute for the award of any degree or diploma.

Date:

Prof. S.K.Sarangi
Dept. of Mechanical Engg.
National Institute of Technology
Rourkela - 769008

ACKNOWLEDGEMENT

First I would like to express my deep appreciation and gratitude to Prof. S.K. Sarangi for his constant support and exceptionally helpful guidance through out this study. Working under his supervision greatly contributed to improving the quality of the thesis and to developing my general engineering and management skills.

Further I greatly appreciate the help from Prof. R.K.Sahoo whose technical expertise in the heat transfer area constituted a valuable asset.

I also want to take this opportunity to express my appreciation toward Prof. A.K.Sathpathy. for his valuable suggestions and encouragement through out the project work.

I am indebted to Prof. S.S.Mahaptra for his great help in my project work.

I also extend my thanks to Prof. S.K.Mahapatra and Prof.P.Rath for their constructive suggestions to my project work.

I thank all my friends in Mechanical Engineering for making my stay at N.I.T.Rourkela a pleasant and memorable experience.

Satya Prakash Kar
Roll No. 20503027
Department of Mechanical Engg
National Institute of technology

CONTENTS

Abstract

Printed Circuit compact heat exchangers that are increasingly being used for viscous media thermal processing applications have semicircular flow channels. But due to some manufacturing constraints, these become semi elliptical in nature. In practice, these channels have very small hydraulic diameters and relatively large (L/d_h).Because of length scales and the viscous nature of the fluids being handled, the flows are generally laminar and both hydro dynamically and thermally fully developed.

At first, fully developed laminar flow and heat transfer in straight circular smooth duct under constant heat flux has been studied using FLUENT and fanning friction factor, Nusselt no. and Colburn factor have been calculated to check the accuracy of the solution using this package.

Then following the same procedure, fully developed laminar flow and heat transfer in three-dimensional, periodic straight duct as well as sinusoidal duct with semiellptic cross section with different aspect ratios are considered. Computational Fluid Dynamics (CFD) using FLUENT is used to investigate the effect of Reynolds number ($50 \leq Re \leq 500$),aspect ratio of semi elliptical cross-sections for straight duct and amplitude to wavelength ratio(A/L=0.3 & 0.5) for sinusoidal channel(with L/D=4.5) on heat transfer enhancement and pressure drop for steady ,incompressible ,constant property, air (Pr=0.7044) flows under the constant wall heat flux boundary conditions.

Velocity, temperature fields, Fanning friction factor, Colburn factor, good ness factor are being studied. Due to the interruption of the boundary layers formed near the solid surface and replacement of the boundary layer with the fluid from the core, thus creating a new boundary layer with an increased temperature gradient ,the overall heat transfer coefficient as well as the pressure drop penalty in case of sinusoidal ducts increase as compared to straight ducts.

Finally correlations between the Fanning friction factor and Colburn factor with Reynolds number and geometrical parameters have been found out for the above geometries.

LIST OF FIGURES

LIST OF TABLES

NOMENCLATURE

a	Aspect ratio
A	Amplitude, mm
C	Indices
D	2 x major axis, mm
d_h	Hydraulic diameter
d	Diameter ,mm
f	Fanning friction factor
g_x, g_y, g_z	Acceleration due to gravity in x, y ,z direction,m/s^2
h	Heat transfer coefficient ,w/m^2-k
j	Colburn factor
K	Thermal conductivity ,w/m-k
L_0	Length of the duct, mm
2L	Wavelength,mm
$\dot{m}$	Mass flow rate, kg/s
Nu	Nusselt number
P	Pressure,N/m^2
Re	Reynolds Number
Pr	Prandtl Number
T	Temperature ,K
V_x V_y V_z	Velocity in x,y,z direction/s
w_m	Area weighted average velocity

Geek Symbols

ΔP	Pressure drop
μ	Viscosity , pa-s
ρ	Density of fluid,kg/m^3

Subscripts

b	bulk
h	hydraulic
f	mean
w	wall
x,y,z	Direction

Abbreviations

PCHE	Printed Circuit Heat Exchanger

Chapter 1

INTRODUCTION

- **Definition of PCHE**
- **PCHE of HEATRIC™ type**
- **Objectives of the study**
- **Organization of the thesis**

1.1 DEFINITION OF PCHE

Printed Circuit Heat Exchanger (PCHE) has been commercially manufactured only since 1985 (by HEATRIC^{TM}) and is virtually unmentioned in the heat exchanger literature until the late 1990's. It is a compact heat exchanger. There are several methods used to increase the heat transfer rate in compact heat exchangers.PCHE uses the method of interrupting the boundary layer on the solid surface and replace it with the fluid from core ,thus creating a new boundary layer with an increased temperature gradient.

- Typical plate thickness-1.6mm
- Width=600 mm Length=1200mm
- Channels have semi-circular profile with 1.2-2 mm diameter.
- Etched plates are stacked and diffusion bonded together to fabricate a block.
- The blocks are welded together to form the complete heat exchanger core.
- Fluid flow channels are etched chemically on metal plates

1.1.1 PCHE Features & Capabilities

High Pressures

PCHE cores are designed for the containment of exceptionally high pressures. PCHEs with design pressures of 500 bar (7500 psi) are in operation.

Extreme Temperatures

Materials of construction, such as austenitic stainless steel allow temperatures from cryogenic to 900°C (1650°F).

Enhanced Safety

PCHEs are not susceptible to hazards commonly associated with shell and tube exchangers, such as flow induced tube vibration and tube rupture. Overpressure relief systems can thus be substantially reduced. The highly compact nature of PCHEs also means that they have relatively low inventory, compared to shell and tube exchangers.

Flexible Fluid Pressure Drop

Despite the compact nature of PCHEs, there is no restriction on the pressure drop specification for fluids passing through them, even with gases or highly viscous liquids. Whilst the passages are small relative to conventional equipment, they are also short.

Close Approach Temperatures

Fluid contact can be counter flow, cross flow, or a combination of these to suit the process requirements. Counter current design enables deep temperature crosses and temperature approaches of 3-5°C.

Multi-Fluid Contact

One of the features of plate type heat exchangers is that they are capable of containing more than two process streams in a single unit. PCHEs extend multi-stream capability to high temperature and pressure processes. Multi-stream heat exchangers have obvious space and weight advantages through reduced exchanger and piping weight. Also process control can be simplified or eliminated. Fluids can enter or leave the heat exchanger core at intermediate points, and can be contacted in series or in parallel, allowing flexibility on inlet/outlet temperatures.

High Effectiveness

PCHEs have met process requirements for high thermal effectiveness in excess of 97% in a single compact unit. High effectiveness heat exchangers can reduce the duty, size and cost of other heating/cooling operations in the overall process scheme.

Injection of Fluids

The unique construction of PCHEs cores enables accurate injection of one fluid into another, passage-by-passage.

Two-Phase Fluids

PCHEs handle boiling and condensation of fluids, and can also be employed in more complex duties involving absorption and rectification. It is also possible to evenly distribute two phase inlet streams in the PCHE core.

Functional Integration

PCHE hardware is not restricted to heat exchange - it may also incorporate additional functions, such as chemical reaction, mass transfer and mixing

1.1.2 CONSTRUCTION

PCHEs are constructed from flat metal plates into which fluid flow channels are chemically etched. The chemical etching technique is similar to that employed for etching electrical printed circuits and hence is capable of producing fluid circuits of unlimited variety and complexity.

The required configuration of the channels on the plates for each fluid is governed by the temperature and pressure-drop constraints for the heat exchange duty. Once an optimal thermal design has been developed for an exchanger, the artwork required for plate manufacture is quickly and conveniently computer-generated.

1.1.3 APPLICATIONS:

- Hydrocarbon gas & NGL Processing
- Gas processing
    - Liquids recovery

- LNG & cryogenic
- Synthetic fuels production

- Chemicals processing

  - Acids- nitric, phosphoric etc.
  - Alkalis - caustic soda, caustic potash
  - Fertilizers - ammonia, urea

- Refining

  - Reactor feed/effluent exchangers
  - Air separation

- Power & Energy

  - Chillers & condensers
  - Cascade condensers
  - Absorption cycles
  - Geothermal generation
  - Nuclear applications

1.2. PCHE OF HEATRIC™ TYPE

1.2.1 Design

The HEATRIC™ HX falls within the category of compact heat exchangers thanks to its high surface density area (>2500 m^2/m^3) . In particular, it is generally categorized as a printed circuit heat exchanger (PCHE). This name originates from its manufacturing method. More precisely, the fluid passages are photo chemically etched into both sides of a metal plate . As the name PCHE implies, this is the same technique as the one developed for producing standard printed circuit boards for electronic equipment.

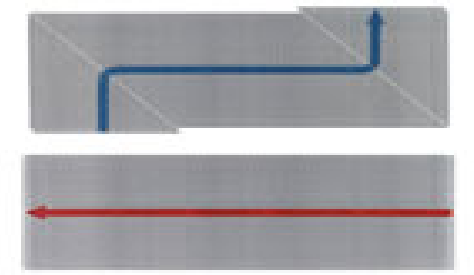

Figure 1.1. Step 1. Plate passages (courtesy HEATRIC™)

Moreover, the milled (etched-out) plates are thereafter joined by diffusion bonding, which results in extremely strong and all-metal heat exchanger cores (Figure 1-2). The diffusion bonding process allows grain growth, thereby essentially eliminating the interface at the joints, which in turn acquire parental metal strength. Because of the diffusion bonding, the expected lifetime of the HXers is longer than for any other HX based on a brazed structure.

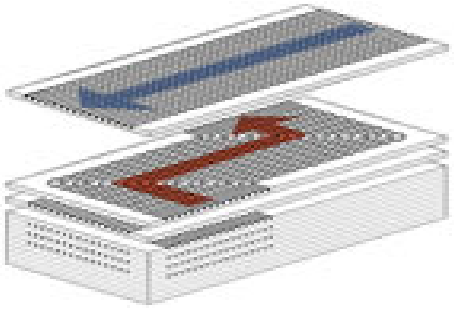

Figure 1.2. Step 2. Diffusion bonding of plates (courtesy HEATRIC™)

A stack of milled plates that have been bonded together comprise a block. The complete heat exchanger core is composed by welding together as many of these blocks as the thermal duty (flow capacity) of the HX requires (Figure 1-3).

Figure1.3. Step 3. A block composed of diffusion bonded plates (courtesy HEATRIC™)

Fluid headers and nozzles are usually welded directly onto the core (Figure 1-4). The geometry contributes to reducing the header maldistribution.

Figure 1.4. Step 4. Welding of nozzles and headers to HX (courtesy HEATRIC™)

The flow passages typically have a semi-circular cross section, as illustrated in Fig. 1-5 and may also be radially corrugated as needed (Fig. 1-6). Their width and depth vary between 1.0-2.0 mm and 0.5-1.0 mm, respectively. Representatives of HEATRIC™ have suggested that a channel diameter of 2.0 mm maximizes thermal performance and economic efficiency [Heatric workshop]. Moreover, the HXers are usually priced by weight. A HEATRIC™ HX for non-nuclear applications, which is fabricated of chrome duplex, costs approximately $50/kg. For nuclear applications, HEATRIC™ estimates the price of a standard product in stainless steel to be around $30/kg . If high coolant temperatures exclude the use of stainless steel, the HXers may be manufactured of titanium, which will inflate the price to $120/kg.

Figure 1.5. Cross-sectional view of HEATRIC™ Showing the semi-circular passages (black) (Courtesy HEATRIC™)

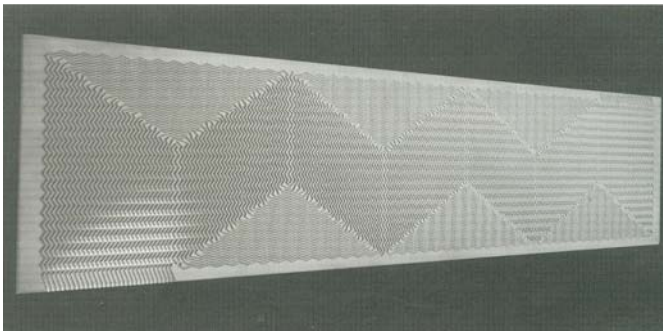

Figure 1.6. Side view of passage shapes

Figure 1-7 shows what the finished HX, while Fig. 1-8 illustrates the flow paths in a typical HEATRIC™ design.

Figure 1.7. Step 5. The final product (courtesy HEATRIC™)

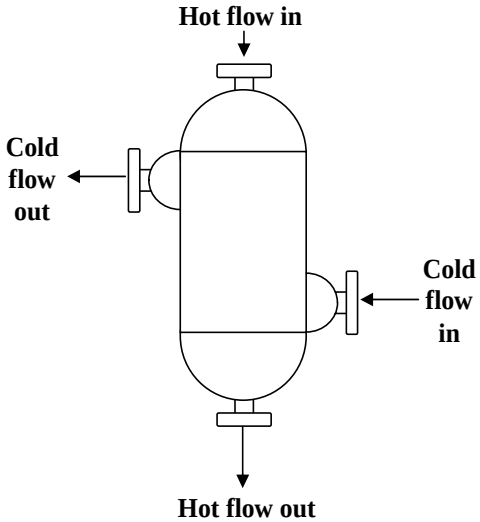

Figure 1.8. Sketch of fluid flow

1.2.2 Characteristics

There are several unique characteristics that contribute to the superior performance of HEATRIC™ HXers. The most distinctive ones are the high allowable pressure and temperature limits. Specifically, the manufacturing company claims that, thanks to its original design, HEATRIC™ HXers are able to operate at pressures up to 50 MPa and temperatures not exceeding 900 °C. To allow operation under such extreme conditions, the materials commonly employed in PCHE include austenitic stainless steel, titanium and nickel (pure/alloys), all which are corrosion resistant. Carbon steel is typically not used for two reasons. First, because of the small channel diameter, the HXers are designed for essentially zero corrosion allowance in order to avoid channel blockage. Second, carbon steel is unsuitable for diffusion bonding. Regarding mechanical considerations, HEATRIC™ HXers are based on the design code ASME VIII Division 1 and ASME III for non-nuclear and nuclear applications, respectively. In all of the shaded area of Fig1-9, HEATRIC™ has supplied HXers. As noted above, the MIT GFR Project has down selected the cycle fluids to helium at 8.0 MPa on the primary side and S-CO_2 at 19.9 MPa on the secondary side. The helium and S-CO_2 design points are represented by a black square and triangle, respectively, in Fig. 1-9. Both are within the shaded area representing HEATRIC™ operating experience from previously supplied HXers.

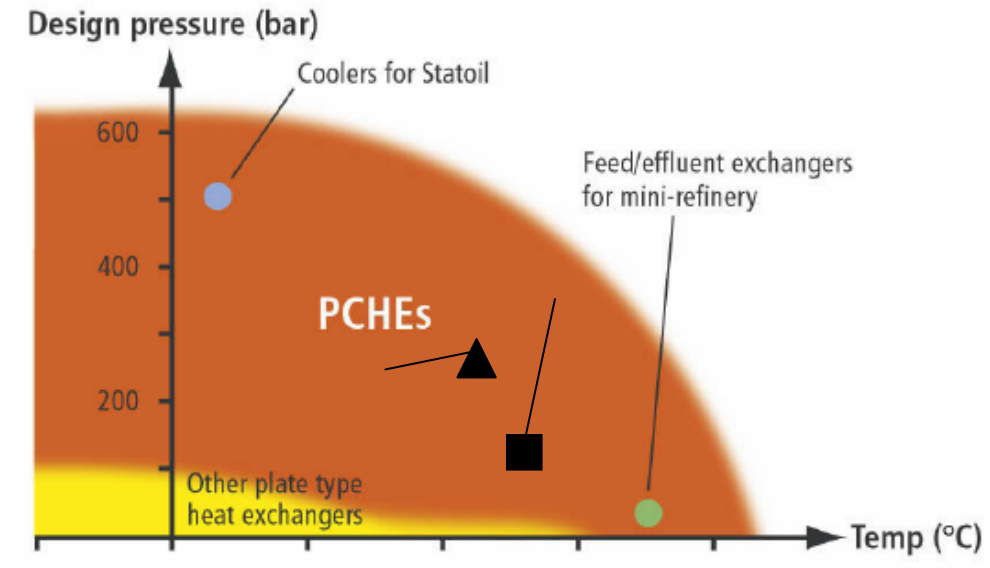

Figure 1.9. Design range of actually manufactured PCHE of HEATRIC™ type

In addition to the wide operating range, the great potential of HEATRIC™ type HXers is also illustrated by its enhanced safety features. Thanks to its construction, it does not use or contain any gaskets or braze material. Consequently, the risk of leaks or fluid incompatibility is substantially reduced. In particular, the risk of leaks in a HEATRIC™ HX is approximately two orders of magnitude lower than for any other HX thanks to its continuous passages. During its total commercial runtime of 100 years, there has never been a leak to atmosphere . Also, the micro channel design efficiently prevents any flow induced vibration damage and tube rupture. As the need for an over pressurization relief system subsides, the system's size may be reduced, which lowers equipment cost.

For gas-gas applications, fouling does not constitute a significant problem in the HEATRIC™ type HXers. As a result of the high operating temperature, the amount of moisture present to agglomerate particles is negligible or even non-existent. Furthermore, the micro channels are free from discontinuities. Consequently, there are no dead spots where particles would be prone to adhere to the passage wall and cause serious fouling problems.

Flexibility is another distinguishing feature of HEATRIC™ HXers. The versatility is particularly shown in the area of allowed fluid types and flow configurations. The variety of fluids for which HEATRIC™ is a feasible choice includes liquids, gases, and boiling and condensing two-phase flow . The design also allows multi-fluid integration (multi-stream capacity). The most commonly employed flow configurations include, but are not limited to, counterblow, cross flow, co flow, or any combination of these (Fig. 1-10).

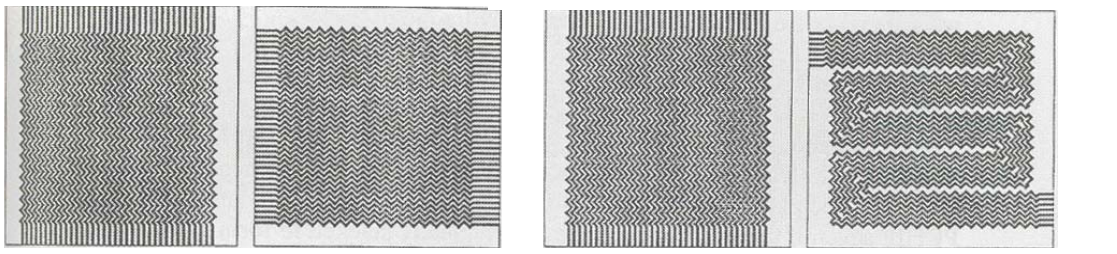

Figure 1.10. Simple cross flow (left) and cross-counter flow (right) configuration (courtesy Hesselgreaves)

Lastly, size and pressure drop considerations also favor the HEATRIC™ HX. Thanks to the compactness provided by its design, the volume of the HEATRIC™ type HX is normally between 4 and 6 times smaller than that of the standard HX type designed for the same thermal duty and pressure drop. With respect to mass, the HEATRIC™ HX has an average mass-to-duty ratio in tones/MW of 0.2, as compared to 13.5 for a shell-and-tube HX Obviously, this reduction in size will cut the material and handling cost noticeably. The characteristic short-and-fat shape as well as the reduced size of the HEATRIC™ HX is demonstrated in Fig.1.11 below. The actual design does not put any constraints on the HX with regard to the pressure drop. As Fig. 1-11 shows, the units are usually short, which compensates for the narrow passages.

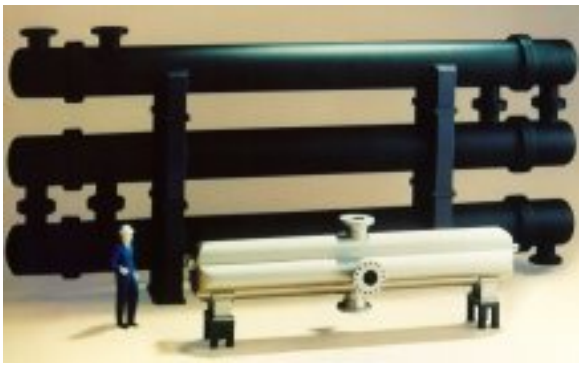

Figure 1.11. HEATRIC™ HX in front of shell-and-tube HX designed for the same thermal duty and pressure drop (courtesy HEATRIC™)

1.2.3 Multiport Printed Circuit Heat Exchanger

This section concentrates on the design and performance of the novel MP PCHE. First, the background leading up to its development is described in brief. Second, the physical dimensions and assembly process are introduced. Third, qualitative and quantitative advantages of this novel concept are presented.

The MP PCHE was developed in order to be able to provide the nuclear market with competitive HXers designed specifically for Generation IV. As indicated earlier, Generation IV HXers are

subject to several stringent requirements. Upon designing the MP PCHE, HEATRIC™ strived to meet the following criteria.

- Effectiveness > 95%;
- Compact size;
- Very low pressure drop;
- Medium to high temperature capability;
- High pressure capability; and
- High integrity to withstand transients

The main feature of the new design is the built-in headers. Incorporating the headers and distributors into the core leads to higher efficiency and less maldistributions. Diffusion bonded block. Two of the diffusion bonded blocks are separated by the inlet and outlet regions added in the middle. The separation distance between the two blocks varies depending on the design, because it is calculated to balance the pressure drop. Another purpose of the separator is, as the name implies, to separate the hot and cold ends of the medium allocated to the space formed by the headers .Normally, the high pressure fluid is assigned to this space in order to minimize the module pressure vessel stresses. As an additional benefit, this innovative construction minimizes the temperature difference at the partition thereby contributing to increasing the overall efficiency. Presently, the dimensions of the block are restricted. The upper limit of the width is 1.5 m, because the current applications in the gas and oil industry do not usually require units above this size. However, were a customer to order a large quantity, the width could be extended beyond today's upper limit of 1.5 m. The depth of the block is normally around 0.4 m, but can be increased to 0.6 m. Also, the height is limited to 0.6 m, because this is the upper limit of the film width used during the photochemical etching process. One can weld a number of blocks together and by doing so fabricate a modular construction of desired size. That is, if n blocks are combined, the stack would have the dimensions $(1.5)x(0.4)x(0.6n)$ m. The inlet and outlet piping for the high pressure fluid side have been added, respectively. The final product in its full beauty which shows the pattern of the new design features laid out on half a plate. In a real plate, the other half would consist of a mirror image of the one shown above. All the thin white (light)

lines represent distribution channels. The dark, wavy pattern in the middle symbolizes the actual channels responsible for the heat transfer. All geometrical figures of different shapes correspond to headers for the hot and cold media.

The new MP PCHE design brings more advantages to the already high-performing HX. These benefits manifest themselves primarily in the area of heat transfer, pressure drop and fabrications. Thanks to an increase in the heat transfer coefficient, the heat transfer area required is reduced by approximately 50% compared to the traditional design. Another thermal benefit of this original device is its ability to strongly limit thermal expansion problems. In particular, the design confines the thermal expansion to one single direction, which makes it easier to cope with the problem by facilitating appropriate counter-measures. The logarithmic mean temperature difference is increased by 20% since the new design has no Z-flow or cross flow. In terms of pressure drop, the low pressure medium is not affected, whereas one can anticipate a 55% reduction for the high pressure fluid. The mulitport design also generally reduces the maldistributions substantially. Other improvements include simplified fabrication and assembly, because the internal headers are now integrated into the plate and thus no longer have to be welded onto the core separately. In addition, the amount of necessary piping is reduced, which cuts the cost and increases the deployment flexibility;

1.2.4 Summary and Conclusions

HEATRIC^{TM} HX is a rugged, extremely compact piece of equipment built on the concept of micro channels, which are chemically etched out of plates that then are diffusion-bonded to form building blocks. The compact design enables operation at pressures up to at least 50 MPa, virtually eliminates the risk of leaks, and allows truly minimized volumes with respect to the heat duty. Further, the efficiency of this HX, in principle, is always above 90%, and can be as high as 98%.

At a workshop on PCHE held at MIT in October 2003, HEATRIC^{TM} representatives presented an innovative multiport PCHE (MP PCHE) design based on the concept of integrating the headers and distributors into the core. The MP PCHE was developed in order to meet the needs of the nuclear power market. Compared to the traditional PCHE, this unique design increases the heat transfer coefficients, lowers the pressure drop, and simplifies the fabrication.

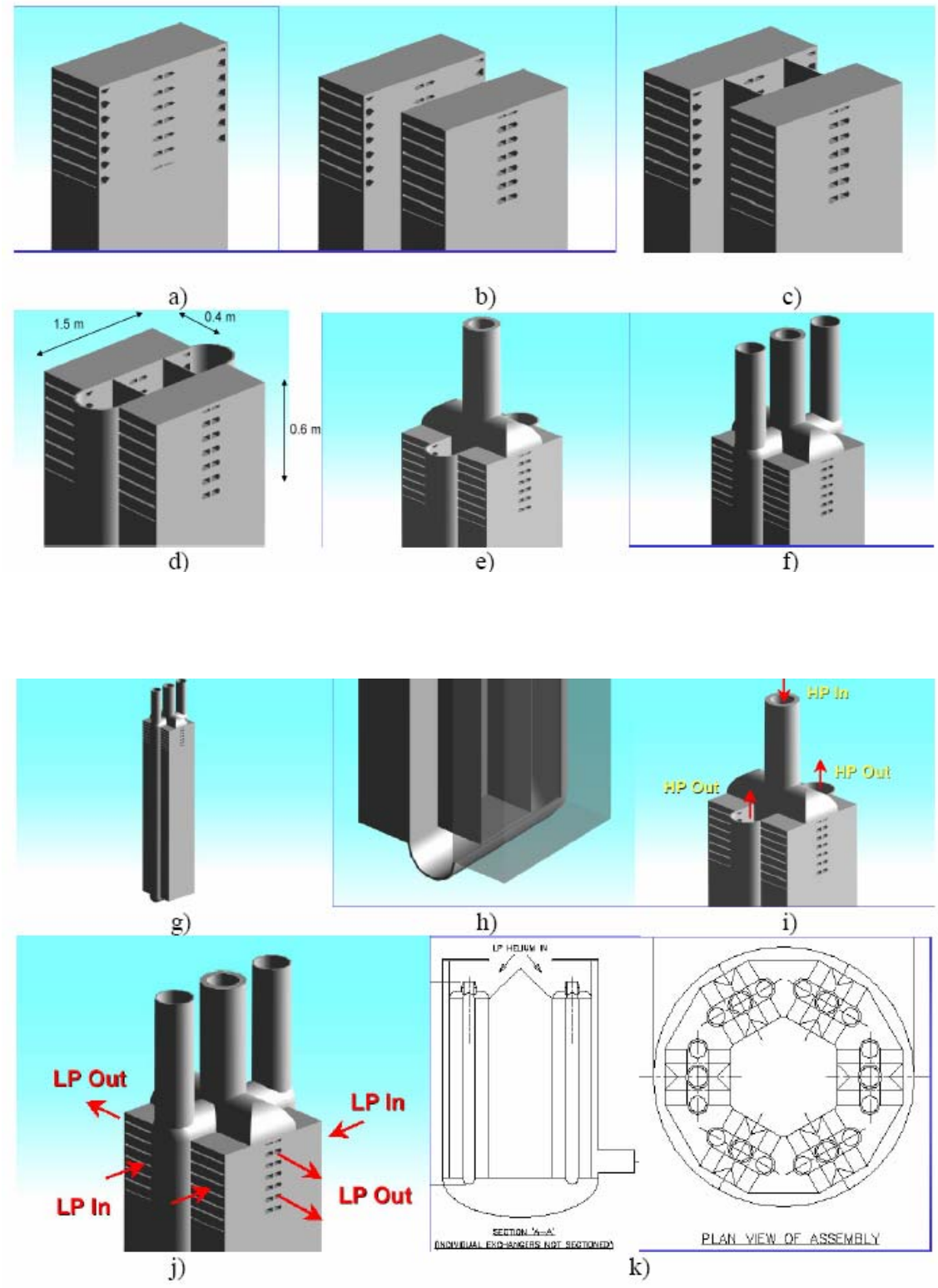

Fig. 1.12 Stepwise assembly of multiported PCHE developed by Heatric™

1.3 OBJECTIVES OF THE STUDY

- To study the flow behavior and heat transfer characteristics of a fully-developed laminar flow in a straight smooth circular straight duct under constant heat flux condition. Fanning friction factor, Nusselt number, Colburn factor, Goodness factor are to be found out and the accuracy of FLUENT package is to be evaluated as these values are already known.

- Following the same procedure, the study is to be focused on semi elliptical cross-sections taking straight and sinusoidal duct which are basically found in the Printed Circuit Heat Exchanger.

- Then the correlations of Fanning friction factor and Colburn factor which can be used in the PCHE manufacturing industry are to be found out taking into consideration of Reynolds Number, and various geometrical parameters.

1.4 ORGANISATION OF THE THESIS

The thesis is being organized in eight chapters as per the followings.

Chapter 1, the current chapter focuses on the introduction to Printed Circuit Heat Exchanger (PCHE).Its construction, features and capabilities have been covered. Then PCHE manufactured by HEATRIC in UK is described. Then the objective of the thesis is being highlighted.
Chapter 2 is based on literature review of the PCHE .PCHE uses the semi elliptical duct .Some literature is given on the fluid flow and heat transfer characteristics of semi elliptical straight duct and sinusoidal duct.

Chapter 3 gives the theory of CFD and overview of FLUENT package.

Chapter 4 covers the study of laminar flow and heat transfer characteristics of the smooth circular duct under constant heat flux boundary condition using FLUENT in both 2D and 3D.

Chapter 5 presents the study of flow behavior and heat transfer characteristics of semi elliptical straight duct in the entrance region under constant heat flux boundary condition using FLUENT.

Chapter 6 highlights on the finding of Fanning friction factor and Colburn factor of semi elliptical straight duct in fully developed region using the periodicity boundary condition using FLUENT.

Chapter 7 covers the flow behavior and heat transfer characteristic of sinusoidal channel using FLUENT.

Chapter 8 makes the conclusion of the thesis .It also focuses the future scope of this work.

Chapter 2

LITERATURE REVIEW

- PCHE
- Semi-elliptical straight duct
- Sinusoidal Duct

2.1 PRINTED CIRCUIT HEAT EXCHANGER (PCHE)

The amount of information about PCHE in the literature is quite meager. Although the concept of using micro channels in heat exchangers has been known for decades, actual units have been produced only since about 1985. Up until 1985, the manufacturing technology was not sufficiently developed. Additionally, microchannel heat exchangers have been fabricated only by one company (HeatricTM.)

One work published by Doty studies laminar flow in micro channels [1]. The findings of this paper were partly used and developed in a previous report which touches on the concept of printed circuit heat exchangers (PCHEs) [2].

The only reference that mentions HeatricTM [4] by name is Hessel greaves' *Compact Heat Exchangers*, published in 2001 [3]. Unfortunately, its section on PCHEs is mainly of a qualitative nature and therefore provides little assistance in the technical design.

The last relevant source of importance is the web site of HeatricTM.Tak, Won-Jae Lee, Jonghwa Jang of Korea Atomic Energy Research Institute have studied on fundamental numerical approach on gas flow behavior in typical PCHE geometry and presented a paper on this in proceedings of ICONE14 International conference [5] on Nuclear Engineering July 2006, Miami, Florida. Konstantin Nikitin, Yasuyoshi Kato and Lam Ngo have used Printed circuit heat exchanger for determining thermal–hydraulic performance in supercritical CO2 experimental loop.

2.2 SEMI-ELLIPTICAL STRAIGHT DUCT

Ducts of semicircular cross section have been analyzed extensively by Hong and Bergles[6],Shah and London [7], Manglik and Bergles[8],Lei and Trupp[9][10],and Ben-Ali et al [11].Fully elliptical ducts have been analyzed by Bhatti[12][13],Abdel-Wahed et al[14],Ebadian et al[15][16], Dong and Ebadian[17][18] and Velusamy and Garg[19].

Laminar flow development in the entrance region of elliptic ducts is described by Bhatti[13],Abdel-Wahed et al[14],Garg and velusamy[19] .Fully developed heat transfer in elliptical ducts is discussed by Bhatti[13],Ebadian et al[18]Dong and Ebadian[15.[16][17].deal with flow and temperature characteristics in curved elliptical ducts, while Dong and Ebadian[17] deal with the interaction of radiation and convection in the

entrance region of elliptical ducts with internal fins. It seems that the problem of fully developed flow and heat transfer in semi-elliptical ducts has not been given any attention [20]and similar earlier reviews)except by Shah .

2.3 SINUSOIDAL DUCT

Rosaguti, Fletcher and Haynes [21] have reported the fully developed laminar flow and heat transfer in three-dimensional, stream wise-periodic sinusoidal channels with circular and semi-circular cross-sections. They have used Computational fluid dynamics (CFD) to investigate the effect of Reynolds Number ($5 \leq Re \leq 200$) and amplitude to half wavelength ratio($0.222 \leq A/L \leq 0.667$) on heat transfer enhancement and pressure drop for steady ,incompressible, constant property, water(Pr=6.13) flows in geometries for the constant wall heat flux and constant wall temperature boundary conditions. Significant heat transfer enhancement is achieved without a large pressure –drop penalty. Heat transfer enhancement exceeds the relative pressure-drop penalty by factors as large as 1.5 and 1.8 for the circular and semi-circular cross-sections, respectively.

Raj M. Manglik,Jiehai Zhang,Arun Muley[22] have numerically investigated the forced convection behavior in three-dimensional wavy plate-fin channels with rectangular cross-sections and the effects of fin density in the steady low Reynolds number regime for air flows. The wavy-wall-surface produces a secondary flow pattern that is made up of multiple counter-rotating vortices in flow cross-sections of the trough region, and its magnitude and spatial coverage increases with Re and fin-spacing ratio. The latter represents wavy-fin density effects, and at low flow rates ($Re < 100$), viscous forces tend to dominate and somewhat suppress or diminish the extent of swirl, whereas at high Re (>100),the multiple-pair counter-rotating helical swirl promotes higher momentum and convective energy transport. The temperature distributions in the wavy-fin channel, subjected to either the uniform wall temperature T or uniform heat flux H1 boundary condition, correspondingly show a local thinning of the boundary layers with sharper wall gradients; the thermal performance with the H1 condition, however, is higher than with the T condition. Also, the cross-section aspect ratio and fin separation appear to have competing effect s on the thermal hydraulic performance ,as measured by the surface area

goodness factor (j/f) or core compactness, and the optimum dependent upon the flow-regime. Nevertheless, increasing fin density (or decreasing fin-spacing ratio) tends to promote a relatively better (j/f) performance under swirl-flow conditions and thus provide for a more compact wavy-plate-fin heat exchanger core.

Harms, jog and Manglik [23] provide a summary of relevant literature available for the fully developed laminar flows in a semicircular duct with temperature-dependent viscosity variations in the flow cross sections.

Velusamy, Garg andVaidyanathan [24] have studied the control volume-based numerical solution for the fully developed laminar flow and heat transfer in ducts of semi-elliptical cross section. Both an isothermal and a uniform axial heat flux condition on the duct walls have been considered. Numerical results for velocity and temperature profiles, friction factor, pressure defect, and Nusselt number are presented for a wide range of duct aspect ratios from 0.1 to 0.999.For ducts in which the baseplate is on the major axis, friction factor and Nusselt number for the uniform heat flux condition increase as the aspect ratio decreases, with values for the lowest aspect ratio of 0.1 being about 25 percent larger than those for a semicircular duct. For ducts with the baseplate on the minor axis, all characteristics exhibit a nonmonotonic behavior with respect to the aspect ratio. While the maximum velocity and pressure defect exhibit a mild maximum for aspect ratio of 0.6, the friction factor and Nusselt number exhibit a minimum at the same aspect ratio. The ratio of Nusselt number to friction factor is higher for semi-elliptical ducts in comparison to that for other ducts, such as sinusoidal, circular segmental, and isosceles triangular ducts.

In recent work, Rosaguti et al.,2006[25] have examined fully developed laminar flow and heat transfer in serpentine passages of various geometrical configurations, and reported the benefits of using such passages to obtain high rates of heat transfer with comparatively low friction factors. One drawback of serpentine passages is that they are not suited for application in plate structures, such as compact plate, plate-fin and plate-and-frame heat exchangers, because the passages cannot be placed close together, i.e., they have poor stackability and make poor use of the available plate area. Research into the flow and heat transfer performance of sinusoidal passages is a natural consequence of the desire for increased surface area density and improved convection heat transfer coefficients in such heat exchangers (Manglik et al., 2005). In this

paper, “stackable” geometries in the form of passages following sinusoidal axial paths are studied.

Sinusoidal channels are widely used in compact heat exchangers (Zhang et al., 2004])[26] due to their simplicity of manufacture and their good thermo-hydraulic performance (Manglik et al., 2005). Manglik et al. (2005) provide a summary of relevant literature available for two-and three-dimensional studies of wavy-walled passages

Rush. T. A, Newell.T.A. Jacobi. A.M [27]. have investigated local heat transfer and flow behavior for laminar and transitional flows in sinusoidal wavy passages. The experimental geometry consists of a channel with a 10:1 aspect ratio bound by two wavy walls. The walls are from 12 to 14 wavelengths long, and the wave amplitude, phase angle, and wall-to-wall spacing are varied during the experiments. Using visualization methods, the flow field is characterized as steady or unsteady, with special attention directed toward detecting the onset of macroscopic mixing in the flow. The location of the onset of mixing is found to depend on the Reynolds number and channel geometry. Instabilities are manifest near the channel exit at low Reynolds numbers (Re =200) and move toward the channel entrance as the Reynolds number is increased; the entire channel exhibits unsteady\ macroscopic mixing at moderate Reynolds numbers (Re =800). The onset of macroscopic mixing is directly linked to significant increases in local heat transfer

Paul E. Geyer et al[28] studied fully developed laminar flow and heat transfer behavior in serpentine channels with a square cross-section using computational fluid dynamics. Studies were performed up to Re=200, beyond which the flow became unsteady. The effect of geometric configuration was examined in detail for Re=110, $0.525<Rc/d<2$ and $3.6<L/d<12$ (where d is the side length of the square section, Rc is radius of curvature of the serpentine bends, and L is the half-wavelength of the serpentine path). Simulations were carried out at (Pr=0.7, 6.13 and 100) constant wall heat flux (H2 boundary condition) and constant wall temperature (T boundary condition). Dean vortices formed at the bends promote fluid mixing transverse to the main flow direction. This leads to significant heat transfer enhancement (up to a factor of 8 at high Pr and Re) with relatively small pressure-drop penalty (factor of 1.8 at high Re). Increasing Rc/d mitigates these effects while the effect of increasing L/d decreases the frictional penalty without greatly affecting the heat transfer enhancement.

Flow in curved passages (such as coiled tube banks in heat exchangers) can give rise to heat transfer enhancement, relative to similar flows in straight pipes (Kalb and Seader 1972)[29]. Although these enhancements come at the cost of relatively higher friction losses, the heat transfer enhancement may significantly exceed the increase in friction factor (Kalb and Seader 1972; Bolinder and Sunde´ n 1996; Ligrani et al. 1996)[30]. These effects are due to the establishment of Dean vortices (Dean 1928)[31] whose axes are aligned with the flow direction and so promote cross-stream mixing without incurring large pressure drops.

Chapter 3

COMPUTATIONAL FACILITIES

- **Introduction**
- **CFD programs**
- **Overview of FLUENT package**
- **Boundary Conditions**

3.1 INTRODUCTION

The subject of Fluid Mechanics deals with the conservation of mass, momentum and energy in a fluid medium. A set of partial differential or integral equations, which result from application of basic conservation principles to microscopic control volumes, constitutes the governing equations of fluid dynamics. There are excellent text books on the subject which derive the equations from first principles, express them in different coordinate systems, and solve them for a variety of idealised situations. Solution of the differential equations over a finite domain leads to macroscopic manifestation of the conservation principles. These macroscopic relations are employed in the design of fluid flow equipment. The following constitute the primary conservation equations of Fluid Mechanics

Conservation of mass (Continuity equation) :

$$\frac{\partial \rho}{\partial t} + \frac{\partial}{\partial x}(\rho v_x) + \frac{\partial}{\partial y}(\rho v_y) + \frac{\partial}{\partial z}(\rho v_z) = 0 \qquad (3.1)$$

Conservation of momentum in x, y and z directions :

$$\rho\left(\frac{\partial v_x}{\partial t} + v_x\frac{\partial v_x}{\partial x} + v_y\frac{\partial v_x}{\partial y} + v_z\frac{\partial v_x}{\partial z}\right) = -\frac{\partial p}{\partial x} + \mu\left(\frac{\partial^2 v_x}{\partial x^2} + \frac{\partial^2 v_x}{\partial y^2} + \frac{\partial^2 v_x}{\partial z^2}\right) + \rho g_x \qquad (3.2)$$

$$\rho\left(\frac{\partial v_y}{\partial t} + v_x\frac{\partial v_y}{\partial x} + v_y\frac{\partial v_y}{\partial y} + v_z\frac{\partial v_y}{\partial z}\right) = -\frac{\partial p}{\partial y} + \mu\left(\frac{\partial^2 v_y}{\partial x^2} + \frac{\partial^2 v_y}{\partial y^2} + \frac{\partial^2 v_y}{\partial z^2}\right) + \rho g_y \qquad (3.3)$$

$$\rho\left(\frac{\partial v_z}{\partial t} + v_x\frac{\partial v_z}{\partial x} + v_y\frac{\partial v_z}{\partial y} + v_z\frac{\partial v_z}{\partial z}\right) = -\frac{\partial p}{\partial z} + \mu\left(\frac{\partial^2 v_z}{\partial x^2} + \frac{\partial^2 v_z}{\partial y^2} + \frac{\partial^2 v_z}{\partial z^2}\right) + \rho g_z \qquad (3.4)$$

Conservation of energy :

$$\rho\hat{C}p\left(\frac{\partial T}{\partial t}+v_x\frac{\partial T}{\partial x}+v_y\frac{\partial T}{\partial y}+v_z\frac{\partial T}{\partial z}\right)$$
$$=k\left\{\frac{\partial^2 T}{\partial x^2}+\frac{\partial^2 T}{\partial y^2}+\frac{\partial^2 T}{\partial z^2}\right\}+2\mu\left\{\left(\frac{\partial v_x}{\partial x}\right)^2+\left(\frac{\partial v_y}{\partial y}\right)^2+\left(\frac{\partial v_z}{\partial z}\right)^2\right\}$$
$$+\mu\left\{\left(\frac{\partial v_x}{\partial y}+\frac{\partial v_y}{\partial x}\right)^2+\left(\frac{\partial v_x}{\partial z}+\frac{\partial v_z}{\partial x}\right)^2+\left(\frac{\partial v_y}{\partial z}+\frac{\partial v_z}{\partial y}\right)^2\right\} \qquad (3.5)$$

Equations (3.1 – (3.5) constitute the complete set of Fluid Dynamics equations in Cartesian coordinates. Along with an equation of state (a relation among p, T and ρ), they make a set of six partial differential equations in terms of six variables : u, v, w, p, T and ρ. For constant physical properties (e.g. Viscosity μ and thermal conductivity k) these six equations completely define a system, while for variable fluid properties additional equations are introduced relating the properties to temperature and pressure. The heat exchanger passages discussed in this thesis consist mainly of flat surfaces and are best described by the Cartesian coordinate system. Therefore equations (3.1 – (3.5) along with appropriate boundary conditions constitute the complete equation set to be solved

The advent of high speed digital computers, combined with the development of accurate numerical algorithms for solving physical problems, has revolutionized the way we study and practice fluid dynamics. This approach, called Computational Fluid Dynamics or CFD in short, has made it possible to analyze complex flow geometries with the same ease as that faced while solving idealized problems using conventional calculus. CFD may thus be regarded as a field of study combining fluid dynamics and numerical analysis. Historically, the early development of CFD in the 1960s and 1970s was driven by the need of the aerospace community. Modern CFD, however, cuts across all disciplines – civil, mechanical, electrical, electronics, chemical, aerospace, ocean, and biomedical engineering being a few among them. CFD complements testing and experimentation, and reduces the total time of design and development. Detailed studies on the philosophy of CFD, various physical models and numerical solution techniques can be found in references.

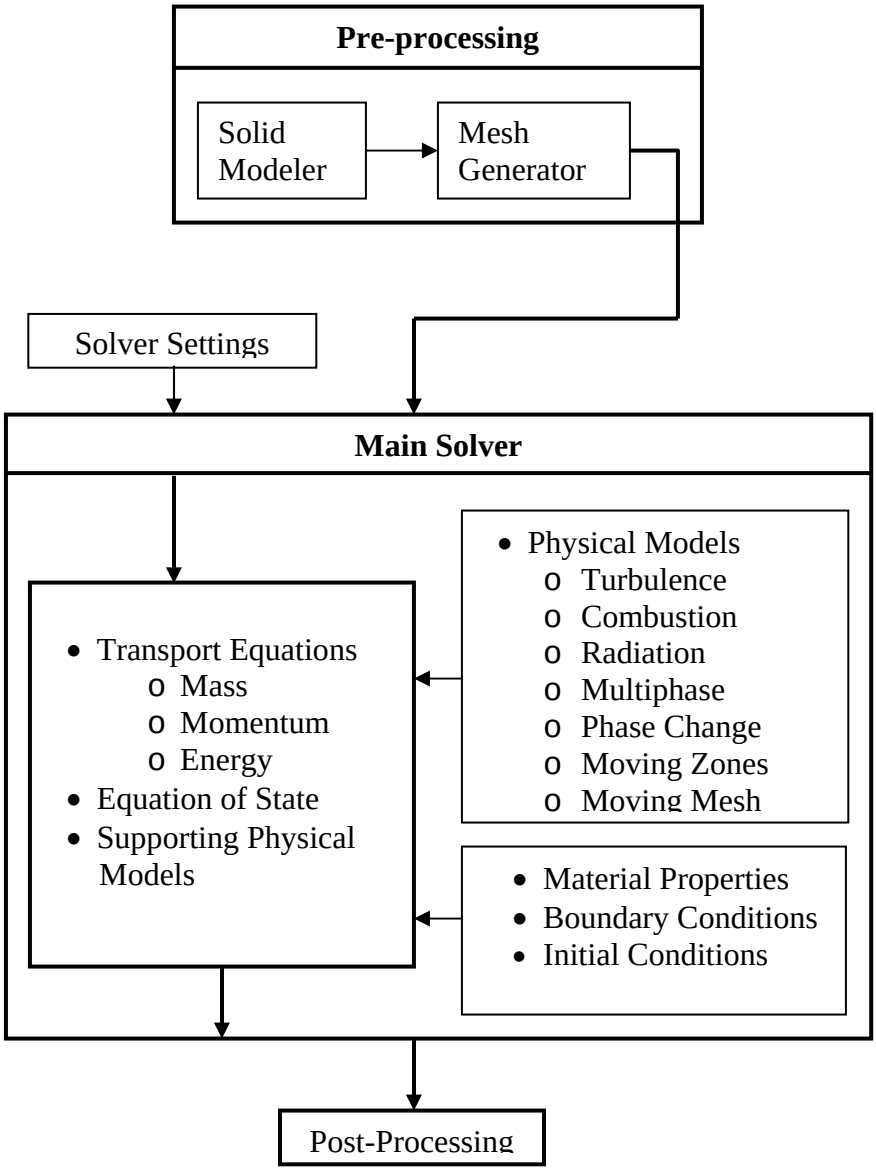

Figure 3.1: Overview of the CFD Modeling Process

3.2 CFD PROGRAMS

The availability of affordable high performance computing hardware and the introduction of user-friendly interfaces have led to the development of commercial CFD packages. Before these CFD packages came into the common use, one had to write his own code to carry out a CFD analysis. The programs were usually different for different problems, although a part of the

code of one program could be used in another. The programs were inadequately tested and reliability of the results were often questioned. Today, well tested commercial CFD packages not only have made CFD analysis a routine design tool in industry, but also have helped the research engineer focus on the physical system more effectively. All formal CFD software contain three elements (i) a pre-processor, (ii) the main solver, and (iii) a post-processor

The Pre-processor

Pre-processing is the first step of CFD analysis in which the user

(a) defines the modelling goals,

(b) identifies the computational domain, and

(c) designs and creates the grid system

The process of CFD modelling starts with an understanding of the flow problem and identification of the computational domain. This is followed by generations of the grid structure, which is the most significant portion of the pre-processing activity. It is said that over 50% of the time spent by a CFD analyst goes towards grid generation. Both computation time and solution accuracy depend on the grid structure. Optimal meshes are often non-uniform – finer in areas where large variation of variables is expected and courser in regions with relatively little change. In order to reduce the drudgery of engineers and maximize productivity, all the major CFD programs include facilities for importing shape and geometry information from CAD packages AutoCAD and I-DEAS, and for applying a meshing procedure. Current research is underway to develop CFD codes with an adaptive meshing capability.

3.2.1 The Main Solver

The solver is the heart of CFD software. It sets up the equation set according to the options chosen by the user and meshes points generated by the pre-processor, and solves them to compute the flow field. The process involves the following tasks:

- selecting appropriate physical model,
- defining material properties,
- prescribing boundary conditions,
- providing initial solutions,

- setting up solver controls,
- set up convergence criteria,
- solving equation set, and
- saving results

Once the model is completely set up, the solution starts and intermediate results can be monitored in real time from iteration to iteration. The progress of the solution process is displayed on the screen in terms of the residuals, a measure of the extent to which the governing equations are not satisfied.

3.2.2 The Post-processor

The post-processor is the last part of a CFD software. It helps the user to examine the results and extract useful data. The results may be displayed as vector plots of velocities, contour plots of scalar variables such as pressure and temperature, streamlines and animation in case of unsteady simulation. Global parameters like drag coefficient, lift coefficient, Nusselt number and friction factor etc. may be computed through appropriate formulas. These data from a CFD post-processor can also be exported to visualization software for better display.

Several general-purpose CFD packages have been published in the past decade. Prominent among them are : PHOENICS , FLUENT , STAR-CD , CFX , CFD-ACE , ANSWER , CFD++, FLOW-3D and COMPACT . Most of them are based on the finite volume method. CFD packages have also been developed for special applications; FLOTHERM and ICEPAK for electronics cooling, CFX-TASCFLOW and FINE/TURBO for turbo machinery and ORCA for mixing process analysis are some examples. Most CFD software packages contain their own grid generators and post processors. Software such as ICEM CFD, Some popular visualization software used with CFD packages are TECPLOT and FIELDVIEW.

3.3 OVERVIEW OF FLUENT PACKAGE

FLUENT is a state-of-the-art computer program for modeling fluid flow and heat transfer in complex geometries. FLUENT provides complete mesh flexibility, solving your flow problems with unstructured meshes that can be generated about complex geometries with relative ease. Supported mesh types include 2D triangular/quadrilateral, 3D FLUENT also allows user to refine or coarsen grid based on the flow solution.

FLUENT is written in the C computer language and makes full use of the flexibility and power offered by the language. Consequently, true dynamic memory allocation, efficient data structures, and flexible solver control are all made possible. In addition, FLUENT uses a client/server architecture, which allows it to run as separate simultaneous processes on client desktop workstations and powerful compute servers, for efficient execution, interactive control, and complete flexibility of machine or operating system type.

All functions required to compute a solution and display the results are accessible in FLUENT through an interactive, menu-driven interface. The user interface is written in a language called Scheme, a dialect of LISP. The advanced user can customize and enhance the interface by writing menu macros and functions..

Program Structure

FLUENT package includes the following products:

- FLUENT, the solver.
- PrePDF, the preprocessor for modeling non-premixed combustion in FLUENT.
- GAMBIT, the preprocessor for geometry modeling and mesh generation.
- TGrid, an additional preprocessor that can generate volume meshes from existing boundary meshes.
- Filters (translators) for import of surface and volume meshes from CAD/CAE packages such as ANSYS, CGNS, I-DEAS, NASTRAN, PATRAN, and others.

.

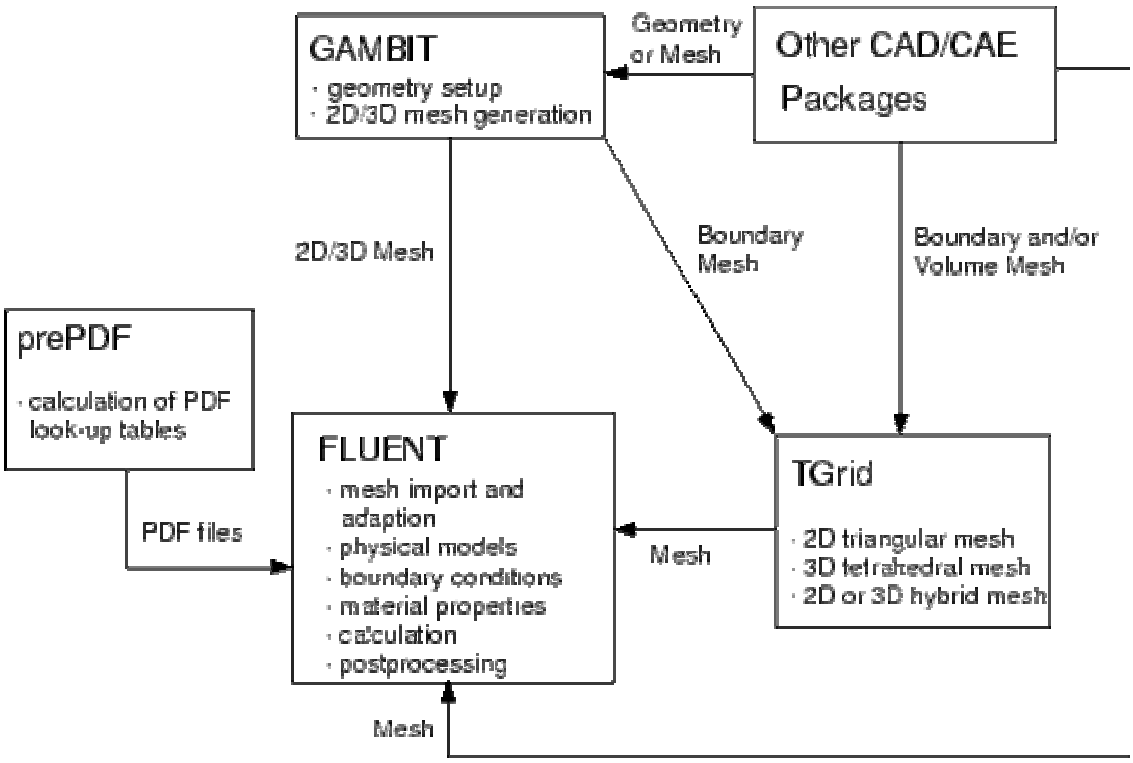

Fig.3.2 shows the organizational structure of FLUENT components

User can create geometry and grid using GAMBIT. User can also use TGrid to generate a triangular, tetrahedral, or hybrid volume mesh from an existing boundary mesh (created by GAMBIT or a third-party CAD/CAE package)It is also possible to create grids for FLUENT using ANSYS (Swanson Analysis Systems, Inc.) , CGNS (CFD general notation system) , or I-DEAS (SDRC) ; or MSC/ ARIES, MSC/ PATRAN, or MSC/ NASTRAN (all from MacNeal-Schwendler Corporation). Interfaces to other CAD/CAE packages may be made available in the future, based on customer requirements, but most CAD/CAE packages can export grids in one of the above formats.

Once a grid has been read into FLUENT, all remaining operations are performed within the solver. These include setting boundary conditions, defining fluid properties, executing the solution, refining the grid, and viewing and post processing the results.

FLUENT is ideally suited for incompressible and compressible fluid flow simulations in complex geometries. Fluent Inc. also offers other solvers that address different flow regimes and

incorporate alternative physical models. Additional CFD programs from Fluent Inc. include Airpak, FIDAP, Icepak, MixSim, and POLYFLOW.

FLUENT uses unstructured meshes in order to reduce the amount of time user spend generating meshes, simplify the geometry modeling and mesh generation process, model more-complex geometries than user can handle with conventional, multi-block structured meshes, and let user adapt the mesh to resolve the flow-field features. FLUENT can also use body-fitted, block-structured meshes (e.g., those used by FLUENT 4 and many other CFD solvers). FLUENT is capable of handling triangular and quadrilateral elements (or a combination of the two) in 2D, and tetrahedral, hexahedral, pyramid, and wedge elements (or a combination of these) in 3D. User can adapt all types of meshes in FLUENT in order to resolve large gradients in the flow field, but user must always generate the initial mesh (whatever the element types used) outside of the solver, using GAMBIT, TGrid, or one of the CAD systems for which mesh import filters exist.

3.3.1 Problem Solving Steps

After determining the important features of the problem user will follow the basic procedural steps shown below.

1. Create the model geometry and grid.

2. Start the appropriate solver for 2D or 3D modeling.

3. Import the grid.

4. Check the grid.

5. Select the solver formulation.

6. Choose the basic equations to be solved: laminar or turbulent (or in viscid), chemical species or reaction, heat transfer models, etc. Identify additional models needed: fans, heat exchangers, porous media, etc.

7. Specify material properties.

8. Specify the boundary conditions.

9. Adjust the solution control parameters.

10. Initialize the flow field.

11. Calculate a solution.

12. Examine the results.

13. Save the results.

14.If necessary, refine the grid or consider revisions to the numerical or physical model.

Step 1 of the solution process requires a geometry modeler and grid generator. You can use GAMBIT or a separate CAD system for geometry modeling and grid generation. You can also use TGrid to generate volume grids from surface grids imported from GAMBIT or a CAD package. Alternatively, user can use supported CAD packages to generate volume grids for import into TGrid or into FLUENT. In Step 2, user will start the 2D or

4. When interphase coupling is to be included, the source terms in the appropriate continuous phase equations may be updated with a discrete phase trajectory calculation.

5. A check for convergence of the equation set is made.

3.4 BOUNDARY CONDITIONS

The governing differential equations of a CFD program need to be provided with boundary and initial (for transient solutions) conditions for complete solution over the space and time domain of interest. The boundary conditions generally involve velocities, (or flow rate in lieu of them), pressure and temperature over the bounding surfaces. The process of solving a fluid flow problem if often considered to be the extrapolation of a set of data defined on the bounding contours or surfaces into the domain interior. It is, therefore, important for the user to supply physically realistic and well-posed boundary conditions to ensure accurate and stable solutions

3.4.1Wall Boundary Condition

For a viscous fluid, a solid wall represents an impenetrable and no-slip boundary. All velocity components vanish on a stationary solid boundary. The shear stress is calculated from the Newton's law of viscosity. For study of heat transfer, isothermal or constant heat flux boundary conditions are generally employed.

3.4.2Symmetry Boundary condition

A symmetry boundary in a flow field is characterized by absence of any scalar flux across the boundary. In other words, flow velocities normal to the boundary vanish, while flow velocity parallel to the boundary line attains a maximum or minimum value. Scalar variables such as temperature and pressure are also symmetric across the boundary, showing a local optimum on the boundary line.

3.4.3 Periodic Boundary Condition

A periodic boundary condition is employed when the flow passage has features repeating at regular intervals. While the velocity, temperature and pressure profiles change monotonically at the entrance to the passages, soon the profiles stabilize and repeat at intervals equal to that of the periodic features. In case of long enough passages, the contribution of the entrance region can be neglected and the entire passage can be considered to have fully developed flow repeating with the period of the geometrical features.

The concept of periodically developed flow and heat transfer has been analyzed by Patankar et al. They have split the pressure term into two components – one related to the global mass flow, the other responding to local motions. The global flow causes a gradual and monotonic fall in pressure along the flow direction due to viscous effects, while the local velocities, governed by the oscillatory changes in flow cross section, cause periodic variation of pressure through the Bernoulli equation. The temperature constraints are represented in two different ways for constant temperature and constant heat flux boundary conditions. In case of constant temperature boundary condition, while the wall temperature Twall remains constant along the flow direction, the dimensionless temperature profile repeats itself at regular intervals. The dimensionless temperature θ is defined by the relation :

$$\theta(x, y) = \frac{T(x, y) - T_{wall}}{T_{bulk}(x) - T_{wall}} \quad \text{----------(3.12)}$$

In case of constant heat flux condition, the bulk fluid temperature Tbulk increases or decreases monotonically. Unlike Eq (3.9), Twall under constant heat flux condition changes monotonically in the flow direction. The nature of the temperature field becomes analogous to that of the

pressure field, the periodic component of temperature repeating with the periodicity of the geometrical features. The periodic boundary condition expresses a relationship between the exit and inlet conditions. A pressure drop or a mass flow rate condition must accompany it over the solution domain.

Chapter 4

STRAIGHT SMOOTH CIRCULAR DUCT (2-D & 3-D Analysis)

- Introduction
- Computational Domain & Boundary Conditions
- Gambit & FLUENT Details
- Results
- Discussion

4.1 2D ANALYSIS

4. 1.1 INTRODUCTION

A circular duct of length L_0=400 mm and of diameter 4 mm has been taken for analysis. Due to symmetry axisymmetry geometry has been taken. So, here d=2 mm. To capture the larger velocity gradient finer mesh has been taken near the wall. Re=50 has been taken .Inlet velocity u=0.2 m/s has been calculated to give Velocity_ Inlet condition as b.c to inlet of the duct .The friction factor & Colburn factor has been calculated to analyzed the fluid flow and heat transfer characteristics. Large length as compared to the diameter has been taken to get the results for fully-developed condition**.**

4.1.2 COMPUTATIONAL DOMAIN& BOUNDARY CONDITIONS

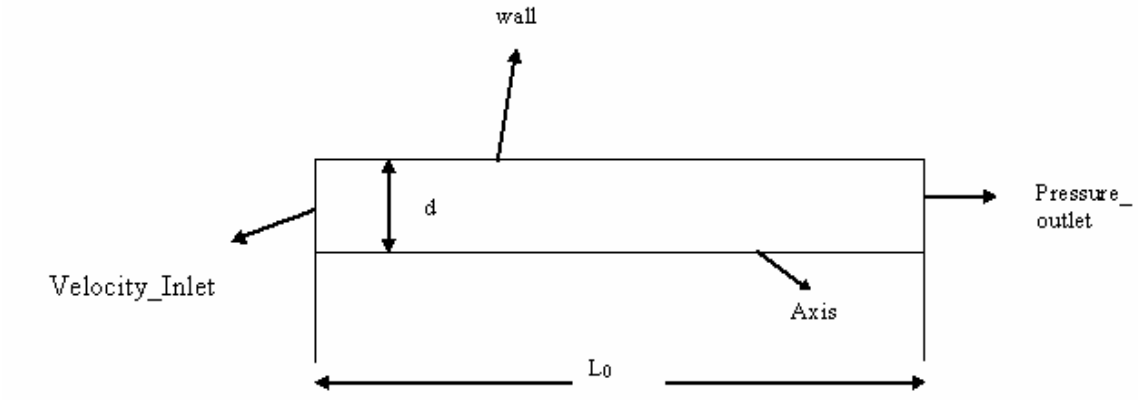

Fig. 4.1 Computational Domain of laminar forced convection in a circular duct with different boundary conditions

Left-inlet-velocity_inlet

Right-outlet-pressure_outlet

Bottom-Axis

Top-Wall

4.1.3 GAMBIT & FLUENT DETAILS:

Laminar, steady, incompressible flow

2-D axisymmetric geometry is created.

Interval count=30 in X & 50 in Y directions

Meshing to be finer near the Wall,

So, Successive ratio in Y- direction is 1.3

Solver-segregated, Implicit, axisymmetric, steady, Laminar

Material properties-default of air selected.

Operating Pressure-101325 Pa.

Wall-constant heat flux (100w/m2 assumed)

Pressure-Velocity Coupling- SIMPLE

Under-Relaxation: - Momentum=0.7, Energy=1.0

Convergence=10-6 for continuity, energy

Grid Independence Test

Table 4.1 Grid Independent Test for laminar forced convection in a circular duct

Grid Size	Nu
20 x 30	4.3692
30 x 30	4.3709
30 x 40	4.3704
30 x100	4.3705

4.1.4 RESULTS

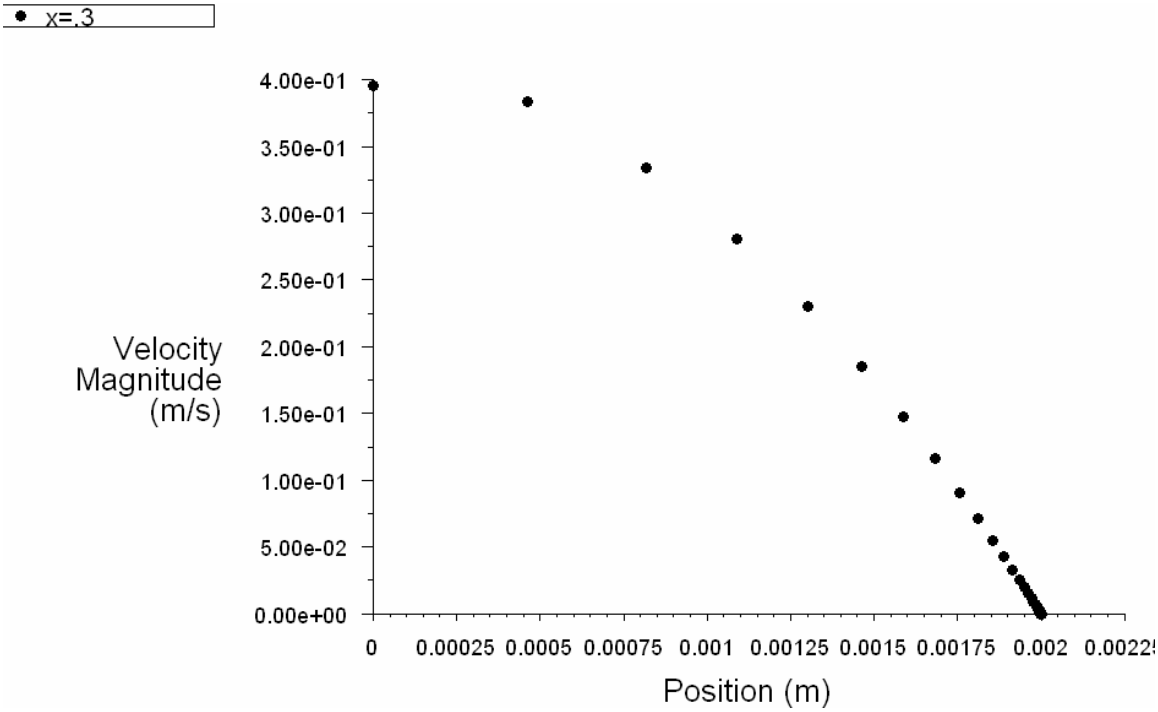

Fig.4.2 Variation of velocity at a section along Y-axis in a circular duct

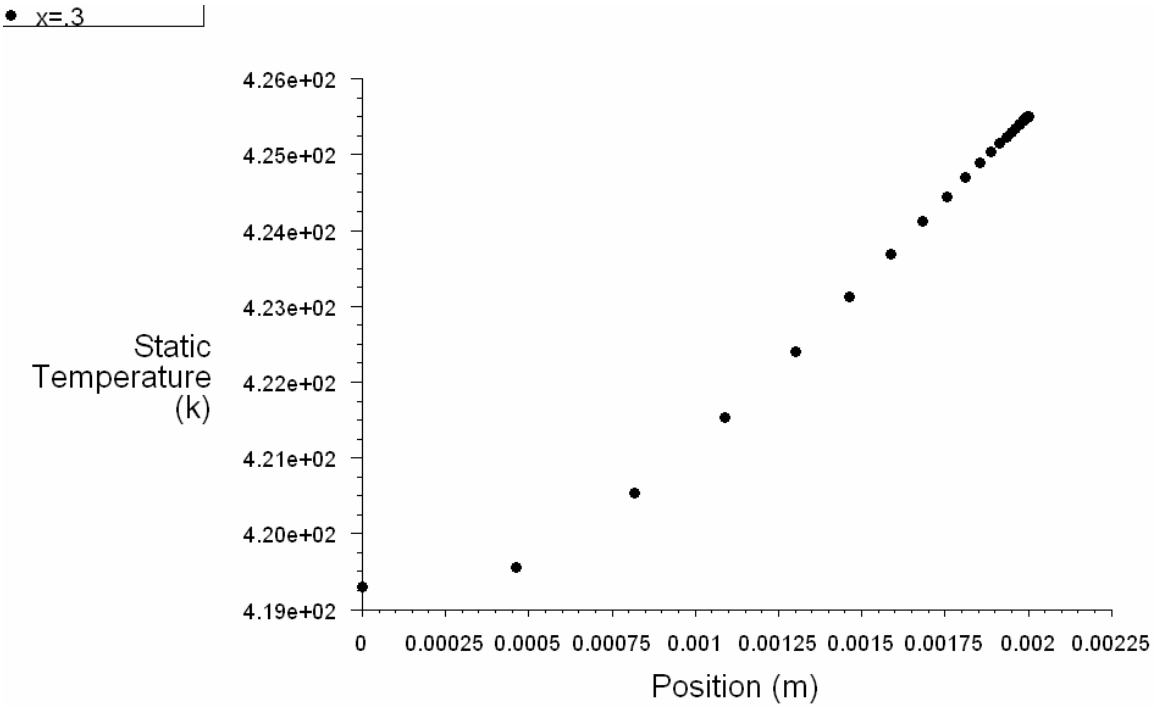

Fig.4.3 Variation of temperature at a section along Y-axis. in a circular duct

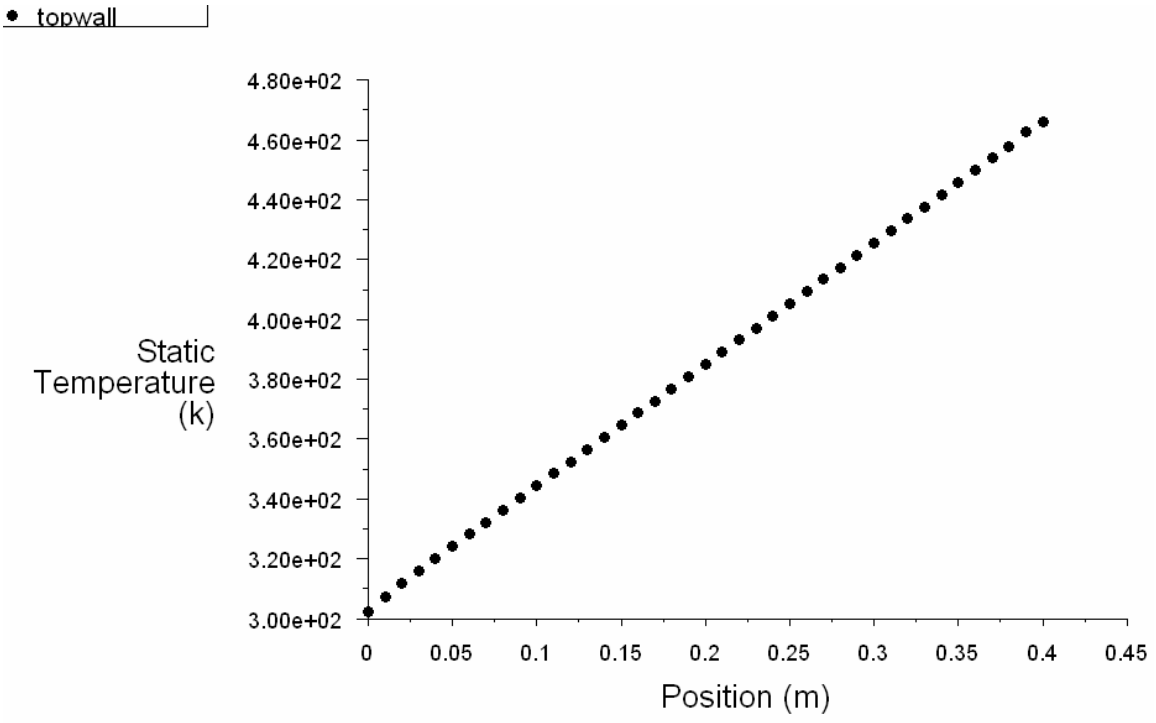

Fig.4.4 Variation of wall temperature along the length of the circular duct

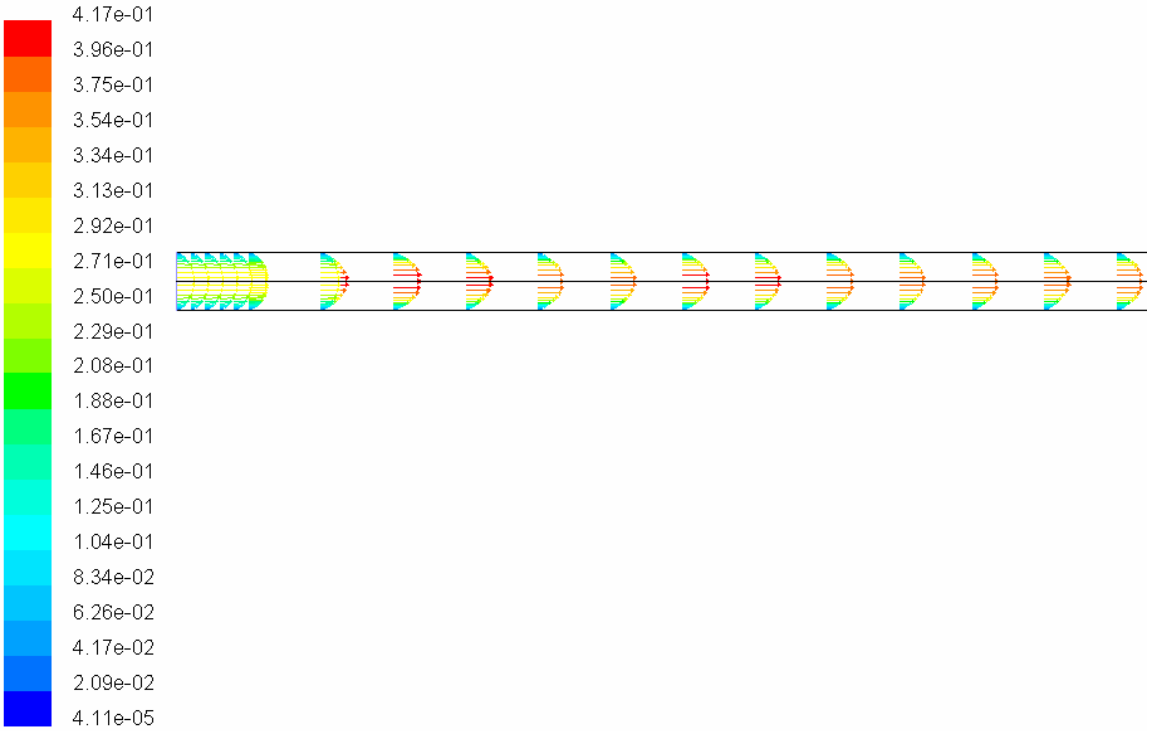

Fig.4.5 Display of velocity vectors showing the flow development.

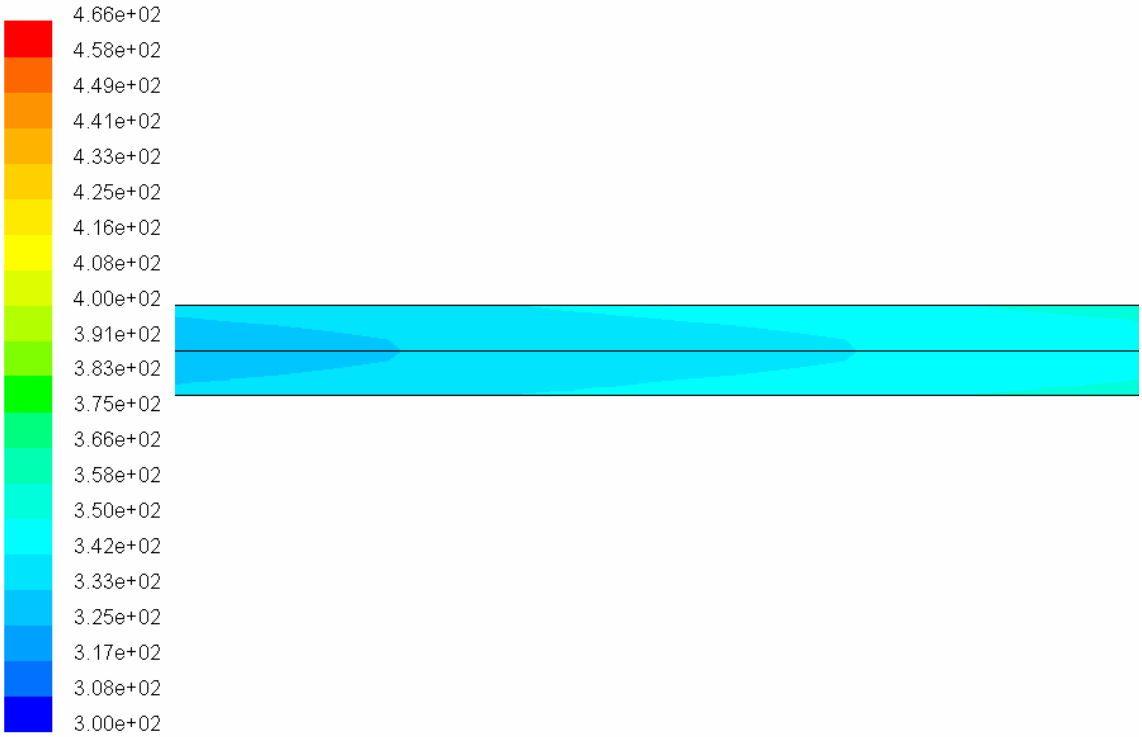

Fig.4.6 Temperature contour along the length of the duct

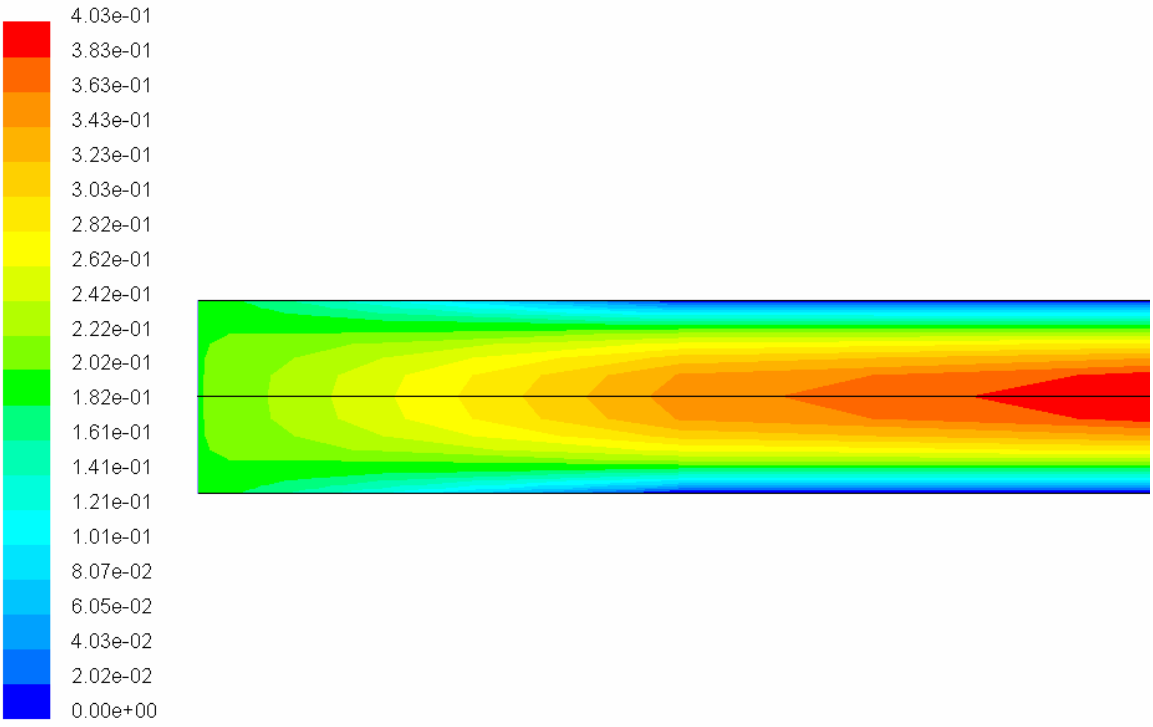

Fig.4.7 Velocity contour along the length of the duct

Taking the grid size 40 x 30

Table 4.2 Calculation of Nusselt no. for a circular duct(2-D)

Section	Tw	Tf	Tw-Tf	h	Nu	f	j
X=.1 m	344.396	340.614	3.781 97	26.4412	4.3704	0.296	0.09811
X=.3 m	425.507	421.725	3.781 99	26.4410	4.3704	0.296	0.09811

The calculations have been done over the fully developed region. Therefore the results have been taken at the sections 100 mm and 300 mm

$$T_w = 1/A\int TdA \quad \text{..... (4.1)}$$

Area weighted average wall temperature has been taken for calculating local nusselt number which is same for all sections after the flow is hydrodynamically and thermally developed.

$$T_f(x) = \left[\iint |u|T(x,y,z)dydz / \iint |u|dydz\right] \quad \text{..... (4.2)}$$

Bulk mean temperature of the fluid is being taken from the mass weighted average temperature from the FLUENT directly.

Nusselt number is calculated from the following relation.

$$Nu = q/T_w - T_f \quad \text{..... (4.3)}$$

Then, Colburn factor, $j = Nu/\mathrm{Re}\,\mathrm{Pr}^{1/3}$ ..... (4.4)

Where Pr=Prandtl number calculated from the thermo physical properties is 0.744

$\Delta P = f\rho Lu^2 / 2D$ …… (4.5)

Where ΔP=P(inlet)-P(outlet)……...(4.6)

h=q/(Tw-Tf)……(4.7)

Nu=h d/k……..(4.8)

ΔP= 2.86Pa

Goodness factor=j/f has been calculated to study the relative surface area compactness.

f.Re =0.296 x 50=14.8

Overall it has been shown that it clearly matches the result f x Re=16and Nu(constant Heat Flux)=4.36

4.1.5 DISCUSSIONS

The friction factor decreases with increase in Reynolds number. The same also happens in case of colburn factor. It is found that the friction factor matches with the correlation f.Re=16 and Nusselt number closes matches with the value of 4.36 under constant heat flux condition.

4.2 3-D ANALYSIS

4.2.1 INTRODUCTION

Fluid flow and heat transfer characteristics for a steady incompressible laminar flow has been investigated taking a 3D geometry. As it is symmetric about the axis ,half of the duct has been taken as the computational domain. Periodic boundary condition has been taken at the inlet and outlet to achieve a fully developed flow. The logic behind this is we are giving mass flow rate inlet at the inlet of the duct. We are keeping the mass flow rate constant through out the duct .Periodic boundary condition will take care of this. So, fully developed flow will be achieved after a certain no of repetitions of the module. Only one module is sufficient for analysis. So, length of the duct can be taken smaller and smaller. Computation time can be reduced very much for analysis of this short domain. Meshing can be made finer and finer to get the accurate result .

4.2.2 COMPUTATIONAL DOMAIN& BOUNDARY CONDITIONS

The whole geometry is taken as half which has been given symmetry boundary condition. The computational domain of length 20 mm and diameter 2 mm has been taken for analysis. At the inlet and outlet periodic boundary condition has been taken. It requires mass flow inlet which is calculated for a fixed Reynolds number. The curved region is given wall boundary condition which is under constant heat flux.

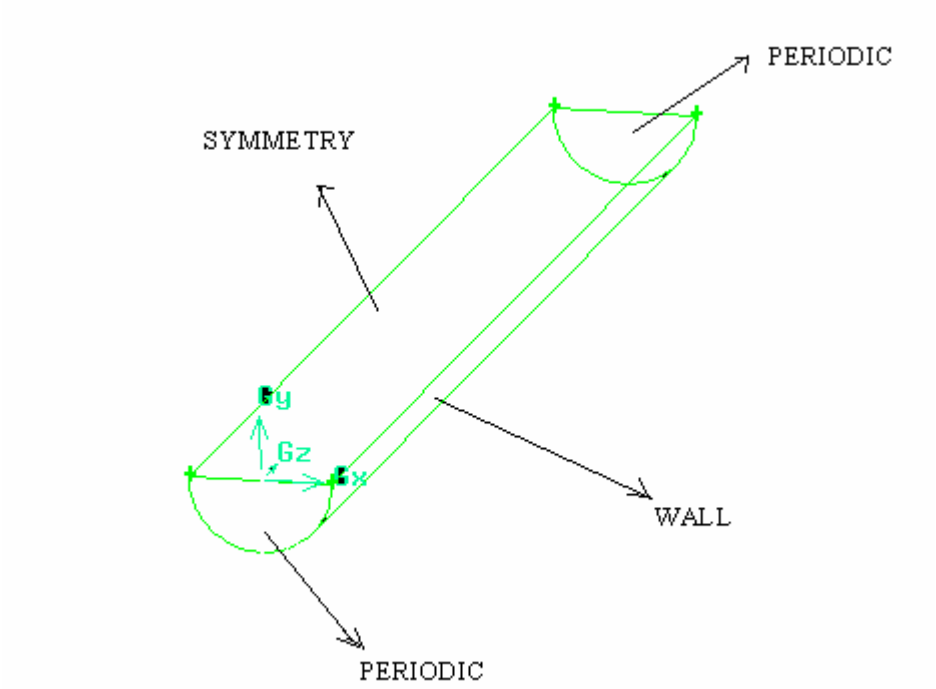

Fig.4.8. 3-D geometry of a circular duct showing different boundary conditions

4.2.3 GAMBIT & FLUENT DETAILS

The geometry is meshed in Gambit.First, the different edges have been meshed .Then the face is meshed quad/pave elements. The inlet and outlet faces are linked so that equal meshing is obtained which is necessary for giving these two faces as periodic boundary conditions. The volume is meshed using cooper meshing**.**

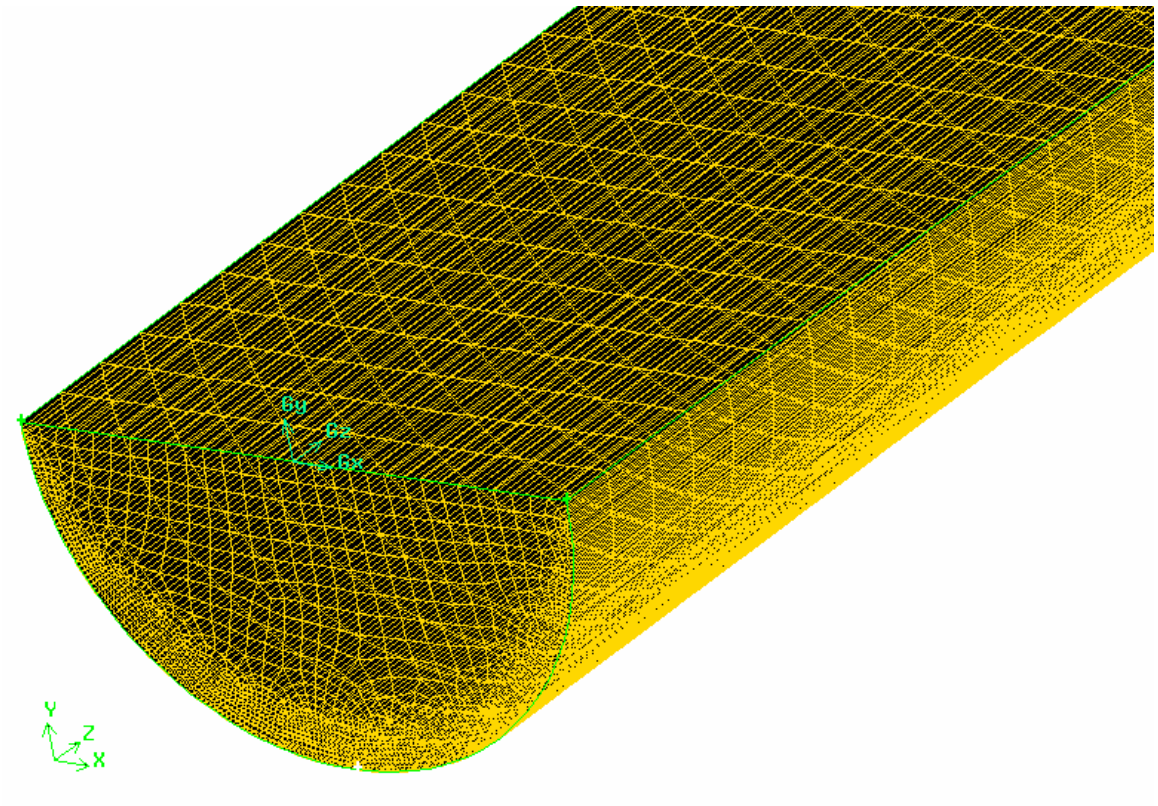

Fig 4.9 Meshing for the whole computational domain

The SIMPLE algorithms evaluate the coupling between pressure and velocity. The under-relaxation factor momentum and energy has been 0.7 and 1 respectively. The second order upwind scheme has been taken for the descretisation of momentum and energy equation. The 3-D double precision solver has been chosen. Convergence criteria have been taken as 1e-06 for continuity and energy. Following grid independent test has been done taking different grid sizes. Nusselt Number variation has been observed

The following thermo-physical properties of air have been taken.

Table 4.3 Thermo-physical properties of air for laminar flow in a circular duct

Fluid -air
Density=1.225 kg/m^3 Thermal conductivity=0.0242 w/m-k Viscosity=1.7894e-05kg/m-s Specific heat at constant pressure=1006.43 J/kg-k

.

For a fixed Reynolds number, mass flow rate is calculated according to the following relation.

$\dot{m} = A\mu \mathrm{Re}/ d_h$ ……(4.9).

Where $\dot{m}$ =mass flow rate

Mass flow rate is being taken as input.

Air temperature at inlet is set at 300K.A constant heat flux(here 100w/m^2) has been provided to the wall as shown as the above fig.

Grid Independence Test (Re=500)

Table 4.4 Grid Inpendence Test for a laminar forced convection in a circular duct(3-D)

Grid Size	**No Of Cells**	**Nu**
60 x 60 x 60	53700	4.673
100 x 100 x 100	243500	4.546
120 x 120 x 30	104340	4.575
200 x 30 x 30	56370	4.512
200 x 30 x 100	187900	4.461

4.2.4 RESULTS

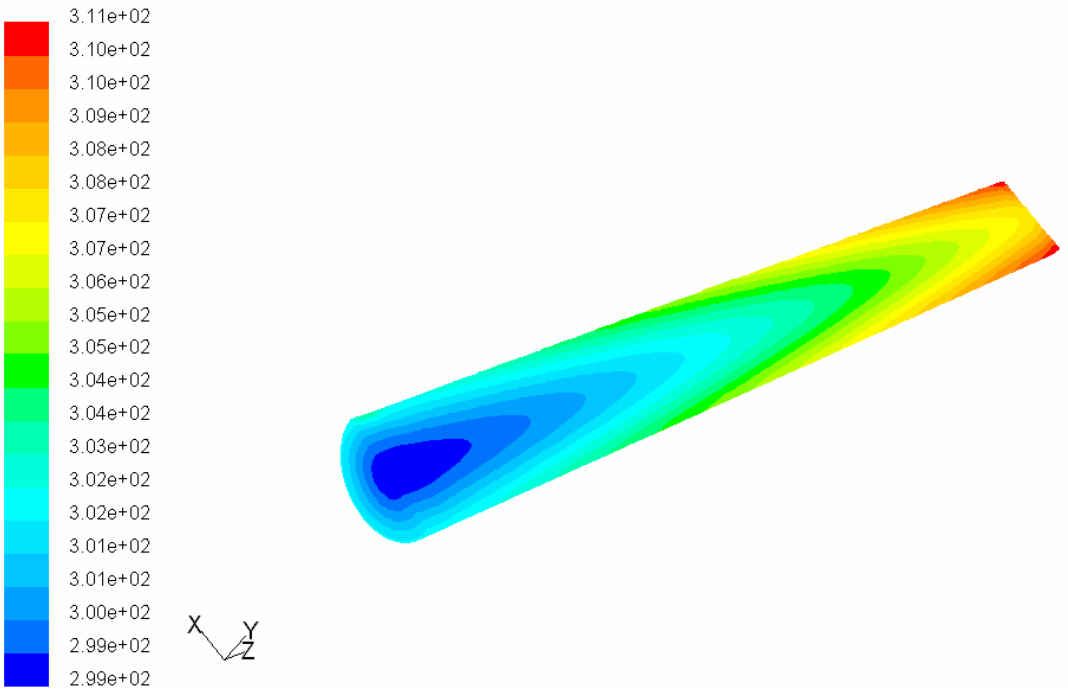

Fig.4.10 Temperature Contour of the circular duct at Re=50

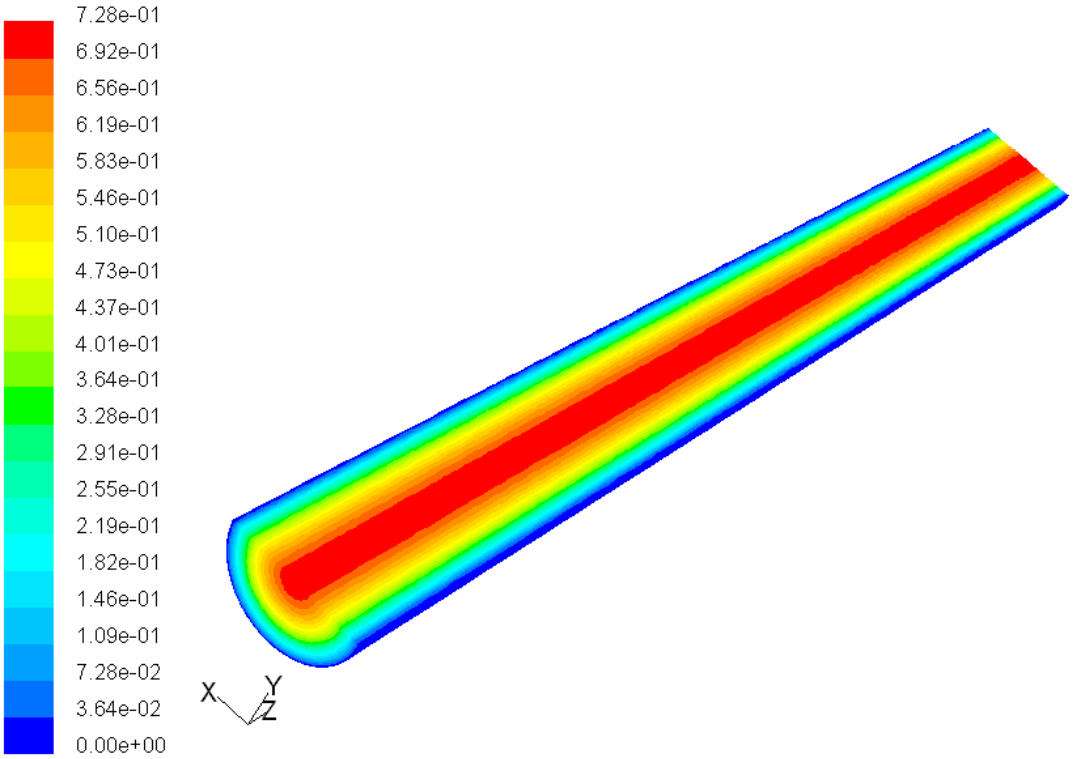

Fig.4.11 Velocity Contour in the circular duct at Re=50

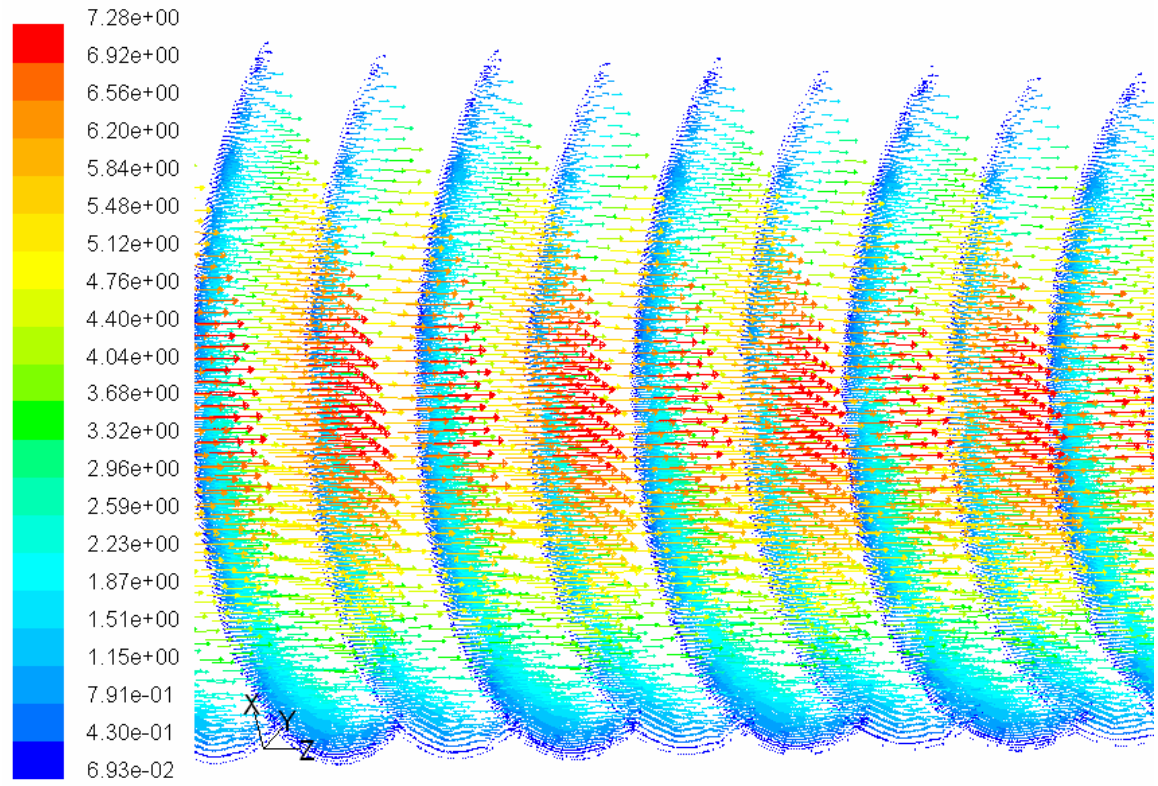

Fig.4.12 Velocity vectors at Re=500 in the circular duct

Computation of Friction Factor (f) and Colburn Factor(j)

$$T_w = 1/A\int T dA \quad \text{.....(4.10)}$$

Area weighted average wall temperature has been taken for calculating local nusselt number which is same for all sections after the flow is hydrodynamically and thermally developed.

$$T_f(x) = \left[\iint |u| T(x,y,z) dydz / \iint |u| dydz\right] \quad \text{.....(4.11)}$$

Bulk mean temperature of the fluid is being taken from the mass weighted average temperature from the FLUENT directly.

Nusselt number is calculated from the following relation.

$$Nu = q/T_w - T_f \quad \text{.....(4.12)}$$

Then, Colburn factor, $j = Nu/\mathrm{Re}\,\mathrm{Pr}^{1/3}$ .....(4.13)

Where Pr=Prandtl number calculated from the thermo physical properties is 0.744

Then Friction factor, $f = d_h \Delta p / 2\rho l w_m^2$ ……(4.14)

Where $\Delta p / l$ = Pressure gradient over the length of the duct.

$w_m = 1/A \int V dA$, the area weighted average velocity calculated from FLUENT directly.

Goodness factor=j/f has been calculated to study the relative surface area compactness.

Table 4.5 Calculation of Fanning friction factor and Colburn factor in a circular duct (3D analysis)

	Re	Wm	ΔP	f	Nu	J	j/f
dh=2	50	0.3651	52.2427	0.3199	4.768	0.1052	0.328853
	100	0.7302	104.4849	0.1599	4.556	0.0503	0.314572
	200	1.4605	208.9673	0.0799	4.501	0.0248	0.310388
	300	2.1907	313.4458	0.0533	4.477	0.0164	0.307692
	400	2.9210353	417.9186	0.0399	4.467	0.0123	0.308271
	500	3.6512	522.3871	0.0319	4.461	0.0098	0.30721

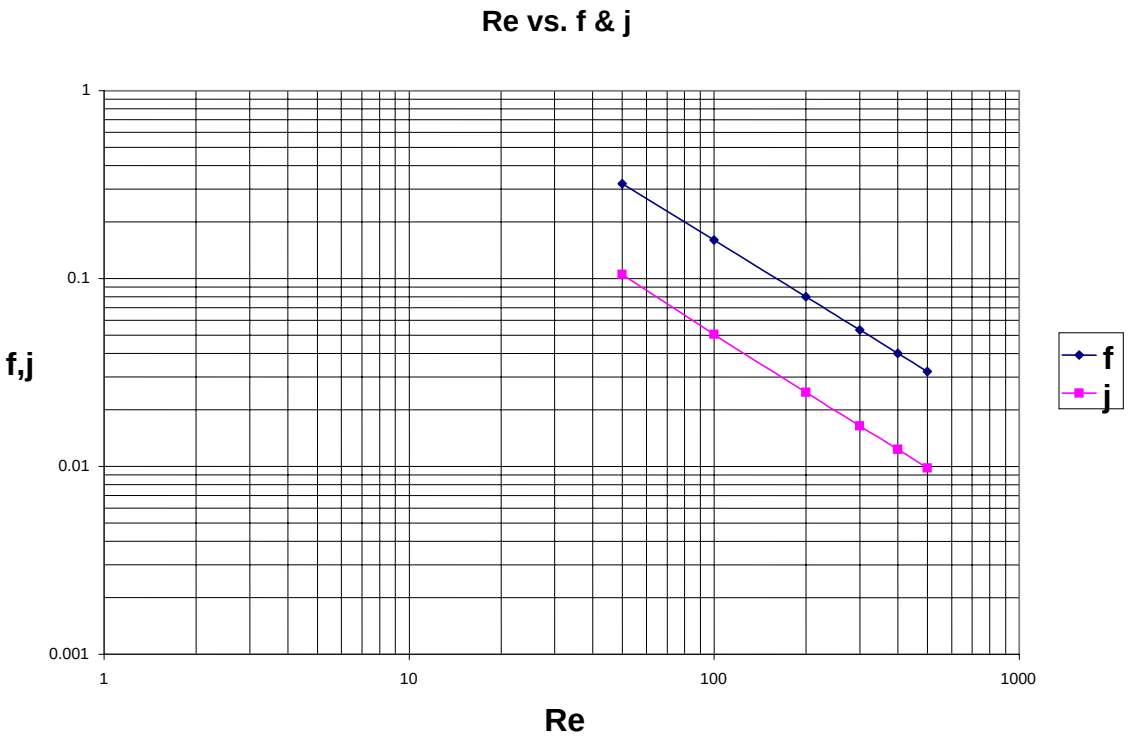

Fig.4.13 Plot of Re vs. f & Re vs. j

Generation Of Heat Transfer and Flow Friction Correlations

The graph between Reynolds number vs. Friction factor and Colburn factor has been plotted. Here it can be seen that the friction factor as well as Colburn factor decrease with increasing Reynolds Number.

The correlation for the given geometry can be found from the following relation.

f or $j=C\ Re^{K}$ .....(4.15)

Firstly the different results have been tabulated .Then the graphs between friction factor and Coburn factor corresponding to different Reynolds number are plotted for the duct.

Then C and K value have been found from the graphs by fitting to a power law.

Table 4.6 Correlation between Reynolds number and friction factor and Colburn factor

Geometry	Correlation	
Dh=2e-03	$f = 16.066 Re^{-1.0011}$	$R^2=1$
	$j = 5.8091\ Re^{-1.0285}$	$R^2=0.9999$

4.2.5 DISCUSSIONS

The friction factor decreases with increase in Reynolds number. The same also happens in case of colburn factor. It is found that the friction factor matches with the correlation f.Re=16 and Nusselt number closes matches with the value of 4.36 under constant heat flux condition..

Chapter 5

SEMIELLIPTICAL STRAIGHT DUCT (ENTRANCE REGION)

- **Introduction**
- **Computational Domain & Boundary Conditions**
- **Gambit & FLUENT Details**
- **Results**
- **Discussion**

5.1 INTRODUCTION

A semi elliptical duct has the cross section of semiellipse, which is defined as major axis of length, D=2mm and minor axis of length a.D. Here we have taken a shorter length duct i.e. 20 mm where the flow is not fully developed. Heat transfer and fluid friction characteristics have been studied.

5.2 COMPUTATIONAL DOMAIN & BOUNDARY CONDITIONS

Length of the duct=20mm

Major axis of the duct (D) =2mm

Minor axis of the duct=0.3x2=0.6mm

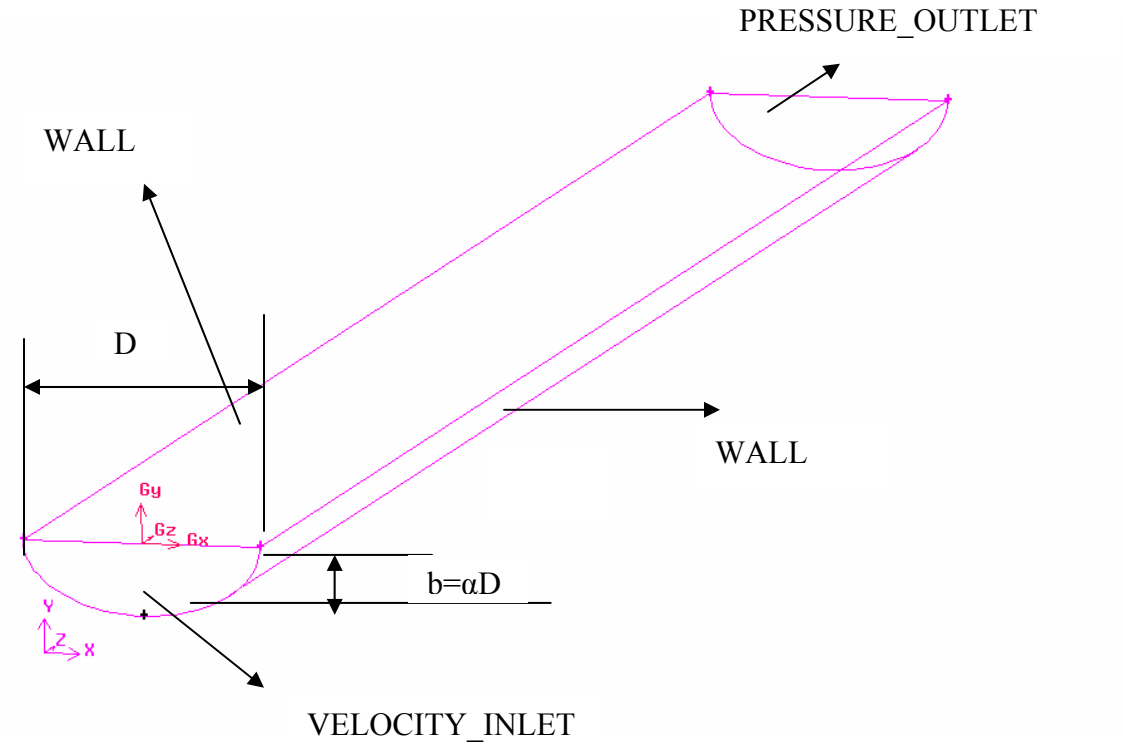

Fig.5.1 Computational domain of semi elliptical straight duct for analysis in the entrance Region

5.3 GAMBIT & FLUENT DETAILS

Meshing=80x60x50

No. of Cells=56350

Specification of Boundary Layer:

First row height=1e-05

Total no. of rows=4

Quadrilateral pave meshing for the face is done. Then the Cooper Hex/wedge meshing has been used for the Volume meshing. The SIMPLE algorithms evaluate the coupling between pressure and velocity. The under-relaxation factor momentum and energy has been 0.7 and 1 respectively. The second order upwind scheme has been taken for the descretisation of momentum and energy equation. The 3-D double precision solver has been chosen. Convergence criteria have been taken as 1e-06 for continuity and energy. Following grid independent test has been done taking different grid sizes. Nusselt Number variation has been observed.

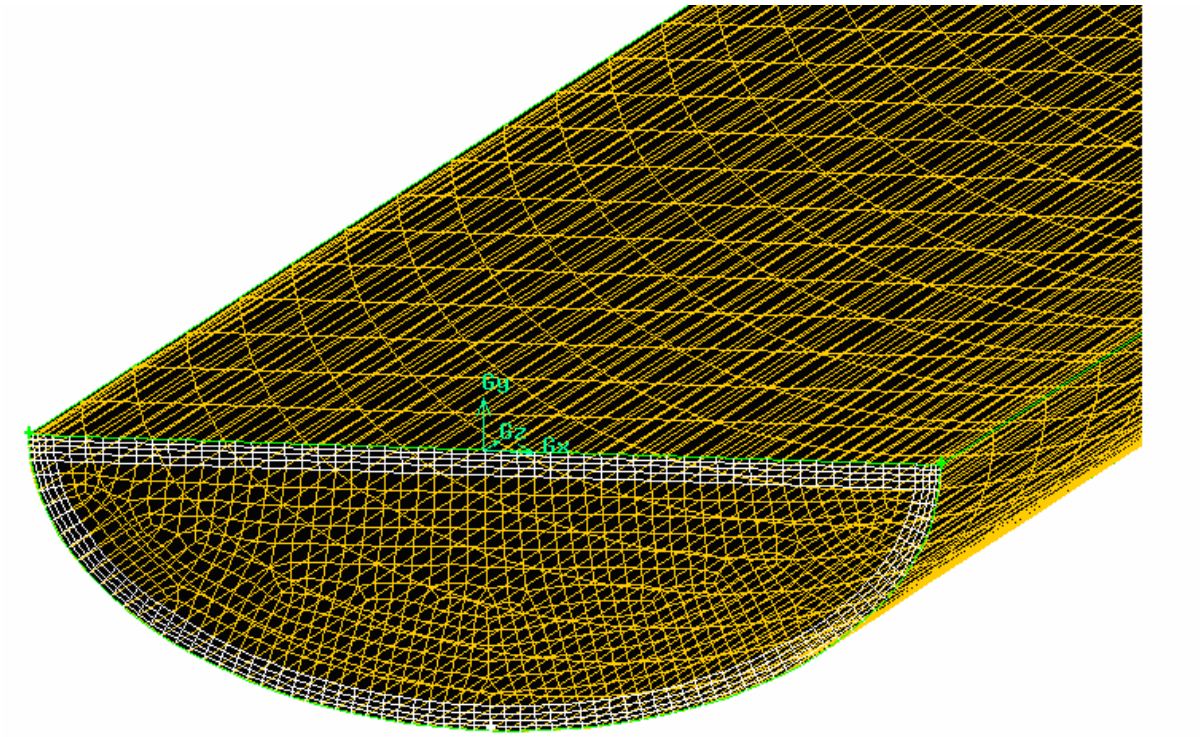

Fig.5.2 Meshing of the semi elliptical straight duct for analysis of heat transfer in the entrance region

5.3.1 Grid Independence Test, Re=50

Table 5.1 Grid Independent Test

a = 0.3

Grid size	Nu
80x60x50	Nu=2.491
120x90x50	Nu=2.509

a = 0.4

Grid Size	Nu
40 x 30 x 50	2.951
80 x 60 x 50	2.978
120 x 90 x 50	2.994

a = 0.5

Grid Size	Nu
40 x 30 x 50	3.244
80 x 60 x 50	3.260

a = 0.6

Grid Size	Nu
40 x 30 x 50	3.405
80 x 60 x 50	3.413

a = 0.7

Grid Size	Nu
40 x 30 x 50	3.483
80 x 60 x 50	3.483
120 x 90 x 50	3.496
40 x 30 x 400	3.214

5.4 RESULTS

5.4.1 Velocity & Temperature Fields

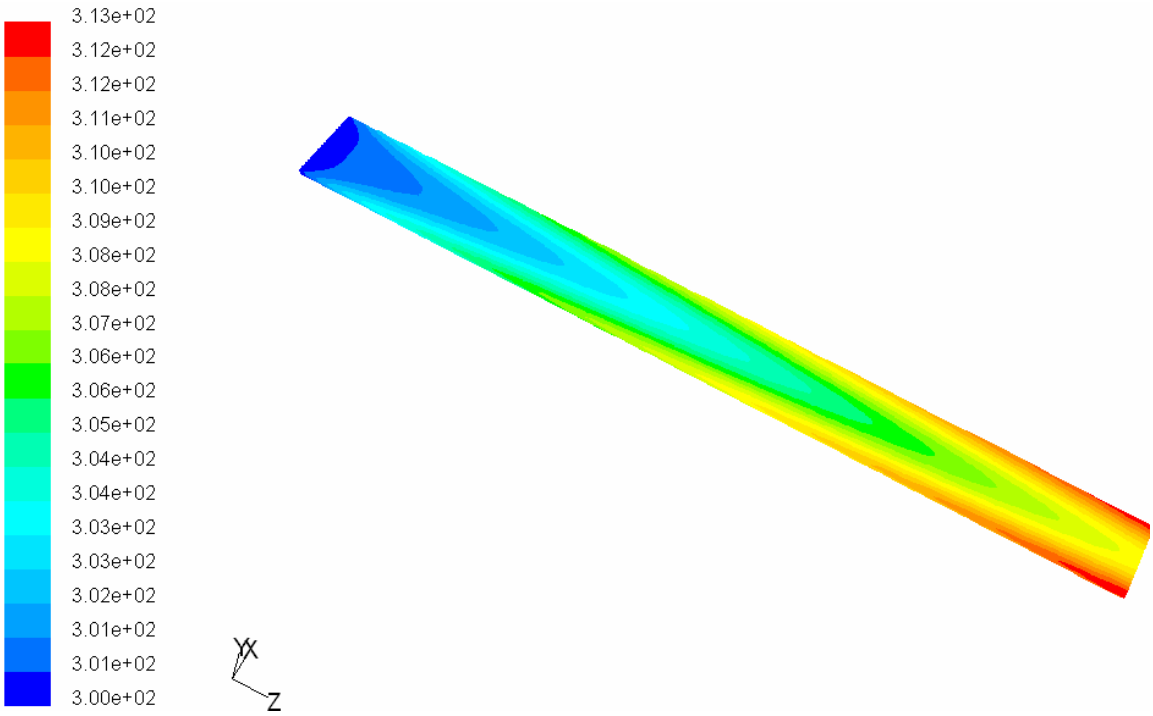

Fig. 5.3 Temperature contour in a semi-elliptical straight duct where a=0.3,Re=50

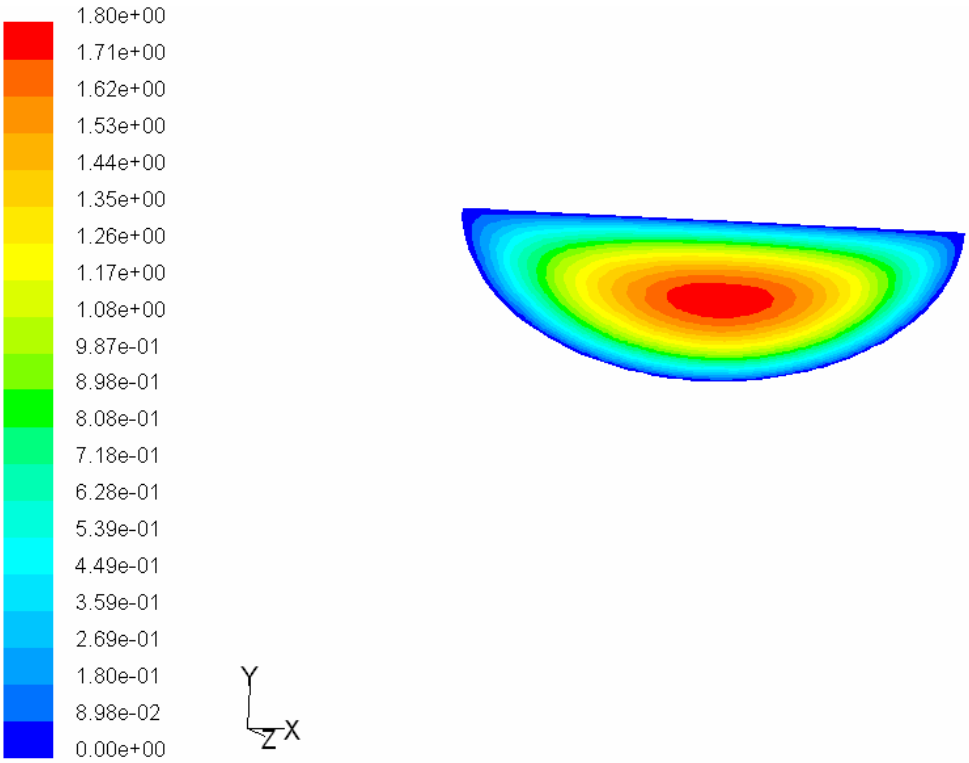

Fig.5.4 Velocity contour at outlet for a semi elliptical straight duct where a=0.3 & Re=50

5.4.2 Computation of Friction Factor (f) and Colburn Factor (j)

$$T_w = 1/A\int TdA \quad \text{..... (5.1)}$$

Area weighted average wall temperature has been taken for calculating local nusselt number which is same for all sections after the flow is hydro dynamically and thermally developed.

$$T_f(x) = \left[\iint |u|T(x,y,z)dydz / \iint |u|dydz\right] \quad \text{..... (5.2)}$$

Bulk mean temperature of the fluid is being taken from the mass weighted average temperature from the FLUENT directly.

Nusselt number is calculated from the following relation.

$$Nu = q/T_w - T_f \quad \text{.....(5.3)}$$

Then, Colburn factor, $j = Nu/\mathrm{Re}\,\mathrm{Pr}^{1/3}$ .....(5.4)

Where Pr=Prandtl number calculated from the thermo physical properties is 0.744

Then Friction factor, $f = d_h \Delta p / 2\rho l w_m^{\ 2}$ ..... (5.5)

Where $\Delta p / l$ = Pressure gradient over the length of the duct.

$w_m = 1/A\int VdA$, the area weighted average velocity calculated from FLUENT directly.

Goodness factor=j/f has been calculated to study the relative surface area compactness

Table 5.2 Calculation of Fanning friction factor and Colburn factor

	Re	Wm	ΔP	f	Nu	J	j/f
a=0.3 Dh=0.82115e-03	50	0.8895	1.5687	0.3323	2.491	0.0559	0.168221
	100	1.7788	3.1383	0.1662	2.538	0.02849	0.17142
	200	3.5577	6.3176	0.0836	2.609	0.0146	0.174641
	300	5.33664	9.6108	0.0565	2.865	0.0107	0.189381
	400	7.1155	13.0423	0.0432	3.107	0.0087	0.201389
	500	8.8944	16.6188	0.0352	3.129	0.0074	0.210227
a=0.4 Dh=1.0374e-03	50	0.704	0.7564	0.3231	2.978	0.0668	0.206747
	100	1.408	1.5137	0.1616	2.847	0.0319	0.197401
	200	2.816	3.0628	0.0817	2.990	0.0167	0.204406
	300	4.2241	4.6994	0.0557	3.224	0.0120	0.21544
	400	5.632	6.4361	0.0429	3.457	0.0097	0.226107
	500	7.04	8.2740	0.0353	3.676	0.0082	0.232295
a=0.5 Dh=1.22194e-03	50	0.5977	0.4502	0.3142	3.26	0.0732	0.232973
	100	1.1954	0.9013	0.1573	3.113	0.0349	0.221869
	200	2.3908	1.834	0.08	3.221	0.018	0.225
	300	3.5862	2.84	0.05506	3.438	0.0128	0.023247
	400	4.7817	3.9259	0.04281	3.665	0.0103	0.02406
	500	5.9771	5.0889	0.0355	3.885	0.0087	0.24507
a=0.6 Dh=1.3783e-03	50	0.5299	0.3062	0.3068	3.413	0.0766	0.249674
	100	1.0598	0.6133	0.1536	3.266	0.0366	0.238281
	200	2.1196	1.2557	0.0786	3.358	0.0188	0.239186
	300	3.1794	1.9626	0.0546	3.567	0.0133	0.24359
	400	4.2392	2.7358	0.0428	3.796	0.0106	0.247664
	500	5.299	3.5697	0.0357	4.021	0.009	0.252101
a=0.7 Dh=1.5108e-03	50	0.4834	0.2254	0.2974	3.214	0.065	0.218561
	100	0.9668	0.4516	0.1489	3.218	0.0361	0.242445
	200	1.9337	0.9329	0.0769	3.375	0.0189	0.245774
	300	2.9005	1.4748	0.0540	3.613	0.0135	0.25
	400	3.8674	2.0753	0.0427	3.866	0.0108	0.252927
	500	4.8342	2.7280	0.036	4.114	0.0092	0.255556

5.4.3 Role Of Reynolds Number and Geometric Parameters

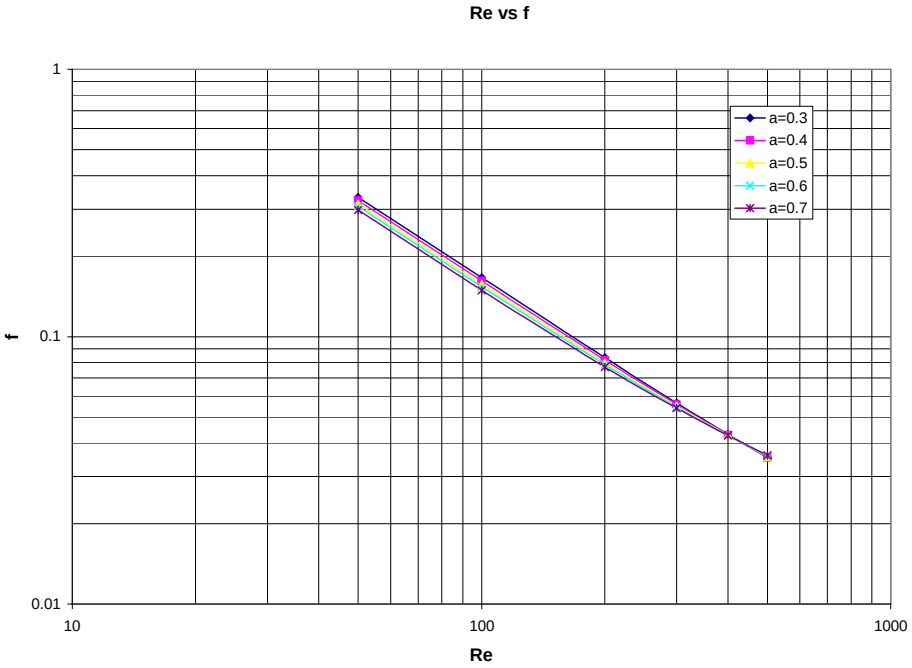

Fig.5.5 Variation of fanning friction factor with Reynolds number in a semi elliptical Straight duct (Entrance Region)

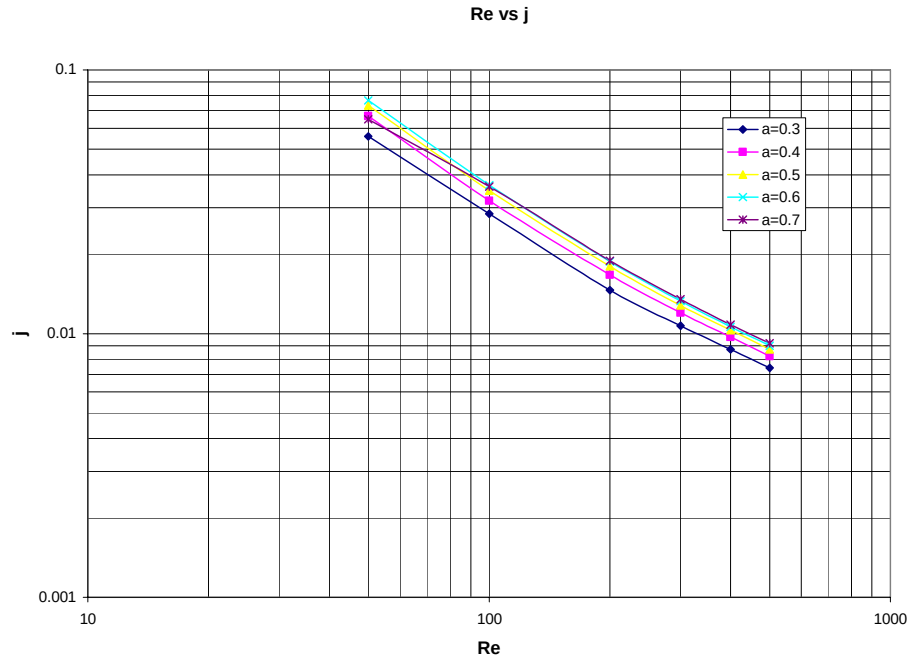

Fig.5.6 Variation of Colburn factor with Reynolds number in a semi elliptical Straight (Entrance Region)

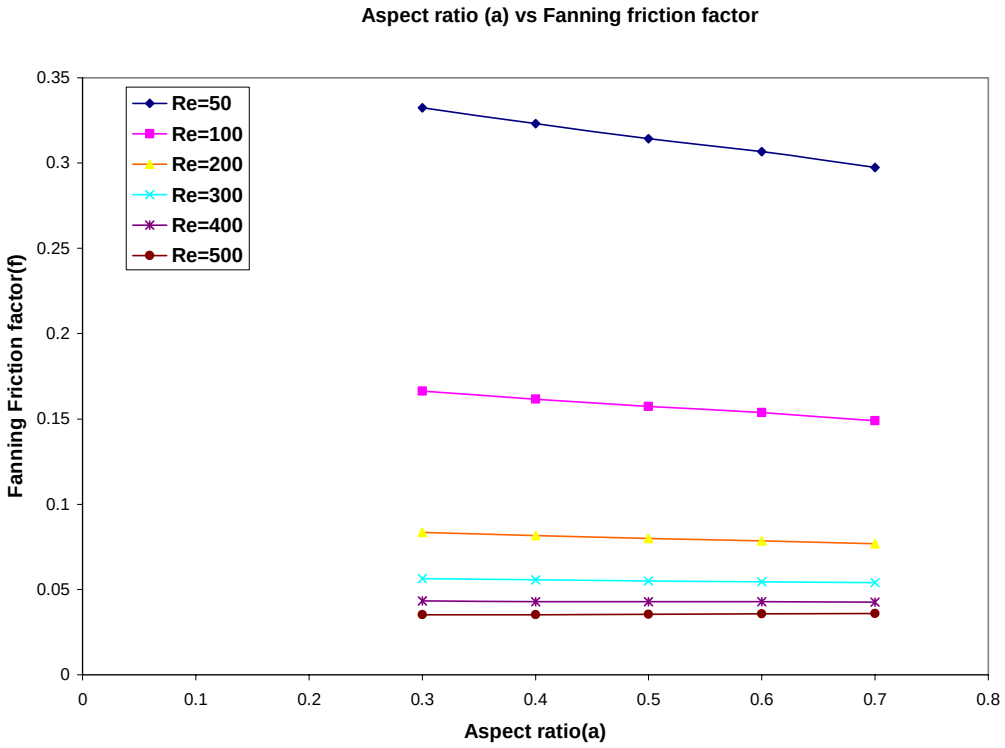

Fig.5.7 Variation of fanning friction factor with aspect ratio at different Re

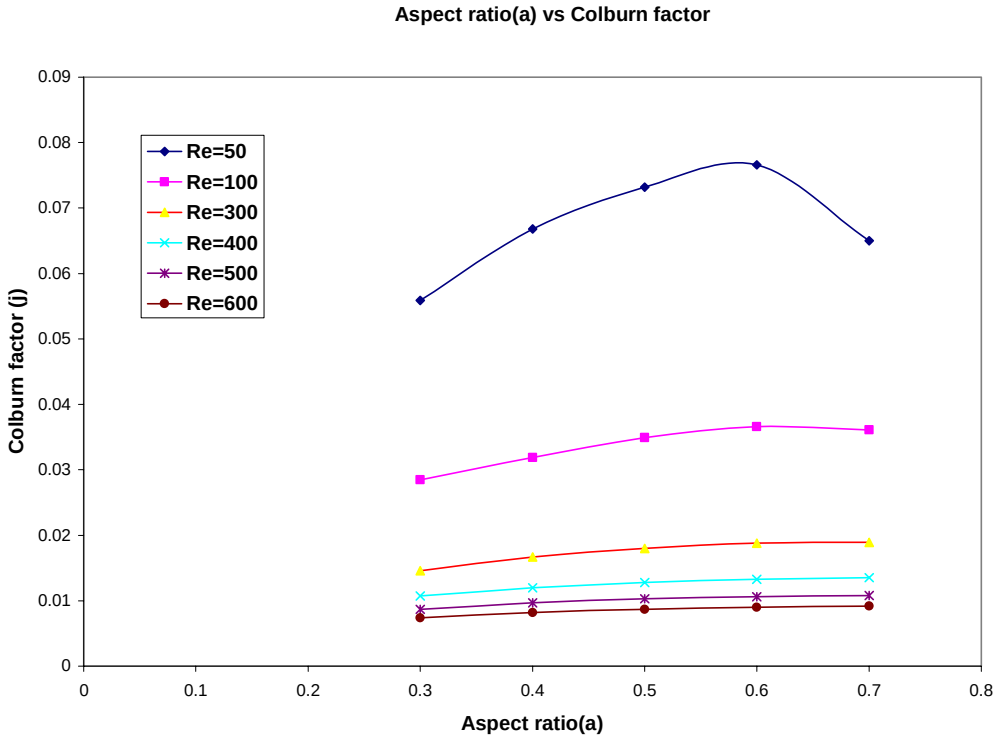

Fig.5.8 Variation of Colburn factor with aspect ratio at different Re

5.4.4 Generation of Heat Transfer and Flow Friction Correlations

The correlation for the given geometry can be found from the following relation.

f or $j=C\ Re^{K}$ …….(5.6)

Firstly the different results have been tabulated .Then the graphs between friction factor and Coburn factor corresponding to different Reynolds number are plotted for various geometry based on different aspect ratios.

Then C and K value have been found from the graphs by fitting to a power law.

Table 5.3 Correlation for semi elliptical straight duct

Geometry	Correlation	
a=0.3	$f=15.024\ Re^{-0.977}$	$R^2=0.9998$
	$j=1.6613\ Re^{-0.879}$	$R^2=0.9958$
a=0.4	$f=13.789\ Re^{-0.9638}$	$R^2=0.9996$
	$j=2.1769Re^{-0.9063}$	$R^2=0.9955$
a=0.5	$f=12.631\ Re^{-0.9499}$	$R^2=0.9992$
	$j=2.5574\ Re^{-0.9232}$	$R^2=0.9961$
a=0.6	$f=11.638\ Re^{-0.9366}$	$R^2=0.9989$
	$j=2.7491\ Re^{-0.9292}$	$R^2=0.9964$
a=0.7	$f=10.504\ Re^{-0.92}$	$R^2=0.9983$
	$j=1.8527\ Re^{-0.8583}$	$R^2=0.9989$

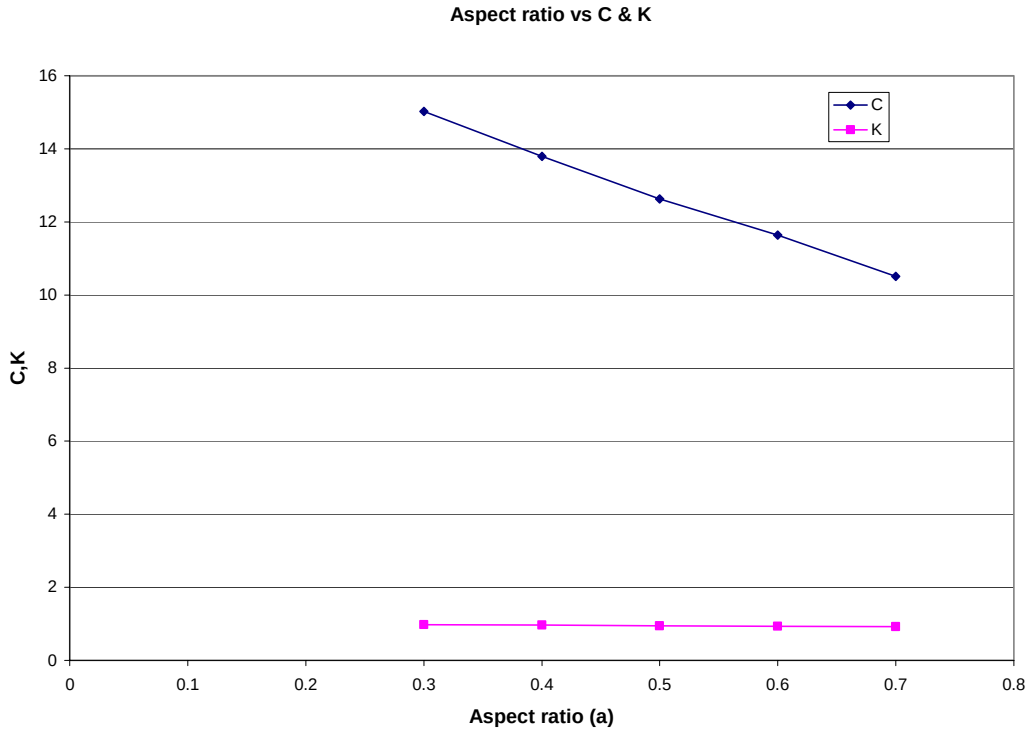

Fig.5.9 Variation of C & K with aspect ratio in a semi elliptical straight duct for Fanning friction factor (f) analysis

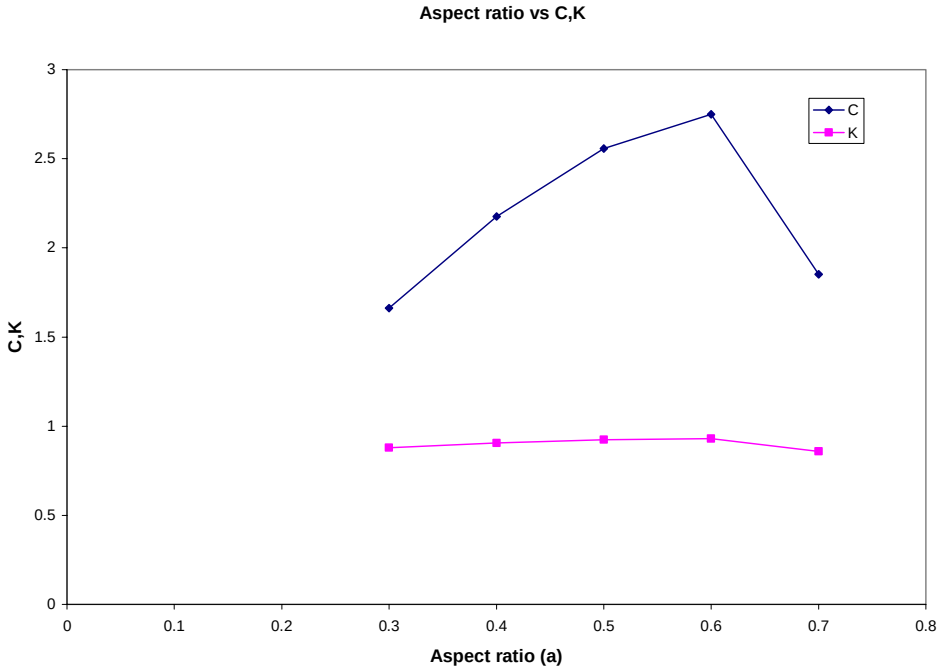

Fig.5.10 Variation of C & K with aspect ratio in a semi elliptical straight duct for Colburn Factor analysis

The final correlation was found using the regression.

$$f = 11.934\ Re^{-0.948}(a)^{-0.067}$$

$$R^2 = 1$$

$$j = 2.785\ Re^{-0.908}\ (a)^{0.292}$$

$$R^2 = 1$$

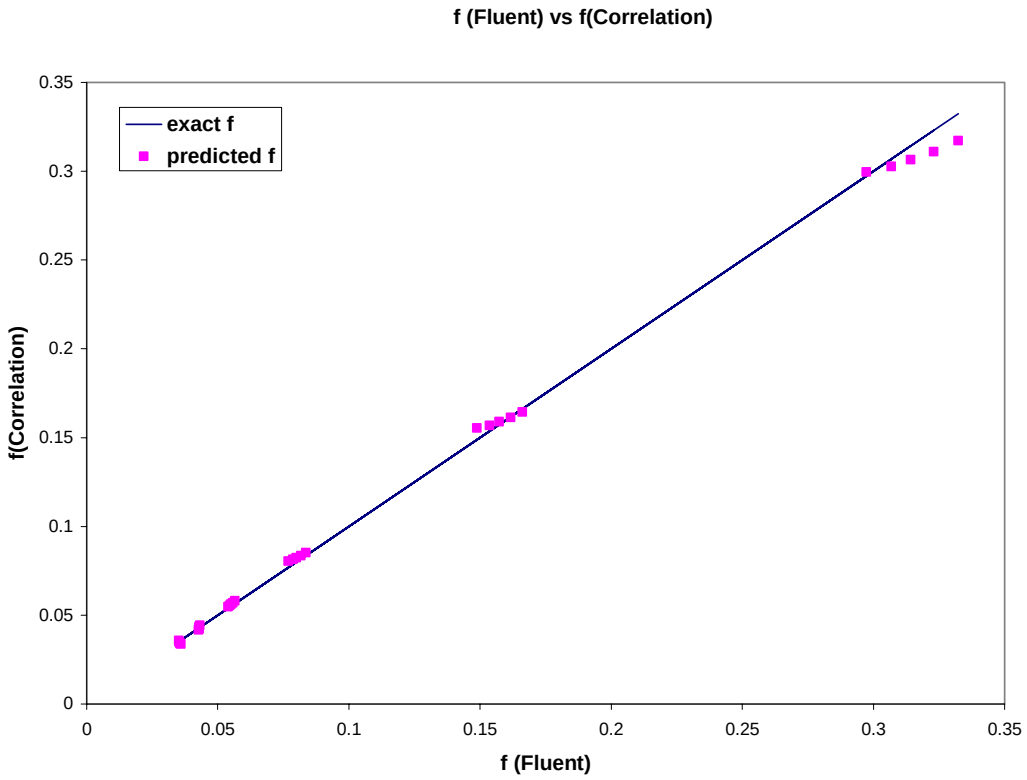

Fig.5.11 shows the comparison of f from fluent and f from correlation
Black line represents the exact f

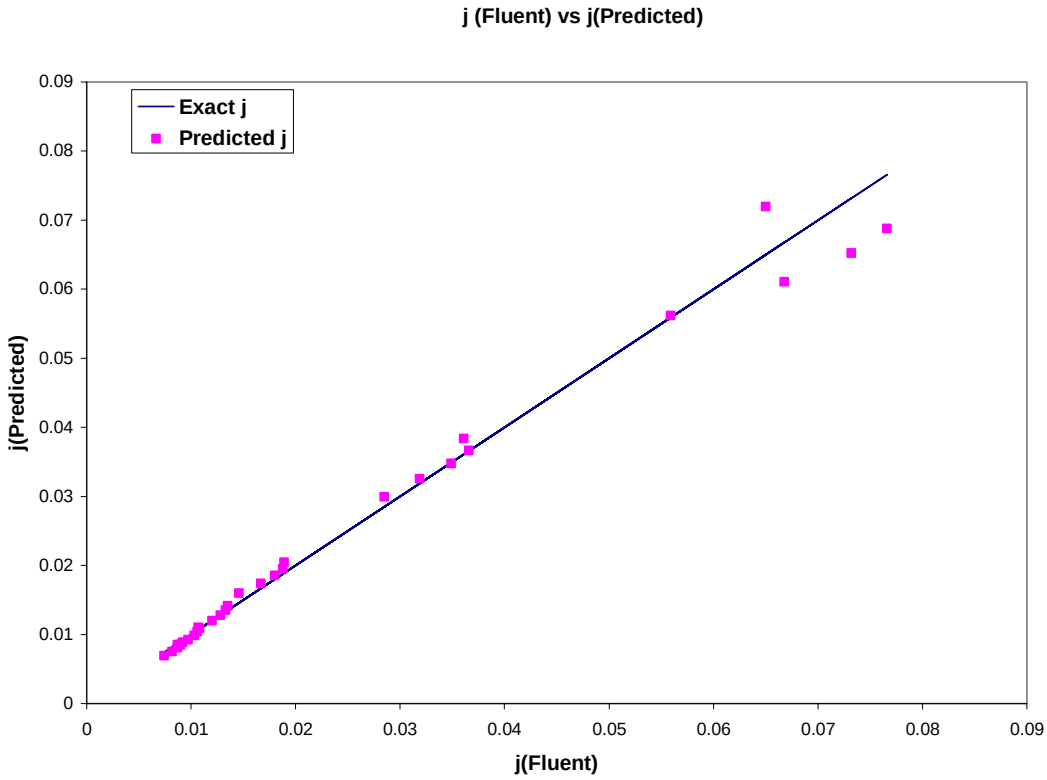

Fig.5.12 shows the comparison of j from fluent and j from correlation Black line represents the exact j.

5.5 DISCUSSIONS

(1) Fig. 5.5 shows that Fanning friction factor decreases with increase in Reynolds Number for all aspect ratios.

(2) From fig.5.6, in the Reynolds number range 50-100, aspect ratio of 0.6 gives the maximum Coburn factor.

(3) From fig.5.7, it is found that the Fanning friction factor becomes independent of the aspect ratio as the Reynolds number increases.

(4) From fig. 5.8, it is seen that Colburn factor also follow the same trend as Fanning friction factor.

(5) The indices k is independent of the aspect ratio for both the correlation for Fanning friction factor and Coburn factor.(from Fig.5.9,5.10)

(6) For fanning factor correlation ,the value of c increases with decrease in aspect ratio(from

fig.5.9)

(7) For Colburn factor correlation, the value of indices c first increase up to aspect ratio=0.6 and then decreases.(from fig.5.10)

(8) From fig. 5.11 and 5.12, it is clear that the predicted correlation is correct to justify the value from FLUENT as the exact line shown by black line passes through most of the points.

Chapter6

SEMIELLIPTICAL STRAIGHT DUCT

(FULLY DEVELOPED FLOW)

- **Introduction**
- **Computational Domain & Boundary Conditions**
- **Gambit & FLUENT Details**
- **Results**
- **Discussion**

6.1 INTRODUCTION

The flow and temperature fields under the assumption of fully developed flow, was studied which means that the flow pattern repeats itself from module to module. In such circumstances it is sufficient to analyze only one segment (module) of the geometry(Patankar,1977).The pressure field in the fully developed region can be expressed (Patankar,1977) as the linear combination of the local pressure, and the overall pressure drop

$P(x,y,z)=p(x,y,\tau)+\beta x$,

Where the local component p(x,y,z) repeats itself from module to module. The overall pressure gradient ß is introduced in the momentum equation as the source term f in the stream wise direction f=ß.i, where ß is the prescribed pressure drop, and i is unit vector in the stream wise direction.So,one module is taken for simulation.

A no-slip boundary condition for velocity is enforced on the walls of the channels, and a periodic boundary condition is applied at the inflow and outflow of the computational domain. For the temperature field, boundary condition of constant heat flux is taken for the wall.

6.2 COMPUTATIONAL DOMAIN& BOUNDARY CONDITIONS

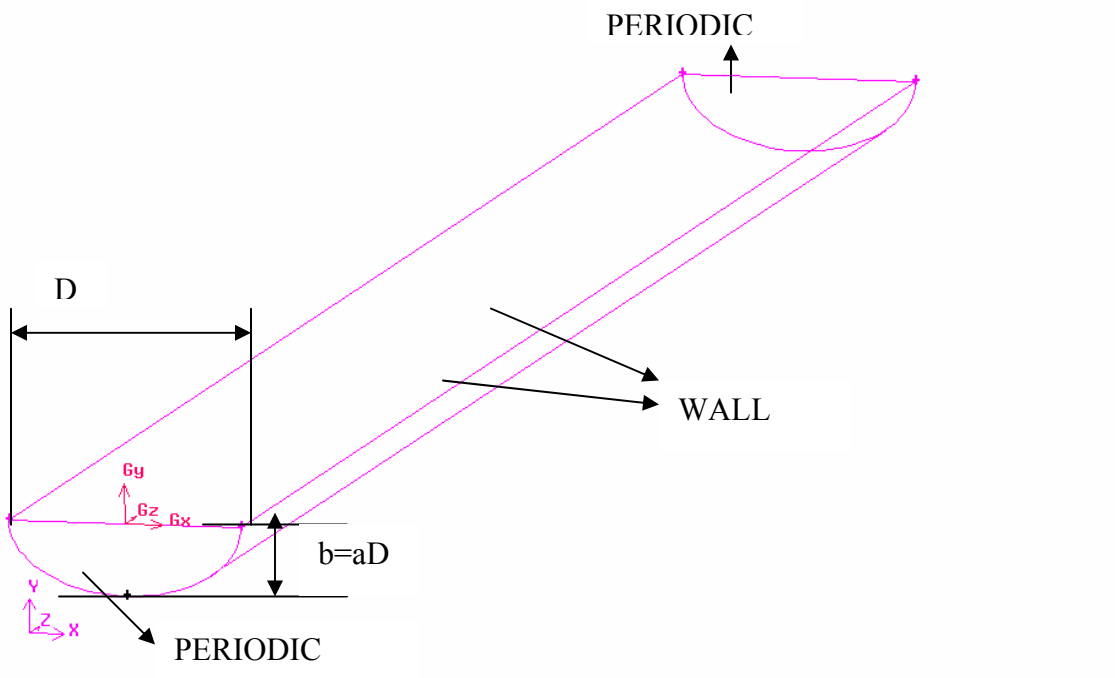

Fig.6.1 Computational domain of semielliptical straight showing boundary conditions

6.3 GAMBIT & FLUENT DETAILS

Length of the duct=20mm

Major axis of the duct(D)=2mm

Minor axis of the duct=0.3x2=0.6mm

Quadrilateral pave meshing for the face is done. Then the Cooper Hex/wedge meshing has been used for the Volume meshing. The SIMPLE algorithms evaluate the coupling between pressure and velocity. The under-relaxation factor momentum and energy has been 0.7 and 1 respectively. The second order upwind scheme has been taken for the descretisation of momentum and energy equation. The 3-D double precision solver has been chosen.

The following thermo-physical properties of air have been taken.

Table 6.1 Thermo physical properties of air

Fluid -air
Density=1.225 kg/m^3
Thermal conductivity=0.0242 w/m-k
Viscosity=1.7894e-05kg/m-s
Specific heat at constant pressure=1006.43 J/kg-k

Convergence criteria have been taken as 1e-06 for continuity and energy. Following grid independent test has been done taking different grid sizes. Nusselt Number variation has been observed.

For a fixed Reynolds number, mass flow rate is calculated according to the following relation.

$\dot{m} = A\mu \mathrm{Re}/d_h$ ……(6.1)

Where $\dot{m}$ =mass flow rate

Mass flow rate is being taken as input.

Air temperature at inlet is set at 300K.A constant heat flux(here 100w/m^2) has been provided to the wall as shown as the above fig.

Hydraulic diameter d_h = 4 x area/perimeter

Area= [π x D x (b)]/2……..(6.2)

Perimeter is being taken as approximation i.e. perimeter=$\pi\sqrt{0.5}$ (D^2+b^2) + 2D

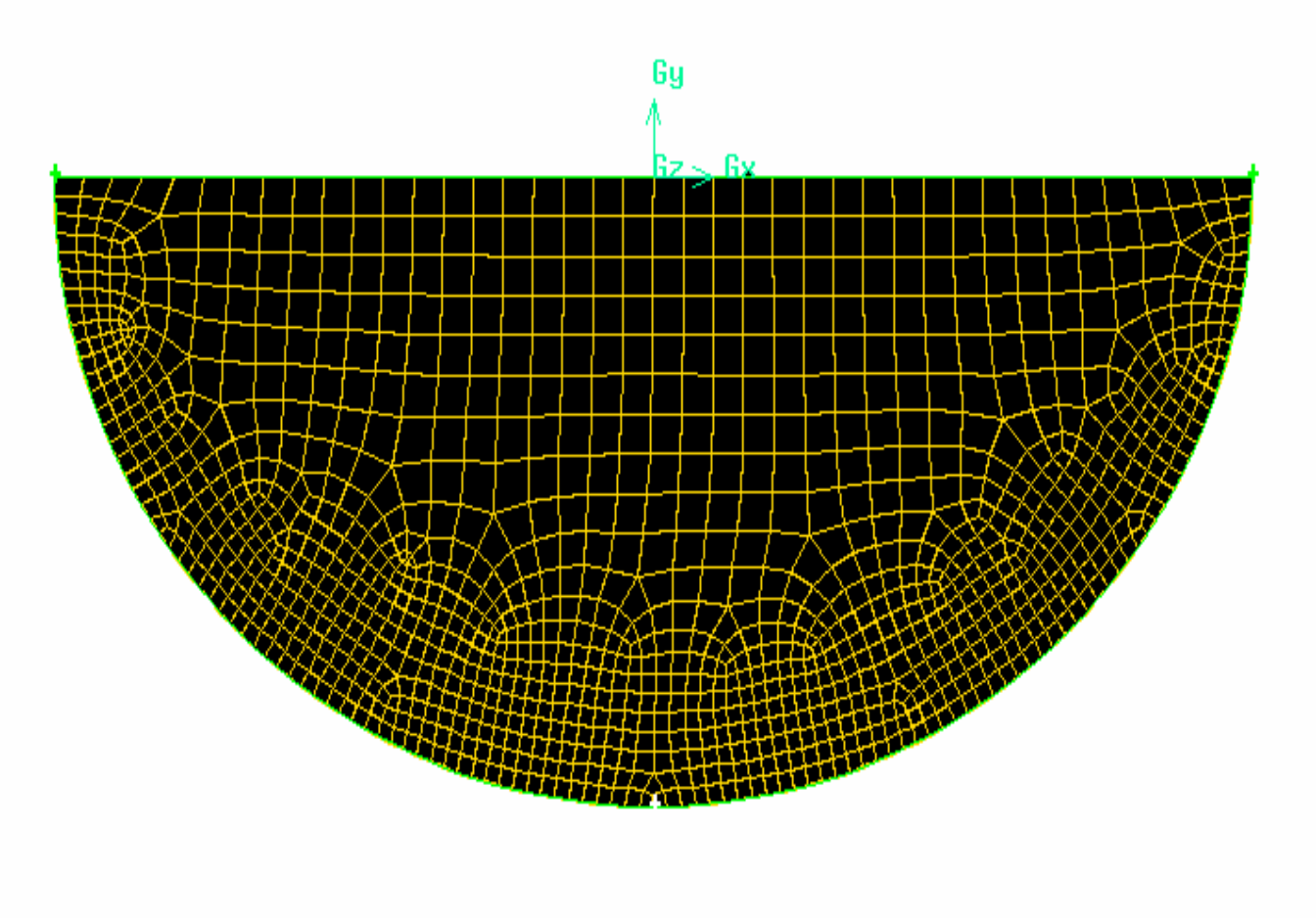

Fig 6.2 Meshing of the semielliptical straight for analysis of heat transfer characteristics in fully developed flow

6.3.1 Grid Independence Test

120x40x30 is the selected mesh size

Table 6.2 Grid Independent Test Re=500,a=0.5

140x30x30	No. of cells=38940	Nu=3.1365	Error from previous value
120x40x30	No. of cells=40830	Nu=3.1366	0.003%
120x60x30	No. of cells=57330	Nu=3.108	0.9%
120x60x40	No. of cells=81660	Nu=3.104	0.128%

6.4 RESULTS

6.4.1 Velocity & Temperature Fields

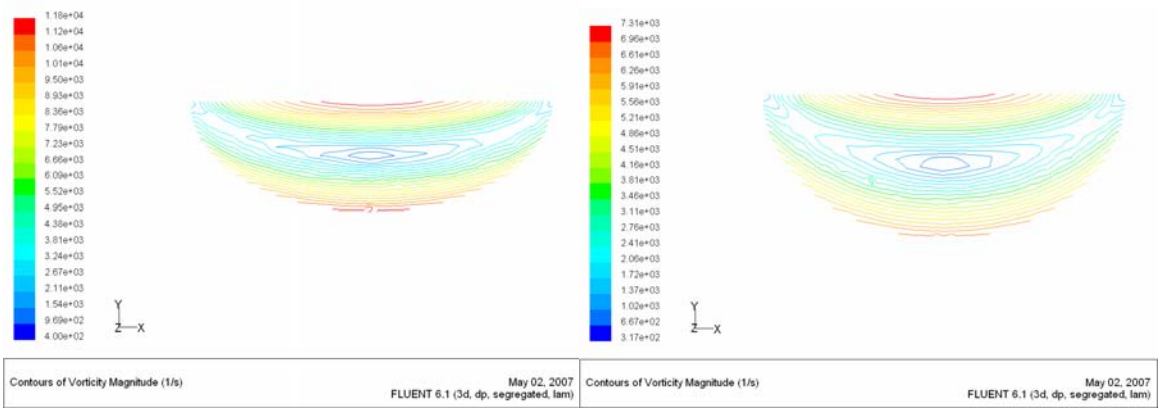

(a) (b)

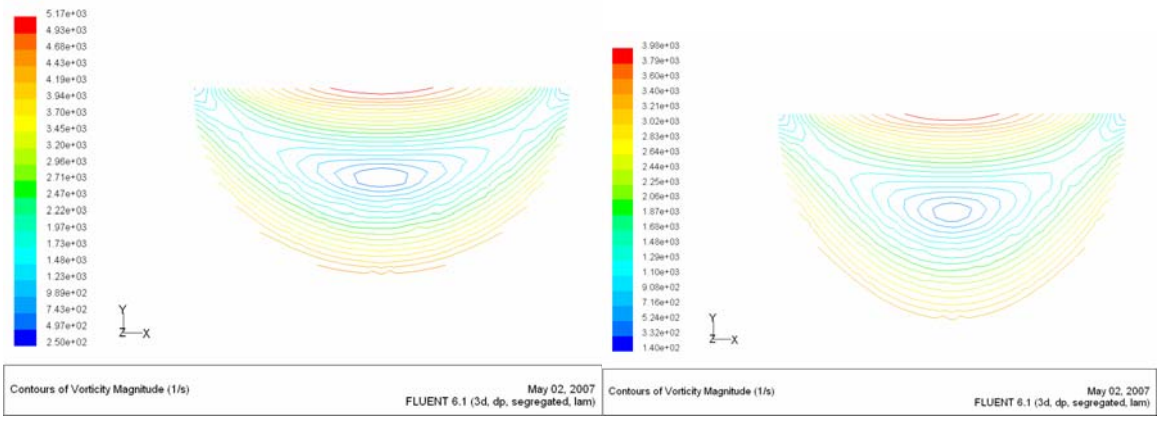

(c) (d)

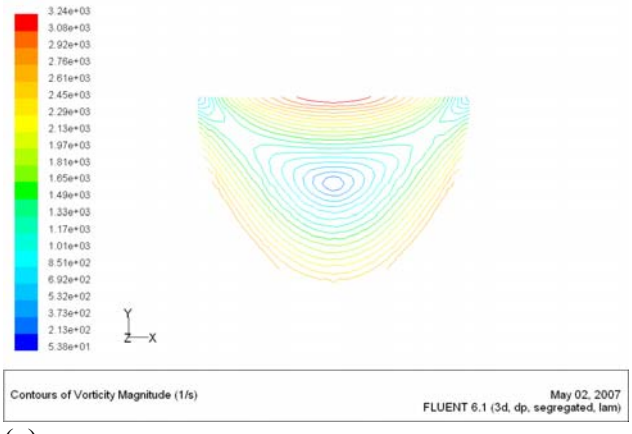

(e)

Fig 6.3 Contour of Vorticity at Re=50 (a) a=0.3(b) a=0.4(c) a=0.5 (d) a=0.6(e) a=0.7

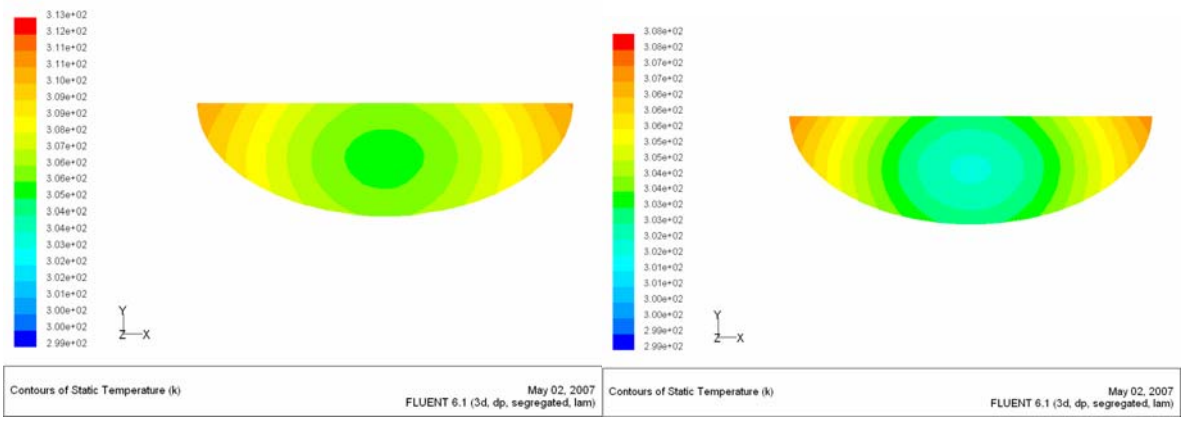

(a) (b)

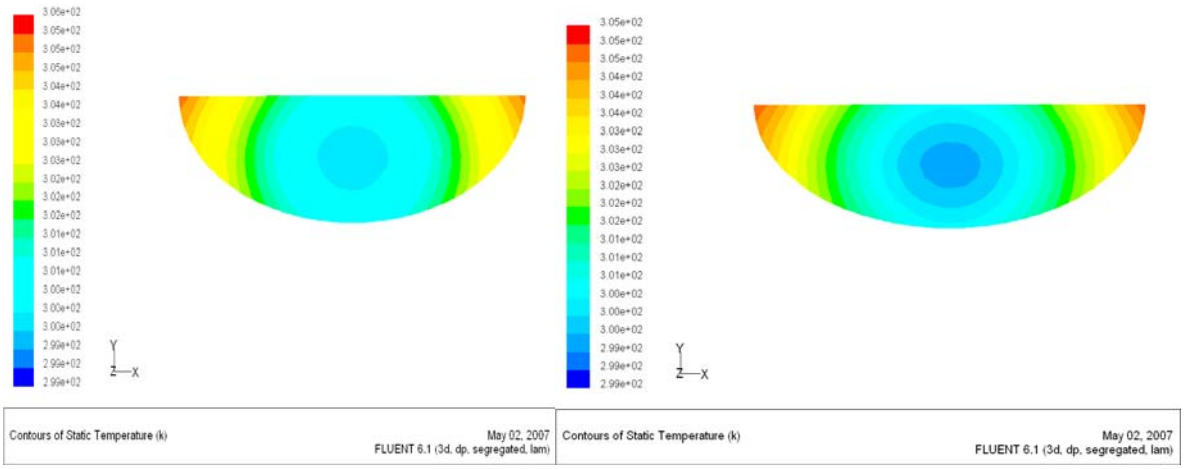

(c) (d)

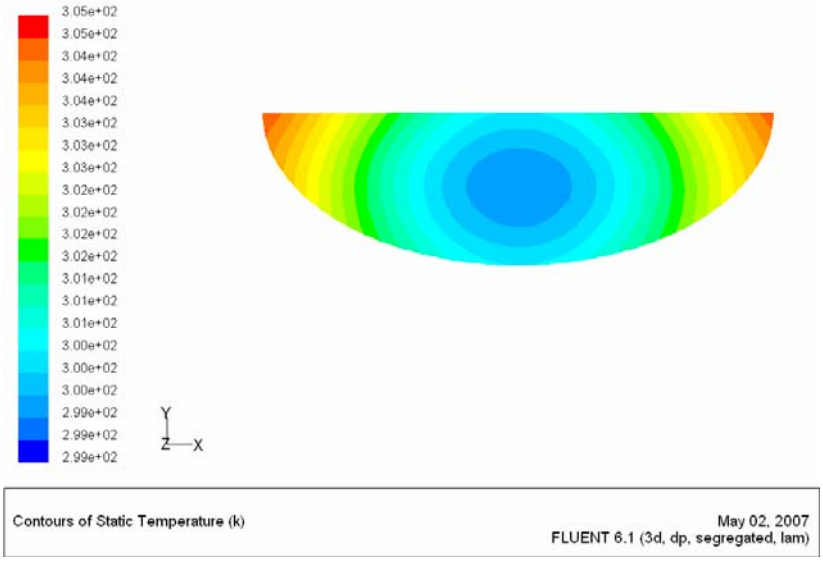

(e)

Fig, 6.4 Contour of Temperature in duct where α =0.3D (a) Re=50 (b) Re=100 (c) Re=200(d) Re=300(e) Re=400(f) Re=500

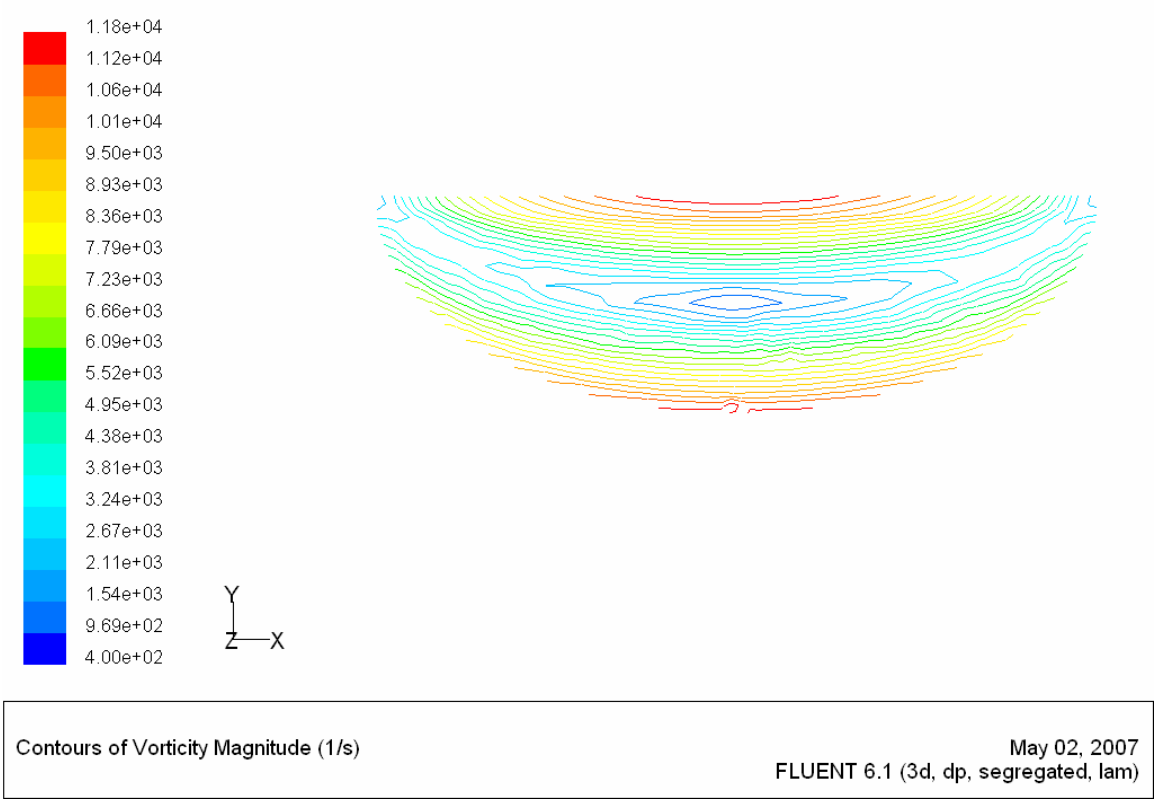
1.18e+04
1.12e+04
1.06e+04
1.01e+04
9.50e+03
8.93e+03
8.36e+03
7.79e+03
7.23e+03
6.66e+03
6.09e+03
5.52e+03
4.95e+03
4.38e+03
3.81e+03
3.24e+03
2.67e+03
2.11e+03
1.54e+03
9.69e+02
4.00e+02
Y
Z
X
Contours of Vorticity Magnitude (1/s)
May 02, 2007
FLUENT 6.1 (3d, dp, segregated, lam)

(a)

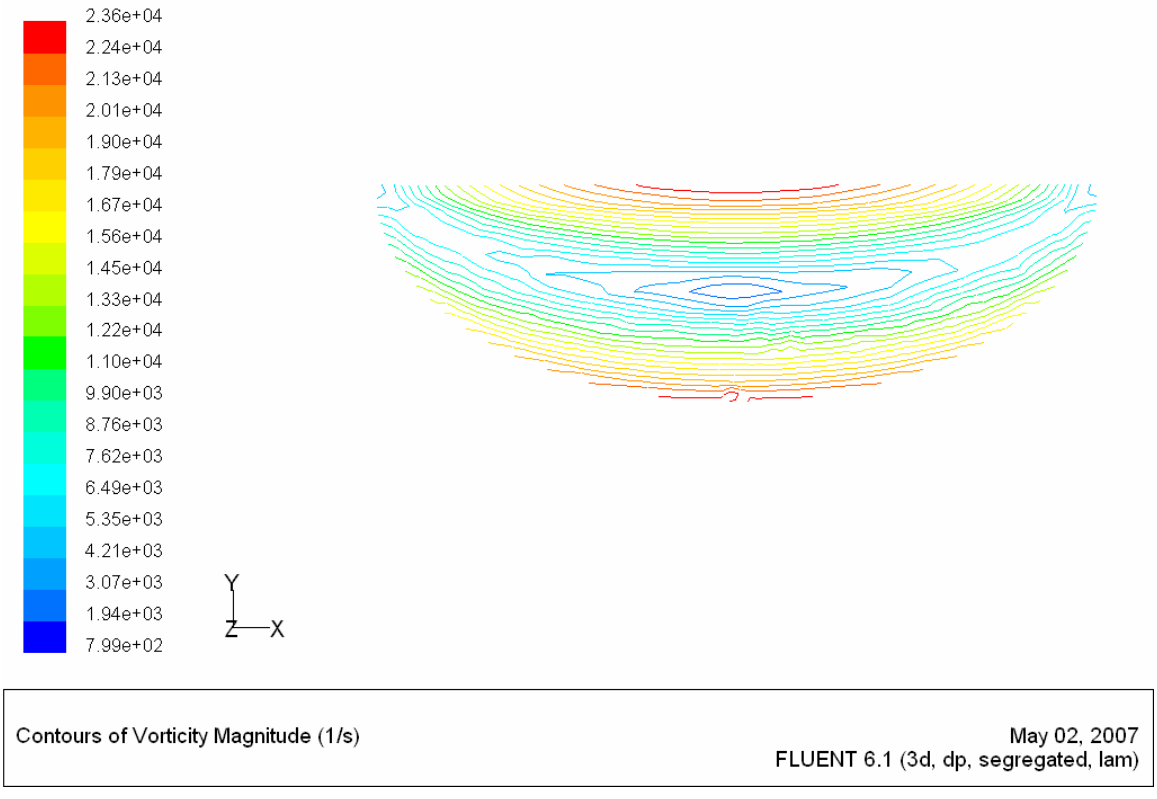
2.36e+04
2.24e+04
2.13e+04
2.01e+04
1.90e+04
1.79e+04
1.67e+04
1.56e+04
1.45e+04
1.33e+04
1.22e+04
1.10e+04
9.90e+03
8.76e+03
7.62e+03
6.49e+03
5.35e+03
4.21e+03
3.07e+03
1.94e+03
7.99e+02
Y
Z
X
Contours of Vorticity Magnitude (1/s)
May 02, 2007
FLUENT 6.1 (3d, dp, segregated, lam)

(b)

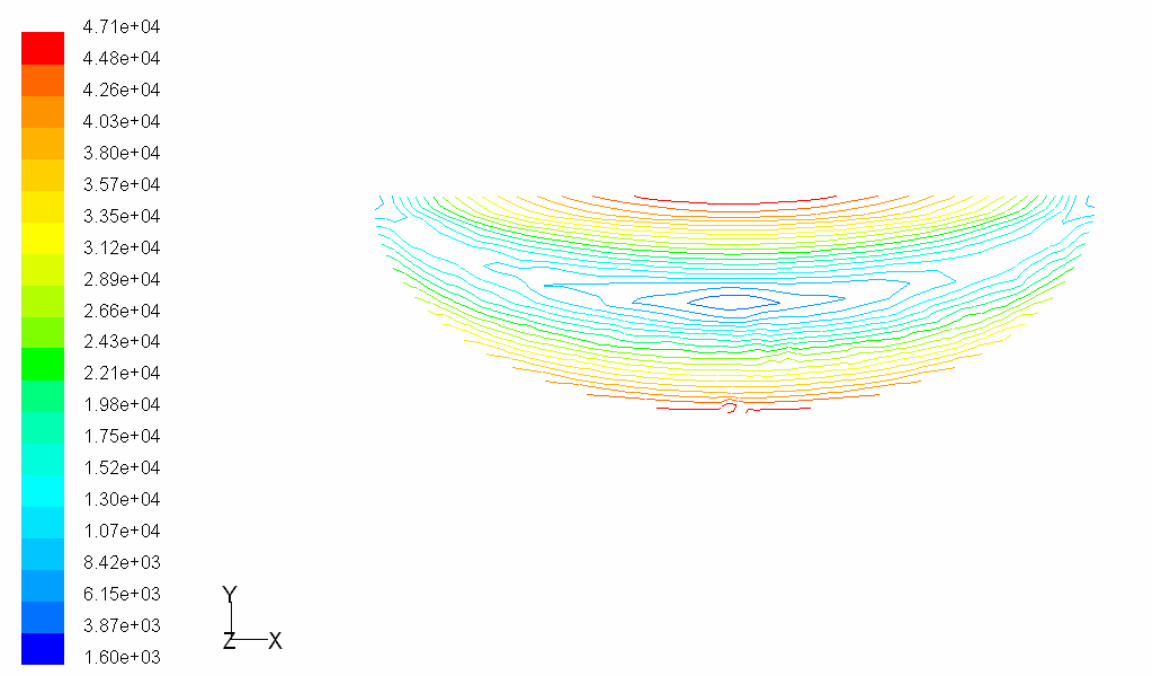
4.71e+04
4.48e+04
4.26e+04
4.03e+04
3.80e+04
3.57e+04
3.35e+04
3.12e+04
2.89e+04
2.66e+04
2.43e+04
2.21e+04
1.98e+04
1.75e+04
1.52e+04
1.30e+04
1.07e+04
8.42e+03
6.15e+03
3.87e+03
1.60e+03
Y
Z
X
Contours of Vorticity Magnitude (1/s)
May 02, 2007
FLUENT 6.1 (3d, dp, segregated, lam)

(c)

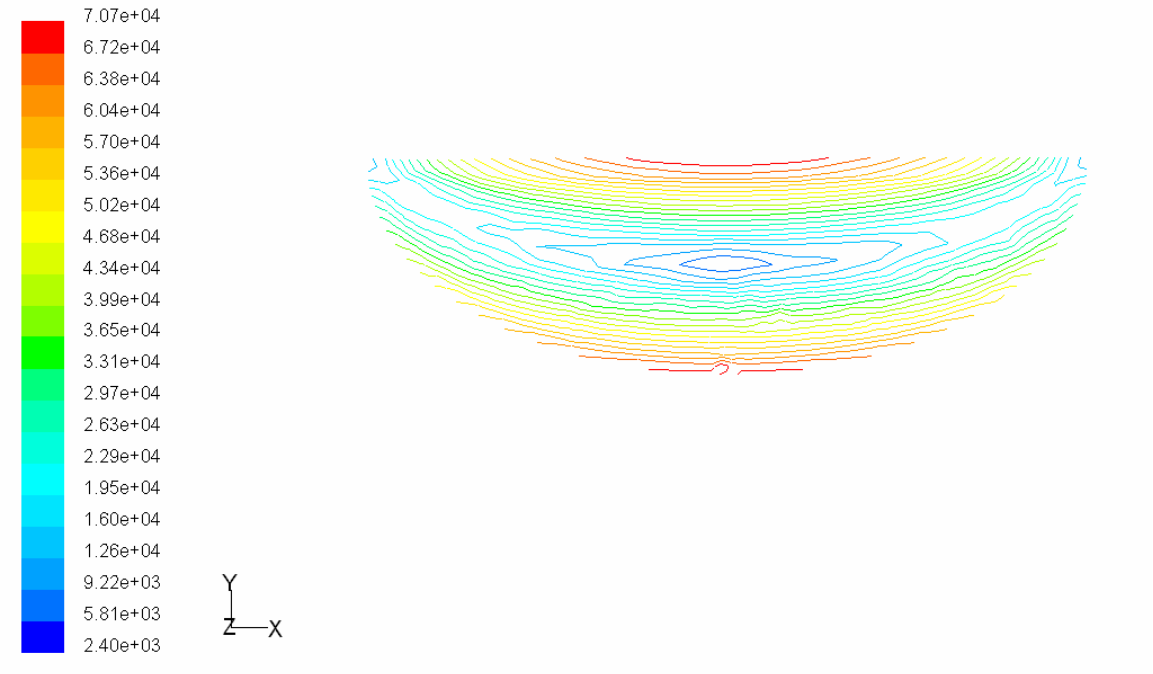
7.07e+04
6.72e+04
6.38e+04
6.04e+04
5.70e+04
5.36e+04
5.02e+04
4.68e+04
4.34e+04
3.99e+04
3.65e+04
3.31e+04
2.97e+04
2.63e+04
2.29e+04
1.95e+04
1.60e+04
1.26e+04
9.22e+03
5.81e+03
2.40e+03
Y
Z
X
Contours of Vorticity Magnitude (1/s)
May 02, 2007
FLUENT 6.1 (3d, dp, segregated, lam)

(d)

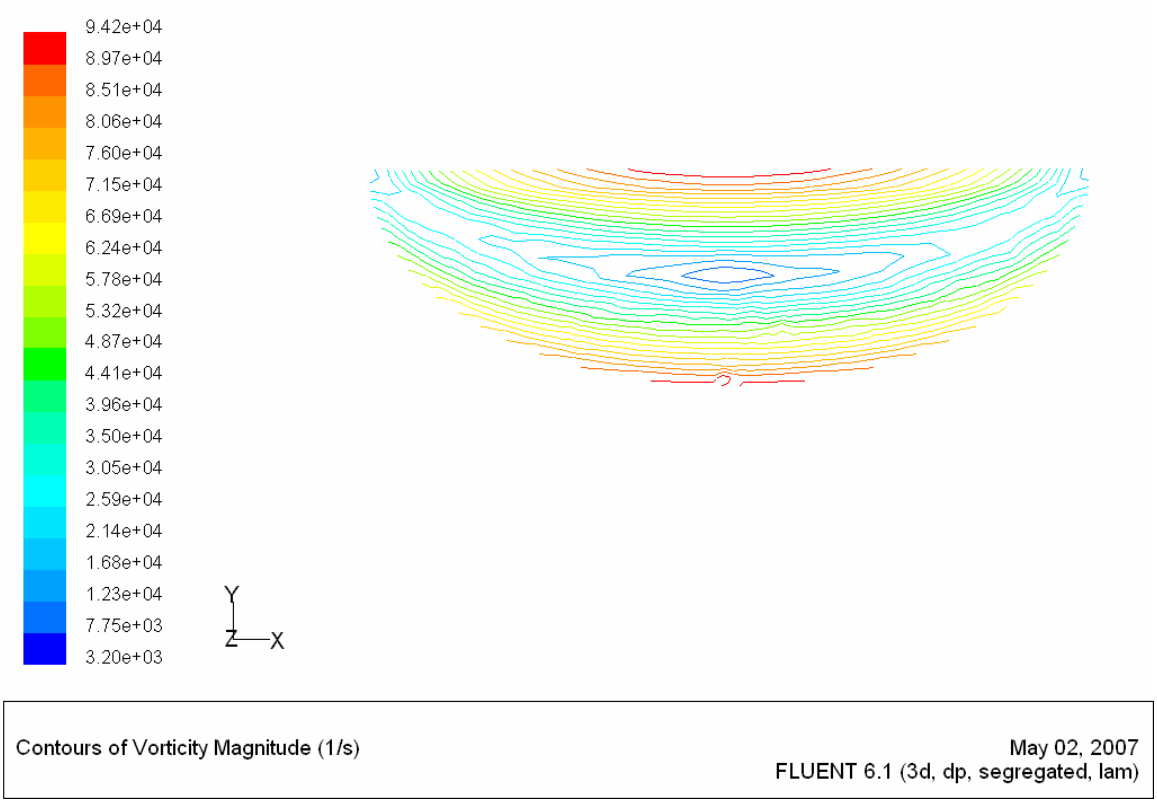

(e)

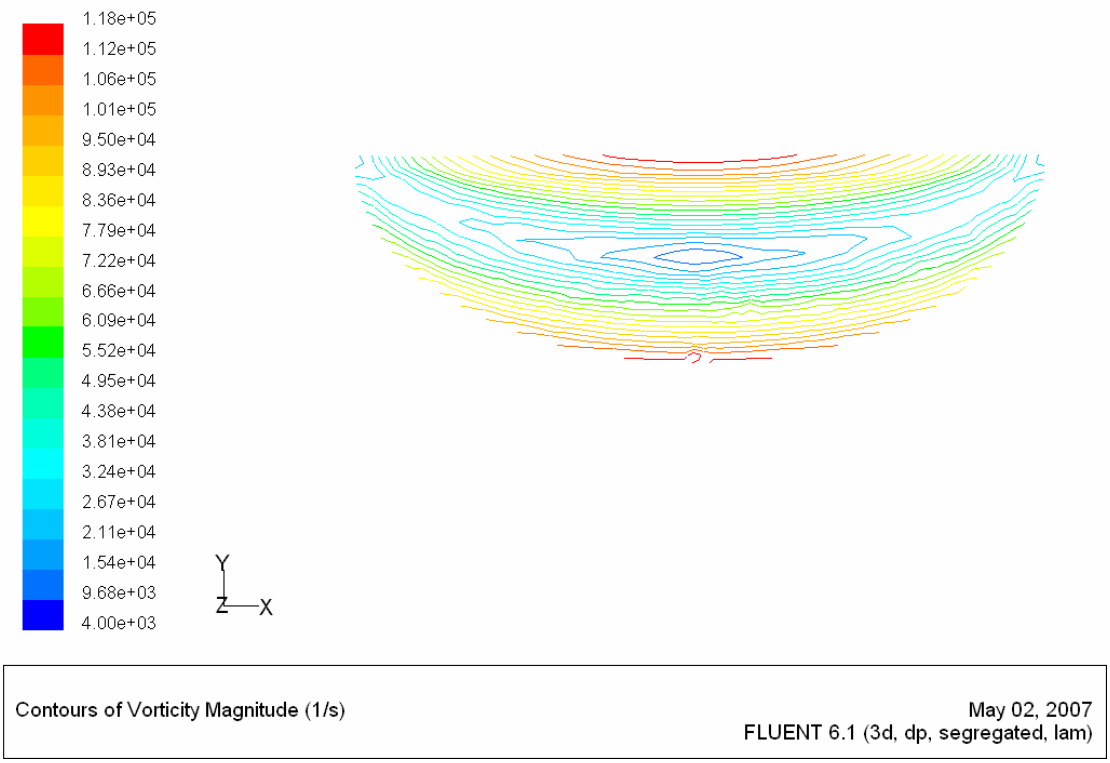

(f)

Fig. 6.5 Contour of Temperature in duct where α =0.3D (a)Re=50 (b)Re=100 (c)Re=200(d)Re=300(e)Re=400(f)Re=500

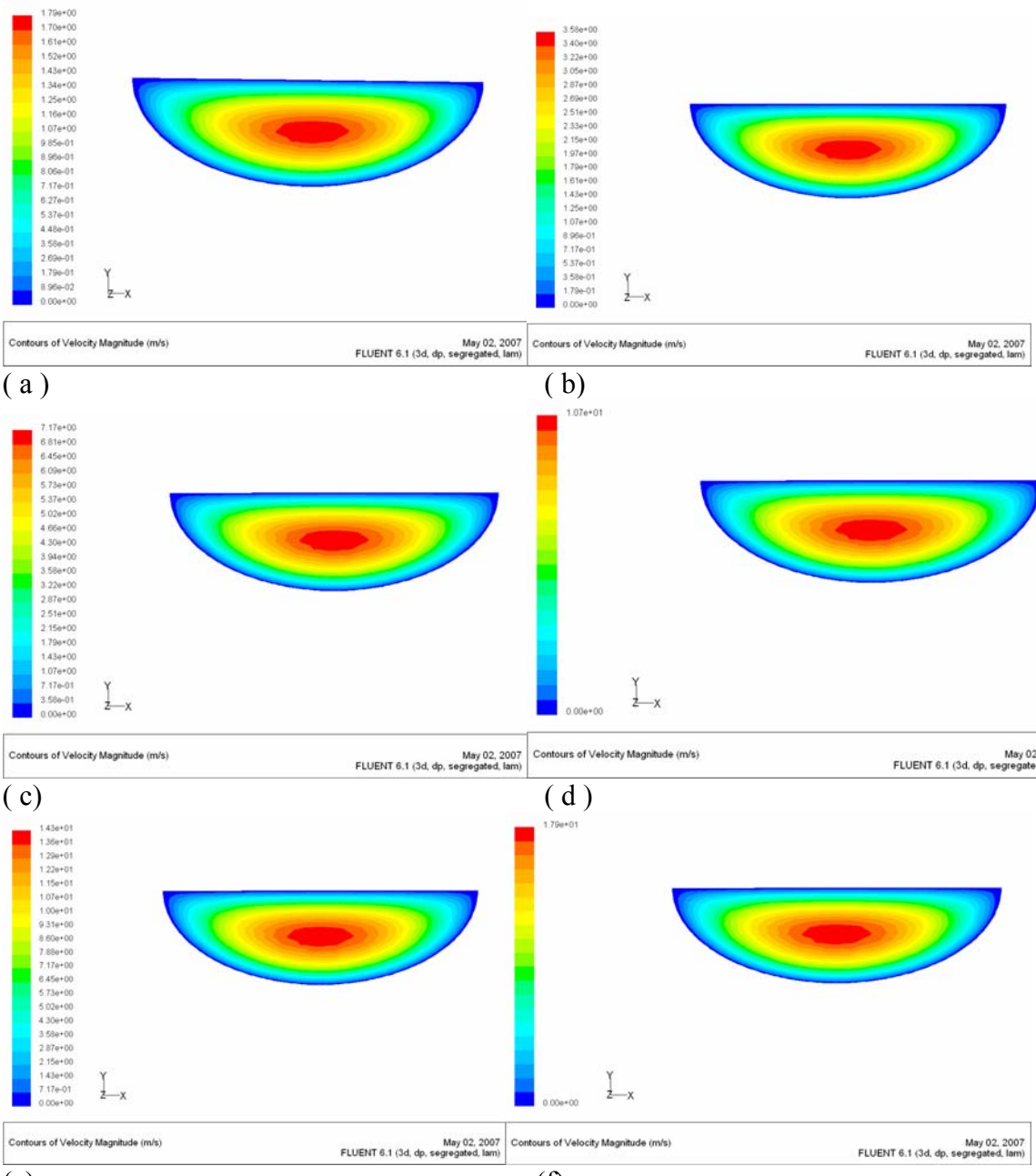

Fig, 6.6 Contour of Velocity in duct where a=0.3(a) Re=50(b) Re=100(c) Re=200(d) Re=300 (e)Re=400(f) Re=500

6.4.2 Computation of Friction Factor (f) and Colburn Factor (j)

$$T_w = 1/A\int TdA \quad \text{.....(6.3)}$$

Area weighted average wall temperature has been taken for calculating local nusselt number which is same for all sections after the flow is hydro dynamically and thermally developed.

$$T_f(x) = \left[\iint |u|T(x,y,z)dydz / \iint |u|dydz\right] \quad \text{.....(6.4)}$$

Bulk mean temperature of the fluid is being taken from the mass weighted average temperature from the FLUENT directly.

Nusselt number is calculated from the following relation.

$$Nu = q/T_w - T_f \quad \text{.....(6.5)}$$

Then, Colburn factor, $j = Nu/\mathrm{Re}\,\mathrm{Pr}^{1/3}$ .....(6.6).

Where Pr=Prandtl number calculated from the thermo physical properties is 0.744

Then Friction factor, $f = d_h \Delta p / 2\rho l w_m^{\ 2}$ ..... (6.7)

Where $\Delta p/l =$ Pressure gradient over the length of the duct.

$w_m = 1/A\int VdA$, the area weighted average velocity calculated from FLUENT directly.

Goodness factor=j/f has been calculated to study the relative surface area compactness.

Table 6.3 f and j for semi-elliptic straight duct taking periodic condition

a=0.3	Re	Wm	ΔP	f	Nu	j	j/f
	50	0.8895	782.477	0.3316	2.8	0.0618	0.186369
dh=0.82115e-03	100	1.7788	1564.996	0.1658	2.53	0.028	0.168878
	200	3.5577	3130.000	0.0829	2.4	0.0132	0.159228
	300	5.33664	4695.013	0.05526	2.36	0.0087	0.157438
	400	7.1155	6260.032	0.04145	2.34	0.0065	0.156815
	500	8.8944	7825.066	0.03316	2.33	0.0051	0.1538
a=0.4	50	0.704	377.5705	0.32245	3.4	0.075	0.232594
	100	1.408	755.1628	0.16123	3.04	0.0335	0.207778
dh=1.037e-03	200	2.816	1510.325	0.0806	2.9	0.016	0.198511
	300	4.2241	2265.038	0.0538	2.85	0.0104	0.193309
	400	5.632	3020.664	0.0403	2.83	0.0078	0.193548
	500	7.04	3775.845	0.0322	2.81	0.0062	0.192547
a=0.5	50	0.5977	224.9318	0.314	3.75	0.0828	0.263694
	100	1.1954	449.8824	0.157	3.38	0.0373	0.23758
dh=1.22194e-03	200	2.3908	899.7834	0.0785	3.22	0.0178	0.226752
	300	3.5862	1349.682	0.0524	3.17	0.0117	0.223282
	400	4.7817	1799.449	0.03926	3.15	0.0087	0.2216
	500	5.9771	2249.49	0.0314	3.14	0.007	0.22293
a=0.6	50	0.5299	153.0577	0.3065	3.9	0.086	0.280587
	100	1.0598	306.1346	0.1533	3.57	0.0393	0.25636
dh=1.3783e-03	200	2.1196	612.3212	0.0766	3.42	0.0189	0.246736
	300	3.1794	918.4863	0.0511	3.37	0.0124	0.242661
	400	4.2392	1224.655	0.0383	3.35	0.0092	0.240209
	500	5.299	1530.825	0.03065	3.33	0.0073	0.238173
a=0.7	50	0.4834	113.973	0.3	4.03	0.089	0.29667
	100	0.9668	227.97	0.1494	3.68	0.04	0.267738
dh=1.5108e-03	200	1.9337	455.9939	0.0752	3.54	0.0195	0.259309
	300	2.9005	683.9944	0.05014	3.5	0.0129	0.25728
	400	3.8674	911.9969	0.0376	3.47	0.0096	0.255319
	500	4.8342	1140.002	0.03	3.46	0.0076	0.253333

6. 4.3Role of Reynolds Number and Geometric Parameters

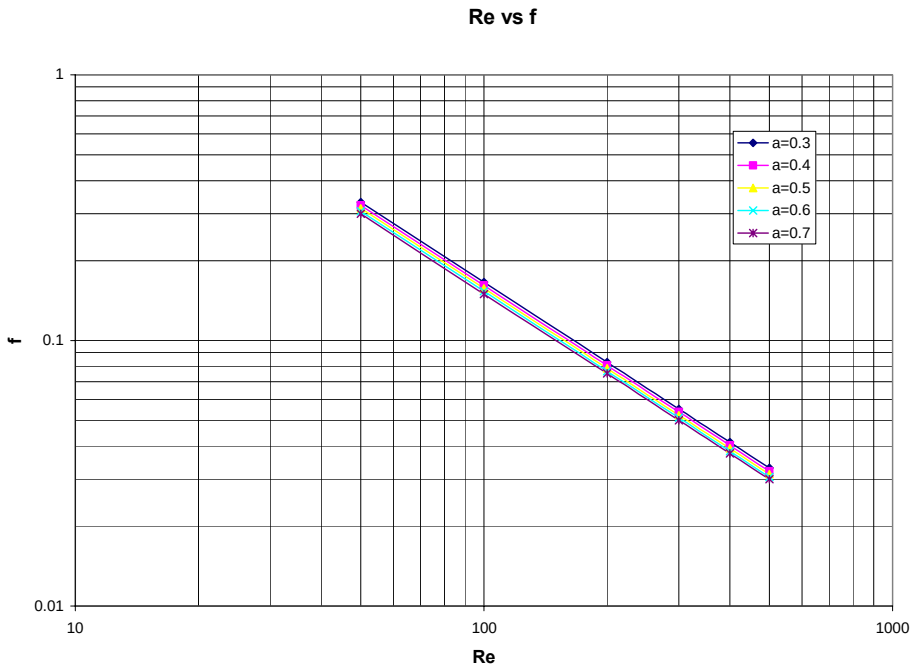

Fig.6.7 Variation of fanning friction factor with different Reynolds no. at different aspect ratios in a semi elliptical straight duct for fully developed region

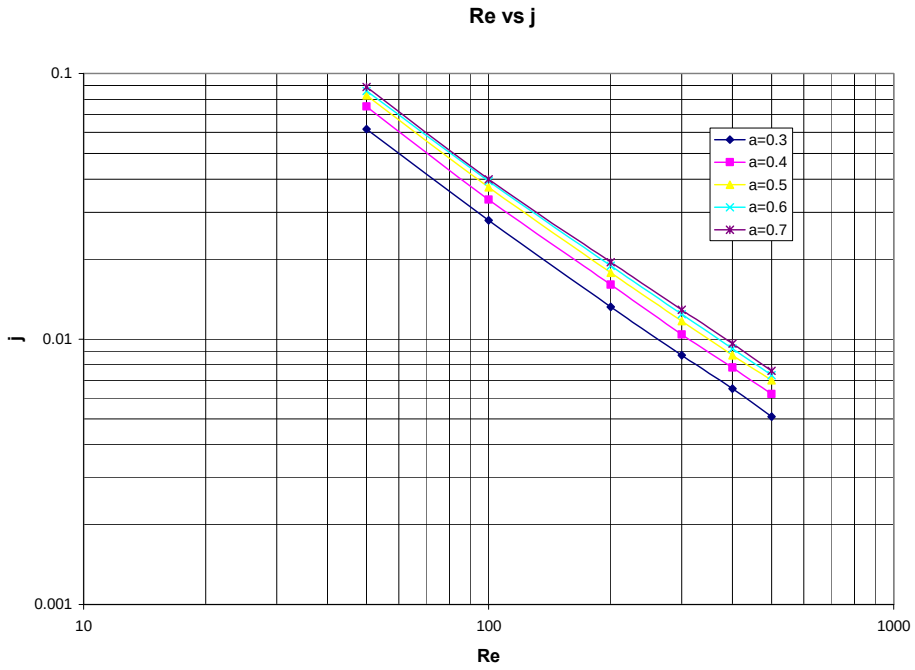

Fig.6.8 Variation of Colburn factor with different Reynolds no. at different aspect ratios in a semi elliptical straight duct for fully developed region

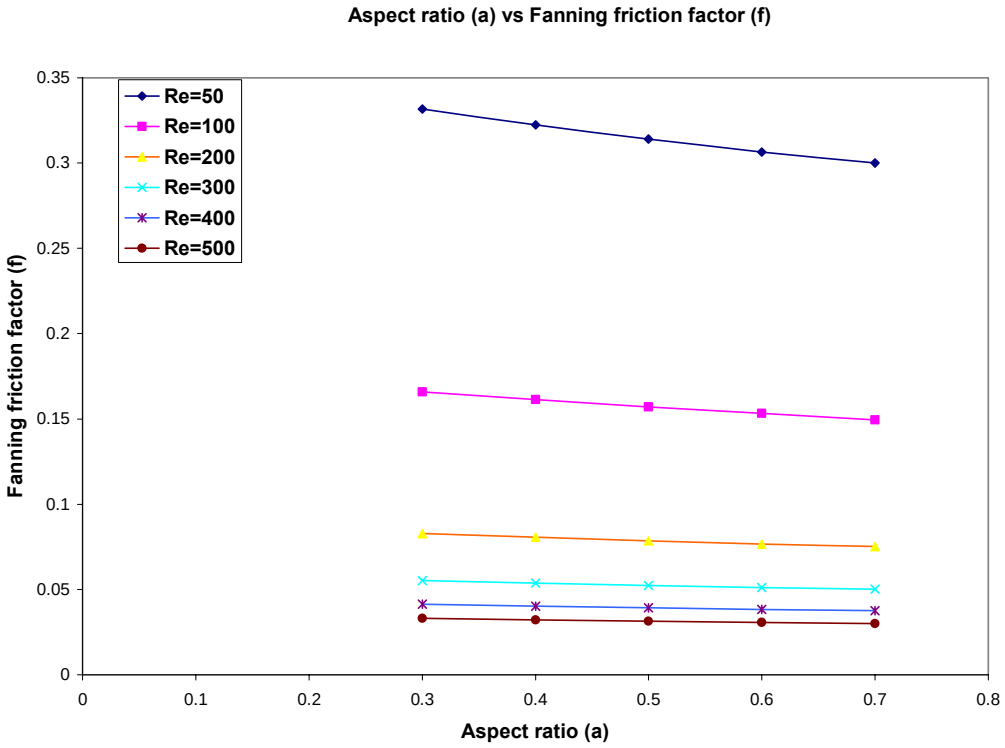

Fig.6.9 Variation of Fanning friction factor with aspect ratio

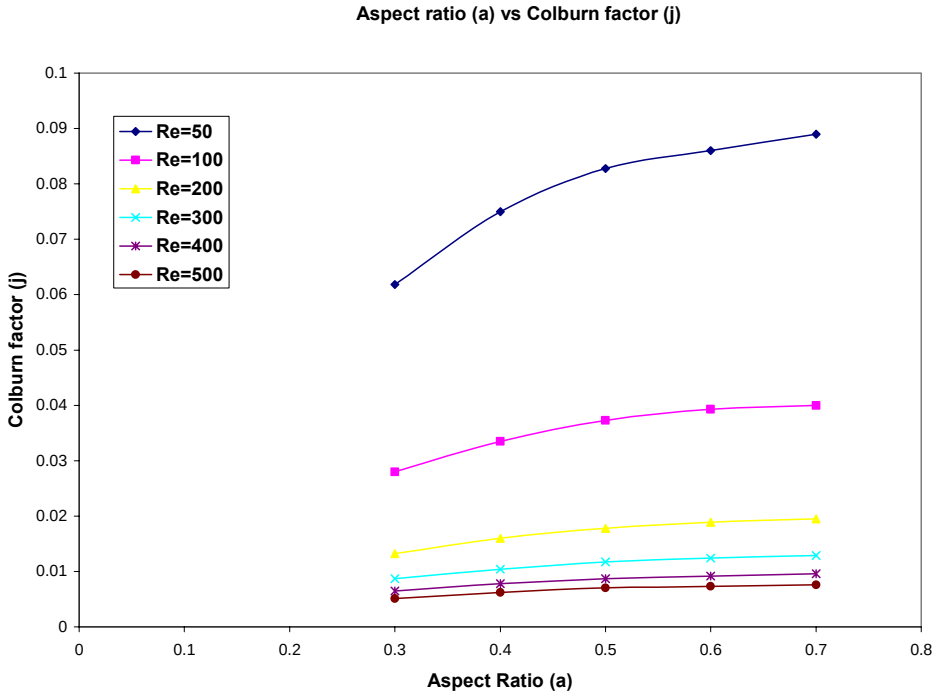

Fig.6.10 Variation of Colburn factor with aspect ratio at fixed Reynolds number.

6.4.4 Generation Of Heat Transfer and Flow Friction Correlations

The correlation for the given geometry for a particular aspect ratio can be found from the following relation.

f or j=C Re^{K}……(6.8)

Firstly the different results have been tabulated .Then the graphs between friction factor and Coburn factor corresponding to different Reynolds number are plotted for various geometry based on different aspect ratios.

Then C and K value have been found from the graphs by fitting to a power law.

Table 6.4 Correlations found out for various geometries based on different aspect ratios.

Geometry	Correlation	
α=0.3D	f =16.581Re^{-1}	R^2=1
	j =4.0874 $Re^{-1.0778}$	R^2=0.9995
α=0.4D	f =16.142 $Re^{-1.0003}$	R^2=1
	j =4.9605 $Re^{-1.0791}$	R^2=0.9994
α=0.5D	f =15.689 $Re^{-0.9998}$	R^2=1
	j =5.3823 $Re^{-1.0741}$	R^2=0.9995
α=0.6D	f =15.332 $Re^{-1.0001}$	R^2=1
	j =5.4199$Re^{-1.065}$	R^2=0.9996
α=0.7D	f =14.892 $Re^{-0.9985}$	R^2=1
	j =5.458 $Re^{-1.06}$	R^2=0.9994

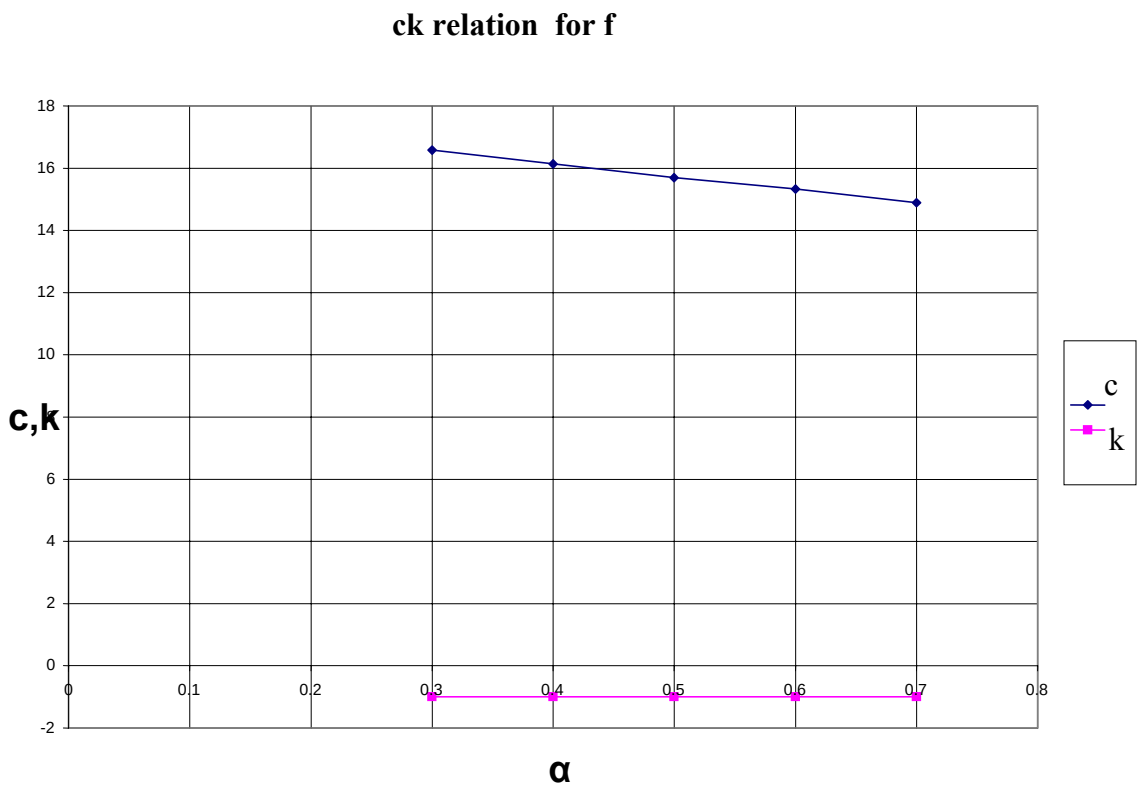

Fig. 6.11 Variation of power indices with different aspect ratios in a semi elliptical straight duct for fully developed region.(For correlation of Fanning friction factor)

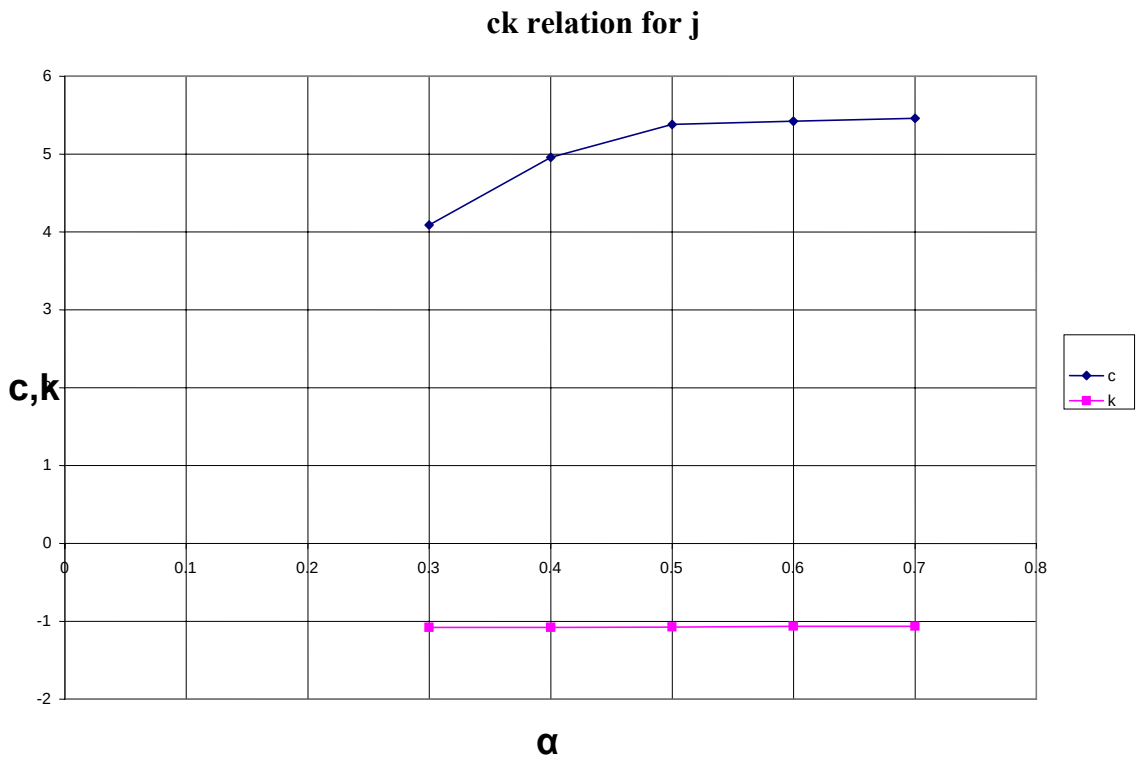

Fig. 6.12 Variation of power indices with different aspect ratios in a semi elliptical straight duct for fully developed region.(for colburn factor correlation)

The final correlation for semi elliptical straight duct irrespective of aspect ratios was found out from regression analysis.

$$f = 14.183\ Re^{-0.997}\ (a)^{-0.121}$$

$$R^2 = 1$$

$$j = 4.557\ Re^{-0.866}\ (\ a\ )^{1.142}$$

$$R^2 = 0.96$$

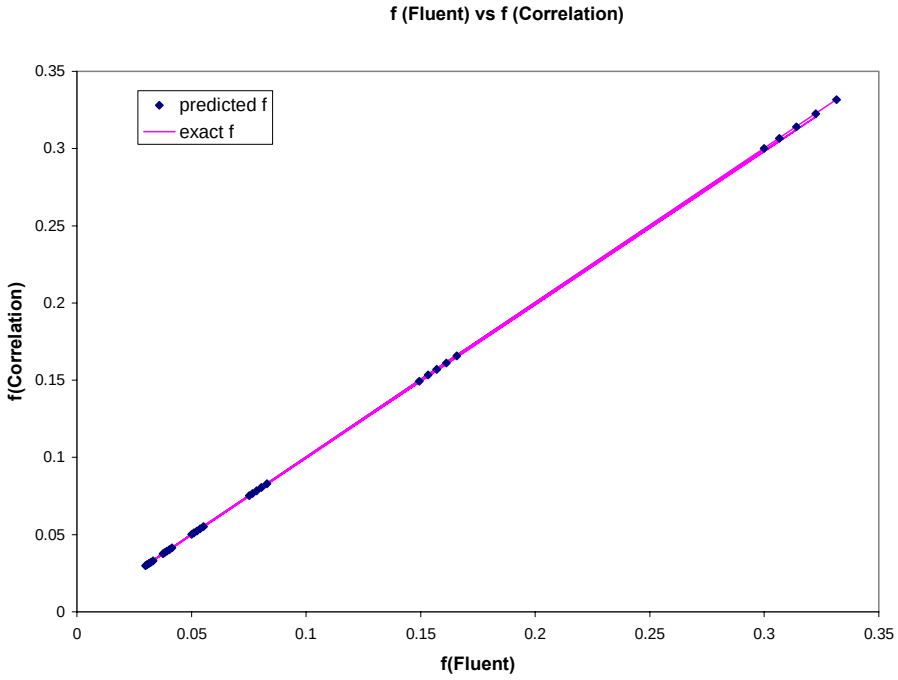

Fig.6.13 shows the comparison of f calculated from Fluent and f found out from correlation. Red line represents the exact f.

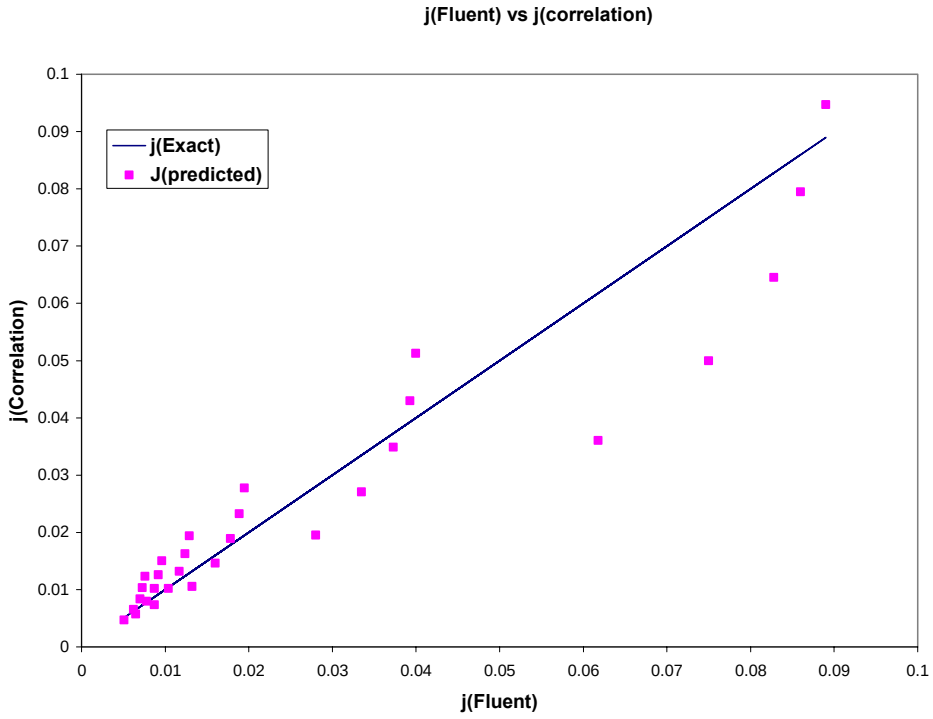

Fig.6.14 shows the comparison of j calculated from Fluent and j found out from correlation. Red line represents the exact j.

6.5 DISCUSSIONS

(1) Fig. 6.7 shows that Fanning friction factor decreases with increase in Reynolds Number for a particular aspect ratio.

(2) For a particular Reynolds number ,the colburn factor is maximum in case of aspect ratio =0.7.It is shown by the fig. 6.8

(3) From fig. 6.9 and fig.6.10, it is clear that there is no significant variation in Fanning friction factor with aspect ratio as the Reynolds number increases. The same happens in the case of Colburn factor.

(4) The indices k is independent of the aspect ratio for both the correlation for Fanning friction factor and colburn factor.(fig.6.11& fig.6.12)

(5) The value of indices c decreases in case of correlation for Fanning friction factor. This is represented by fig.6.11

(6) The value of indices c increases up to aspect ratio 0.5 and then remains constant in case of correlation for colburn factor. This is represented by fig.6.12

(7) Fig. 6.13 and fig. 6.14 represents the accuracy of the correlation with the data obtained from Fluent for Fanning friction factor and Colburn factor respectively.

Chapter7

SINUSOIDAL DUCT

- **Introduction**
- **Computational Domain**
- **Boundary Conditions**
- **Gambit & FLUENT Details**
- **Results & Discussion**

7.1 INTRODUCTION

The sinusoidal channels under consideration are defined by sweeping a semi ellipse along a sinusoidal path and fully characterized by the geometry wavelength(2L),passage diameter(D) and the half height of the sinusoid (A).We use the non-dimensional parameters L/D,A/L and α to characterize the geometry. Here we report the effect of Reynolds Number ($50 \leq Re \leq 500$) and geometric configuration (A/L=0.3 and 0.5)on the fully developed flow and heat transfer in a sinusoidal channel with different cross sections of various aspect ratios (a=0.3 to 0.7).

The thermal boundary condition of constant heat flux is being investigated in the absence of peripheral wall conduction. Repetitive or periodic geometric modules in compact heat exchangers lead to fully developed flows after a sufficient number of modules ,beyond which flow patterns become invariant at successive downstream locations. Here such fully developed flows, subject also to the constraint that the non-dimensional temperature profiles are invariant from one module to the next.. In such circumstances it is sufficient to analyze only one segment (module) of the geometry (Patankar, 1977).The pressure field in the fully developed region can be expressed (Patankar, 1977) as the linear combination of the local pressure, and the overall pressure drop

$$P(x,y,z)=p(x,y,\tau)+ßx, \quad \text{(7.1)}$$

Where the local component p(x, y, z) repeats itself from module to module. The overall pressure gradient ß is introduced in the momentum equation as the source term f in the stream wise direction f=ß.i, where ß is the prescribed pressure drop, and i is unit vector in the stream wise direction. So, one module is taken for simulation.

7.2 COMPUTATIONAL DOMAIN

Half of the geometry along the length has been taken as symmetry.

A/L=0.3 and 0.5, L/D=4.5

$Y=2A \text{ SIN } (\pi Z/2L)$ ..(7.2)

$y = 9 \text{ SIN } (\pi z/18)$

Length of the duct=36mm

Major axis of the duct (D)=2mm

Minor axis of the duct=a x D, a varies from 0.3 to 0.7.

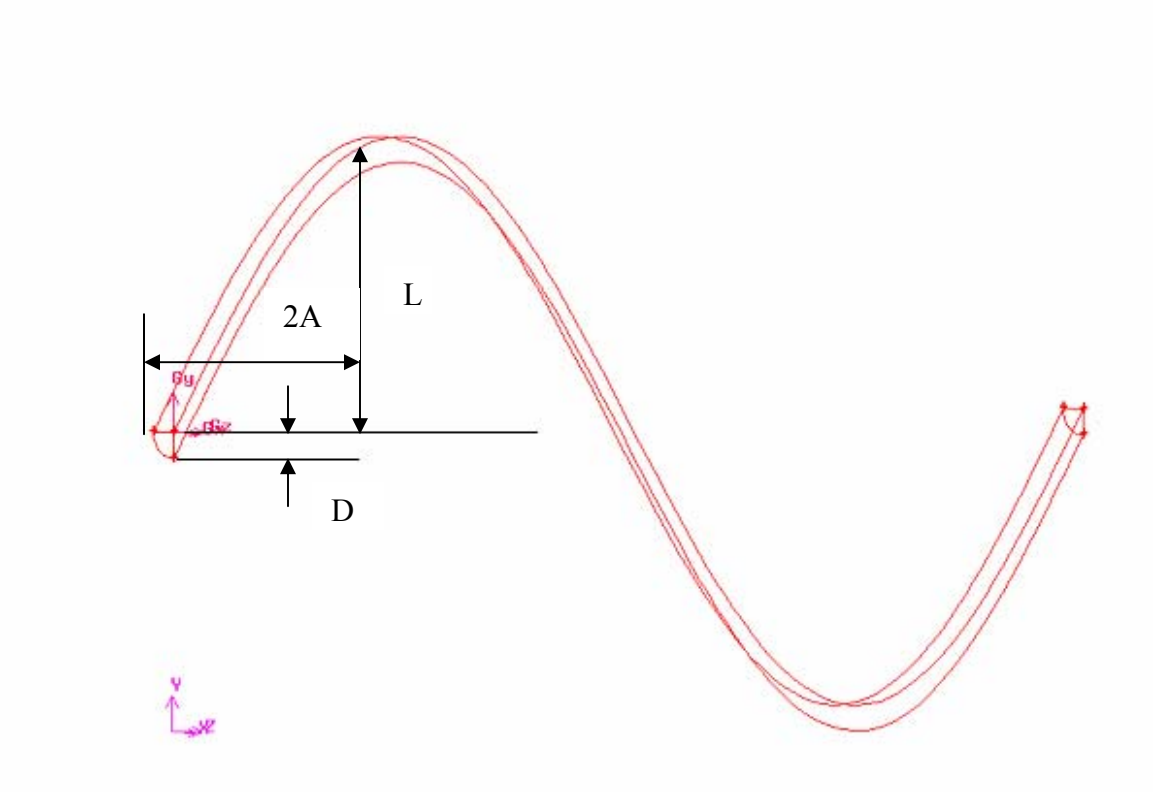

Fig.7,1 Computational domain for Sinusoidal channel

7.3 BOUNDARY CONDITIONS

Fully developed flow field

In case of sufficiently long ducts, the entrance region has a negligible effect on the overall thermo hydraulic performance of a surface. We have assumed fully developed velocity and temperature fields. This assumption is implemented by invoking the periodic boundary condition in association with the uniform cross section of the flow passage [a trivial case of periodic geometry]. This approach reduces the number of grid points and saves on computing time. A no-slip boundary condition for velocity is enforced on the walls of the channels, and a periodic boundary condition is applied at the inflow and outflow of the computational domain. For the temperature field, boundary condition of constant heat flux is taken for the wall

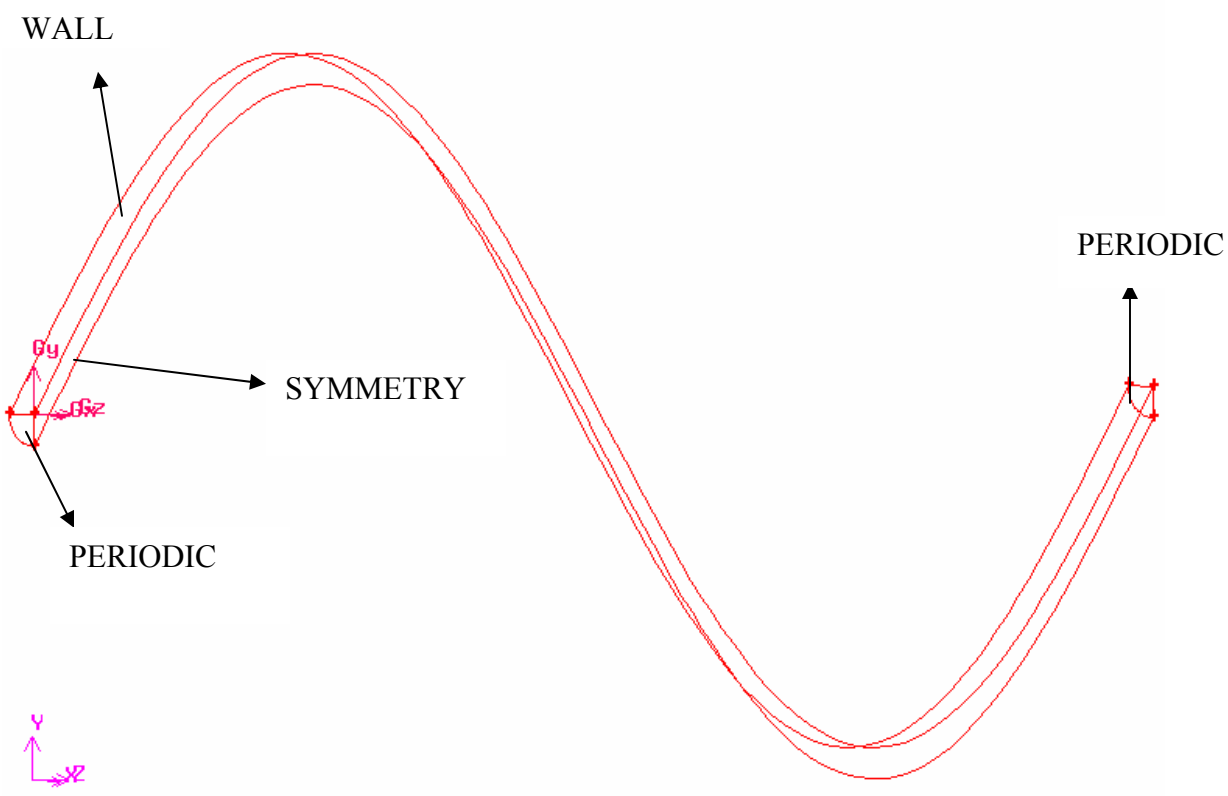

Fig.7.2 Boundary conditions assumed for Sinusoidal Channel

7.4 GAMBIT AND FLUENT DETAILS:

Quad/Tri wedge primitive meshing for the face is done. Then the Cooper Hex/wedge meshing has been used for the Volume meshing. The SIMPLE algorithms evaluate the coupling between pressure and velocity. The under-relaxation factor momentum and energy has been 0.4 and 0.8 respectively. The second order upwind scheme has been taken for the descretisation of momentum and energy equation. The 3-D double precision solver has been chosen. Convergence was achieved for all runs, with normalized residuals being much lower than 10^{-6}.

The following thermo-physical properties of air have been taken

Table 7.1 thermo-physical properties of air

Fluid -air
Density=1.225 kg/m^3
Thermal conductivity=0.0242 w/m-k
Viscosity=1.7894e-05kg/m-s
Specific heat at constant pressure=1006.43 J/kg-k

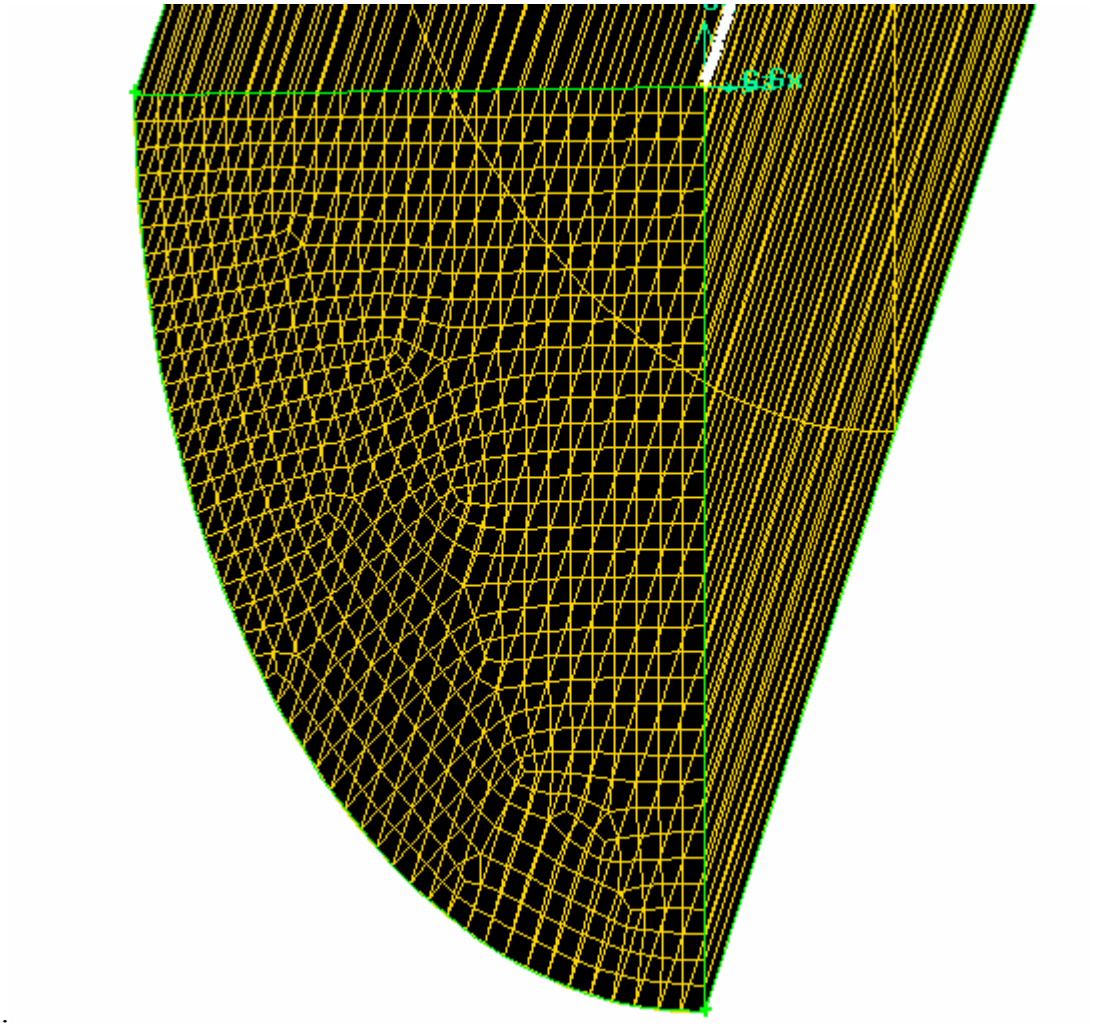

Fig.7.3 Meshing of Sinusoidal Channel

7.4.1Grid Independent Test

Following grid independent test based upon nusselt number has been done taking different grid sizes.

Table 7.2 (a) Grid Independent Test (A/L=0.5,L/D=4.5)

For a =**0.3**

No . Of Cells	Nu
30680	2.297
47200	2.261

For **a = 0.4**

Number of Nodes	Nu
33040	3.1168
51625	3.0592

For **a =0.5**

No. Of Cells	Nu
26078	3.8235
36580	3.75
64350	3.71

For **a =0.6**

Grid Size	No.Of Nodes	Nu
601 x 50	30050	4.22138
1086 x 50	54300	4.20286
100 x 30 x 50	70000	4.21481

For **a =0.7**

No Of Cells	Nu
39744	4.167868
57456	4.131718

Table 7.2 (b)Grid Independent Test (A/L=0.3,L/D=4.5)

For **a =0.3**

No . Of Cells	Nu
22360	2.372(selected for computation)
88088	2.390
172000	2.366

For **a = 0.4**

Number of Nodes	Nu
29376	3.133
40320	3.083(selected for computation)
63000	3.035
83754	3.017

For **a =0.5**

No. Of Cells	Nu
33480	3.676
110110	3.607

For **a =0.6**

No. Of Nodes	Nu
32736	4.035
49880	3.981

For **a =0.7**

No Of Cells	Nu
29160	4.221
39744	4.167
67456	4.132

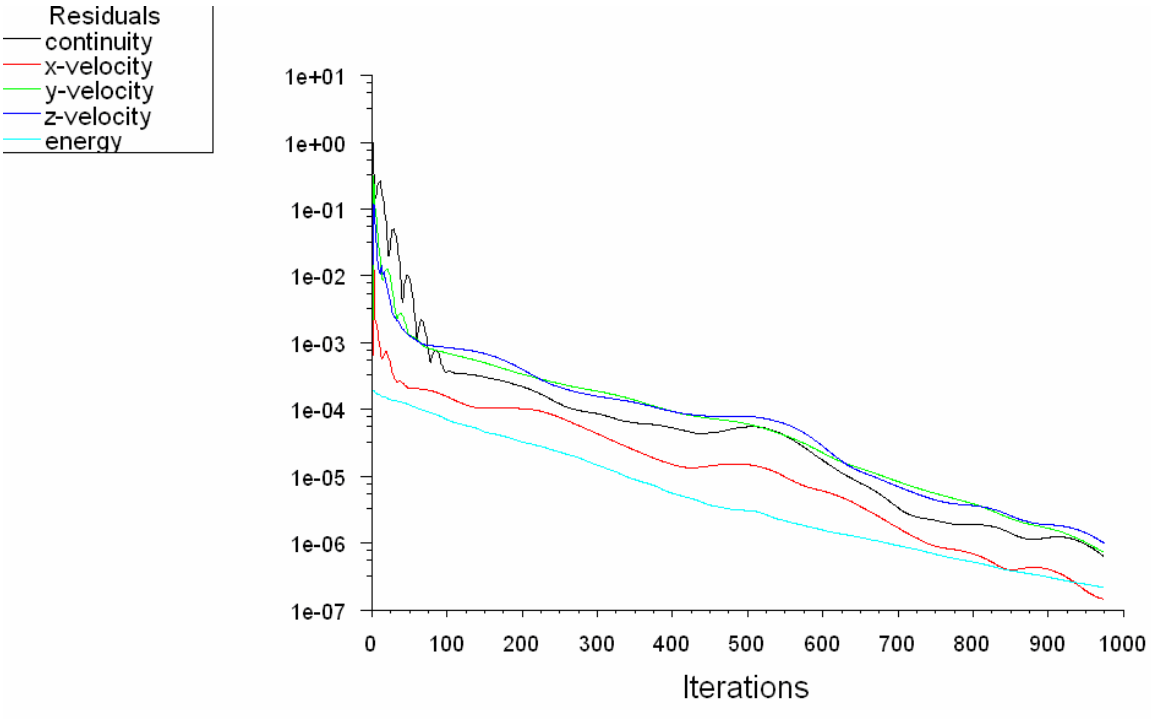

Fig. 7.4 Convergence by iterations in Sinusoidal Channel

7.5 RESULTS

7.5.1 Pressure, Velocity and Temperature Fields

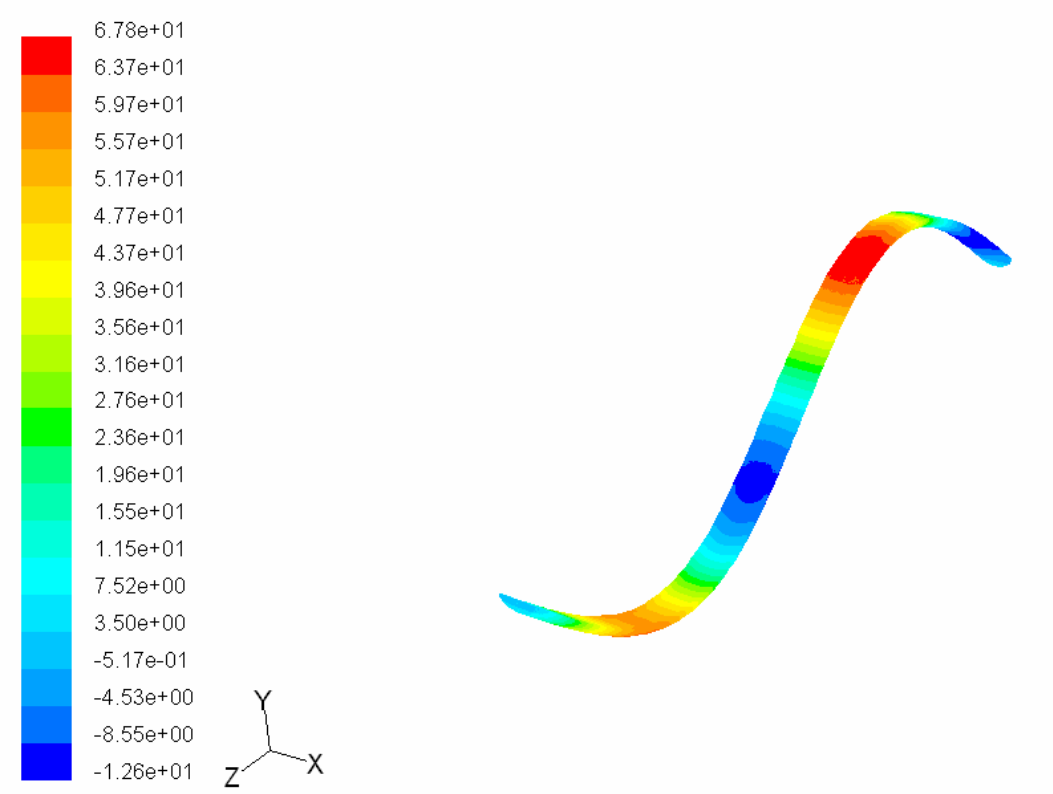

Fig.7.5 Pressure drop in a Sinusoidal channel A/L=0.3,L/D=4.5,Re=100,a = 0.3

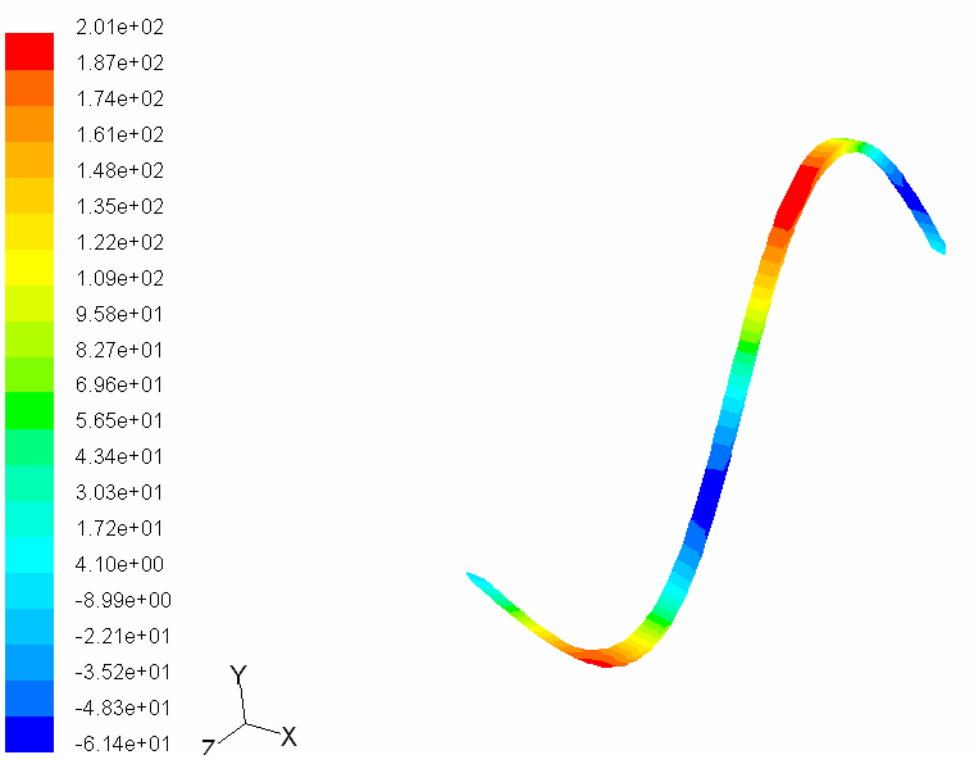

Fig7.6.Pressure drop in a Sinusoidal channel A/L=0.5,L/D=4.5,Re=100,a = 0.3

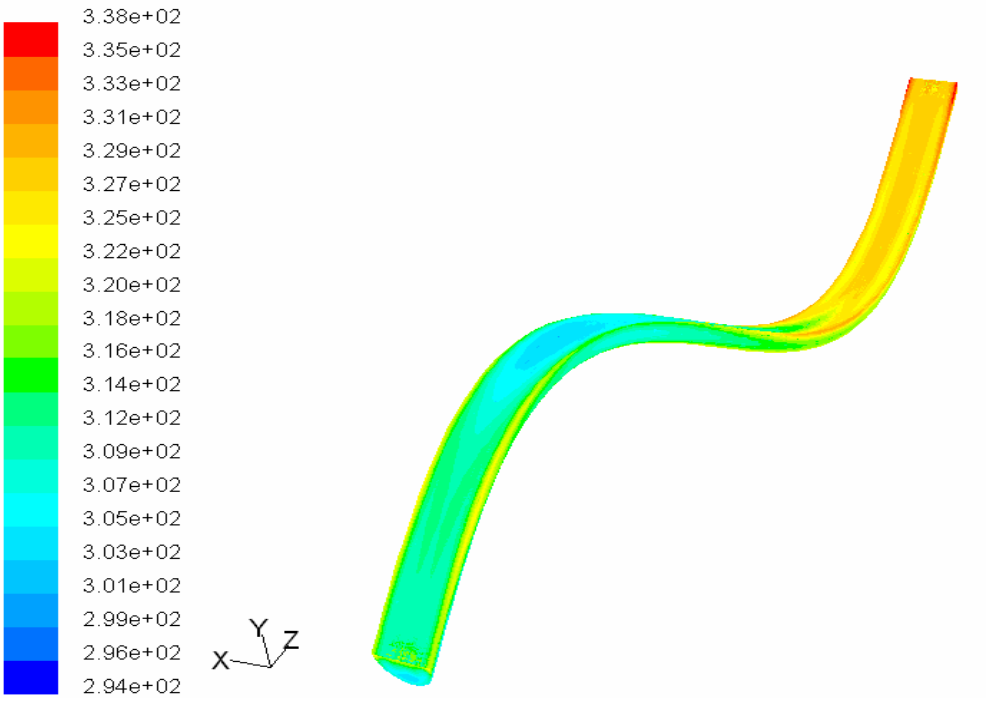

Fig. 7.7 Contour of static temperature in the whole domain. For a =0.6 A/L=0.3, L/D=4.5.Re=500

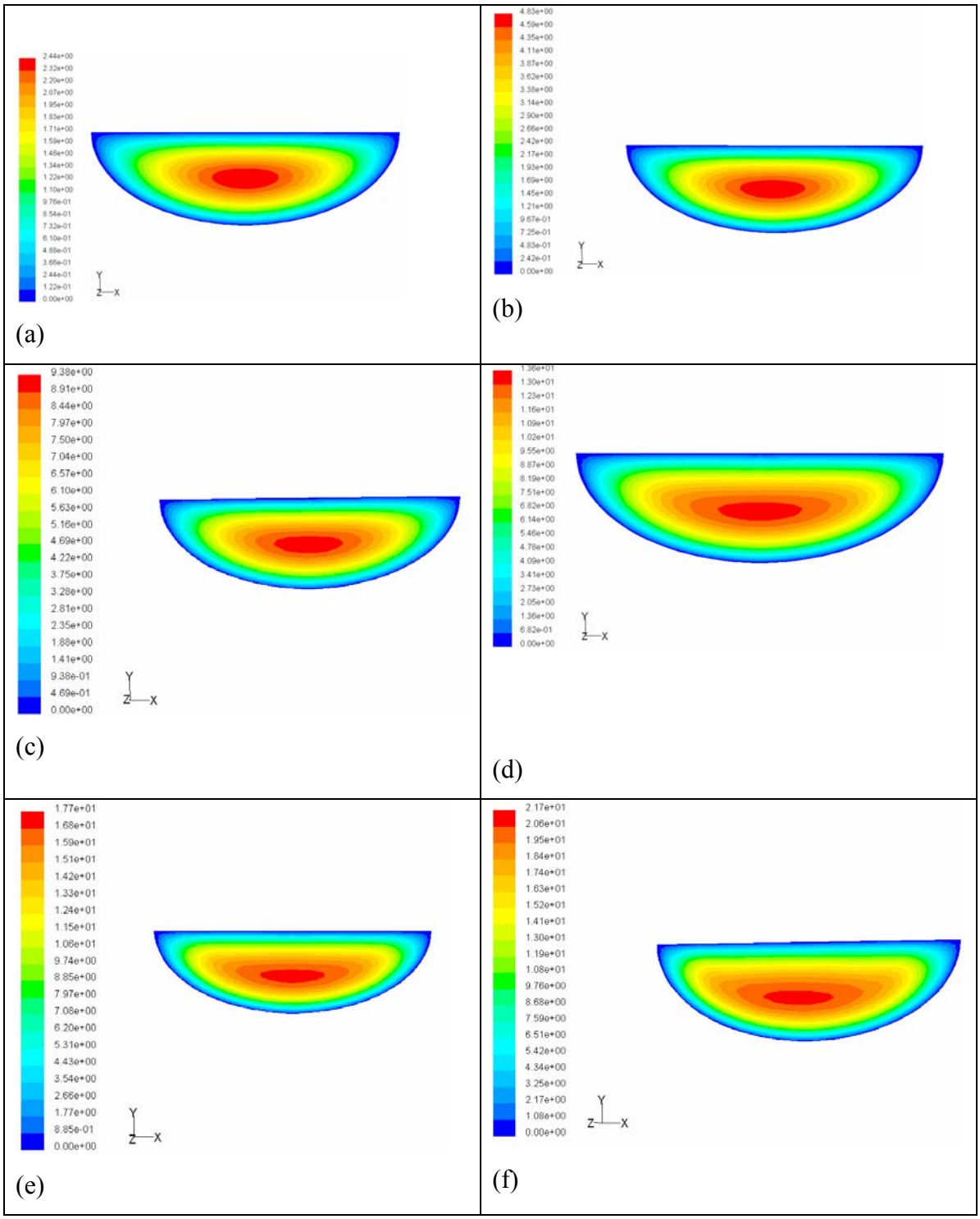

Fig.7.8 Velocity contour at the outlet of the sinusoidal channel where aspect ratio, a=0.3and A/L=0.3 at (a)Re=50,(b)Re=100,(c)Re=300,(d)Re=400,(f)Re=500

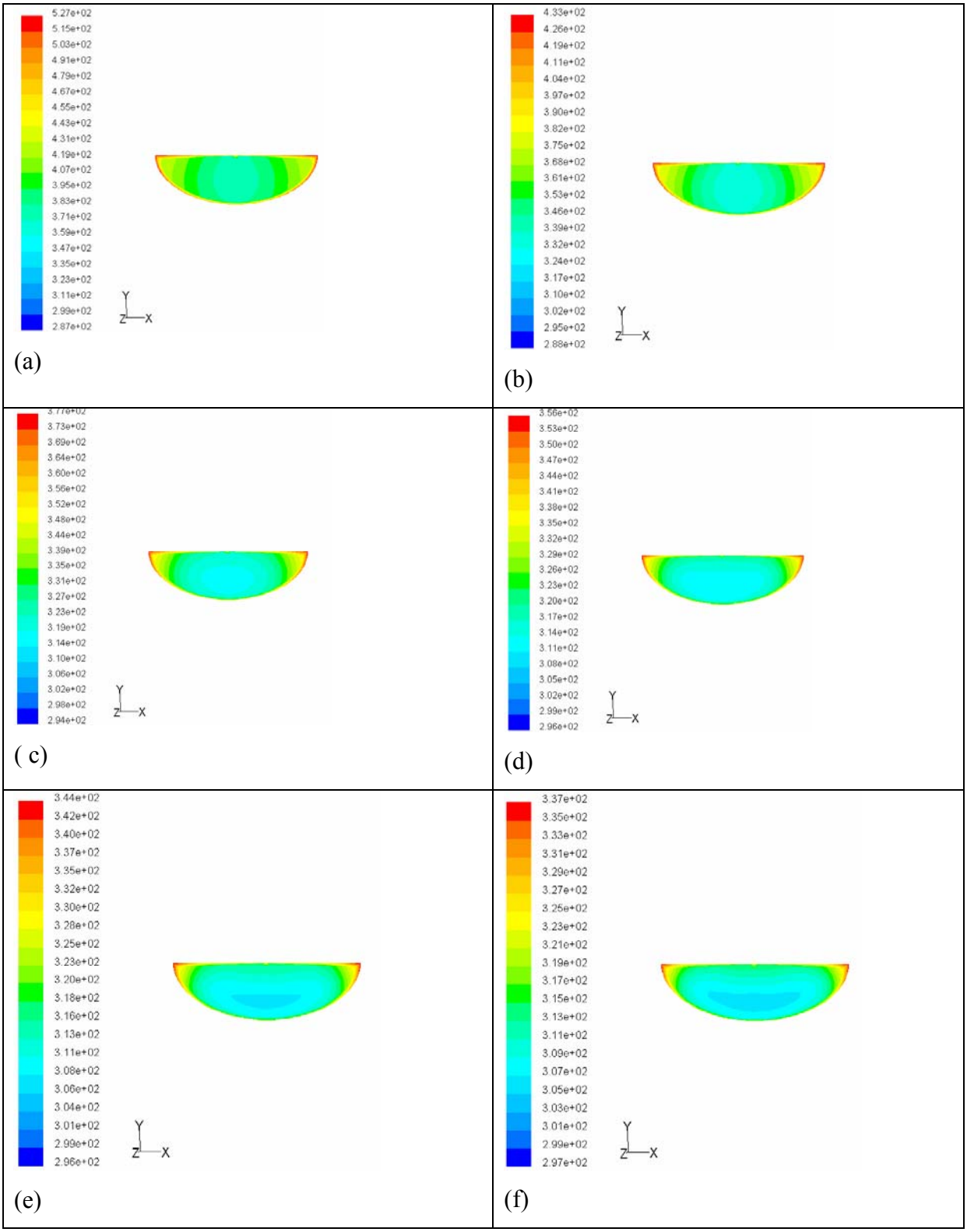

Fig.7.9 Temperature contour at outlet for (a)Re=50,(b) Re=100 (c) Re=200 (d) Re=300 (e) Re=400 (f) Re=500 where aspect ratio, a =0.3

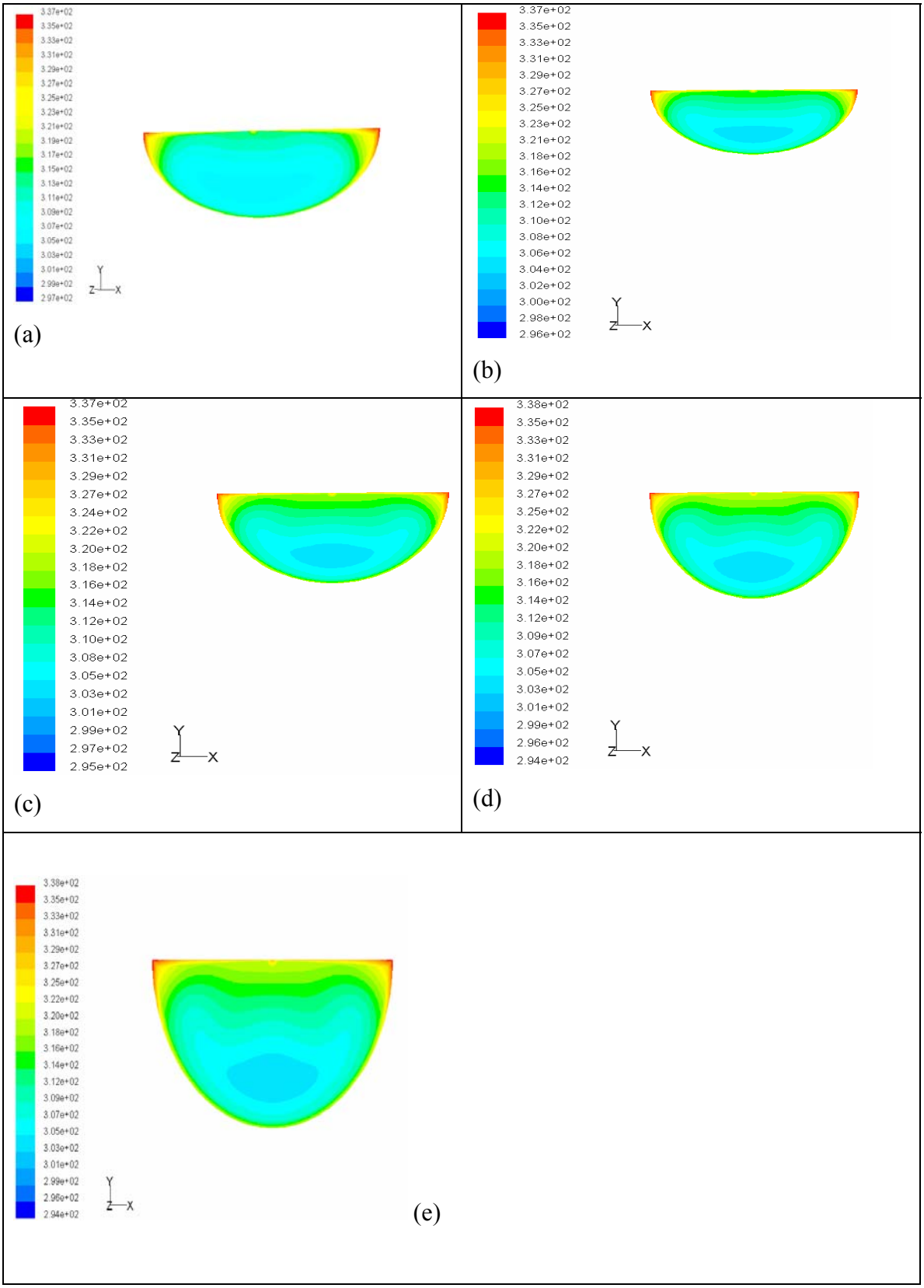

Fig.7.10 Temperature contour at outlet, for Reynolds no=500 at different aspect ratios (a) a=0.3,(b)a=0.4(c)a=0.5 (d) a=0.6 (e)a=0.7

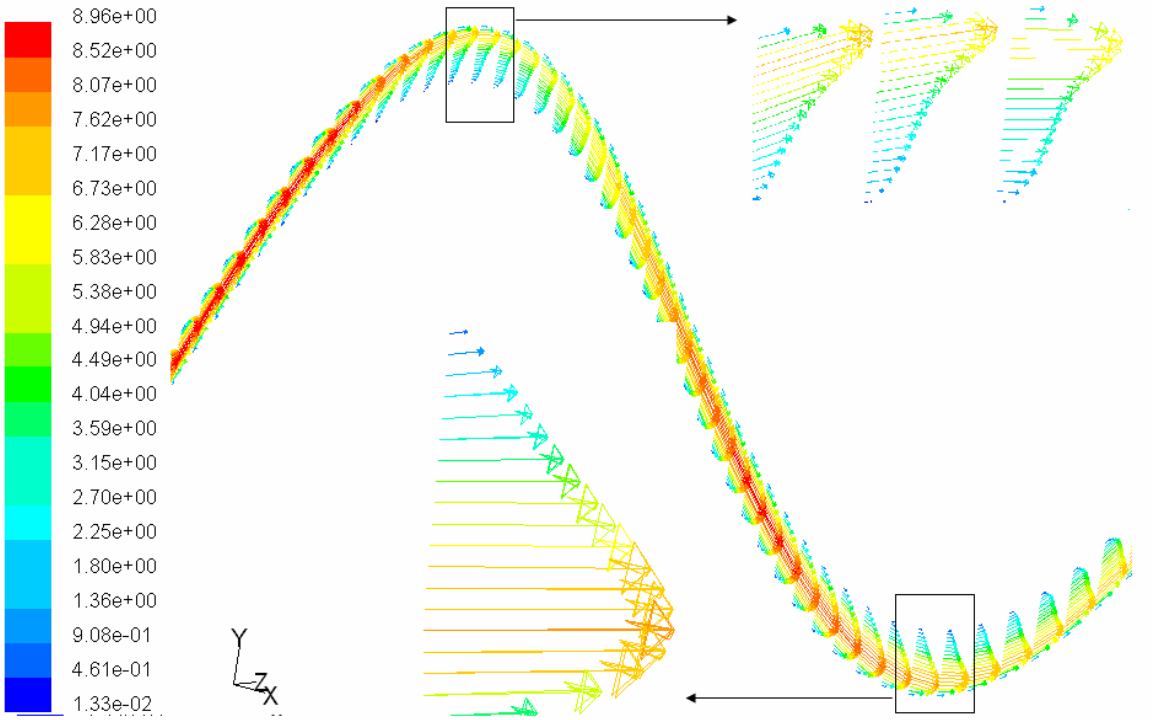

Fig 7.11Velocity vectors showing the changes in the profile at the peak and trough region of the Sinusoidal Channel along the symmetry plane taken in the middle of the domain.

7.5.2 Computation of Friction Factor (f) and Colburn Factor (j)

L=9mm, A=0.5L=4.5mm

2A=9mm

y = 9 SIN (πz/18)

For a fixed Reynolds number, mass flow rate is calculated according to the following relation.

$\dot{m} = A\mu \,\mathrm{Re}/\, d_h$ Where $\dot{m}$ =mass flow rate……(7.3)

Mass flow rate is being taken as input.

Air temperature at inlet is set at 300K.A constant heat flux(here 1000w/m^2) has been provided to the wall

Hydraulic diameter d_h = 4 x area/perimeter

Area=[π x D x (b)]/2

Perimeter is being taken as approximation i.e. perimeter=π√0.5 (D^2+b^2) + 2D

$$T_w = 1/A\int TdA \quad \text{..... (7.4)}$$

Area weighted average wall temperature has been taken for calculating local nusselt number which is same for all sections after the flow is hydrodynamically and thermally developed.

$$T_f(x) = \left[\iint |u|T(x,y,z)dydz / \iint |u|dydz\right] \quad \text{..... (7.5)}$$

Bulk mean temperature of the fluid is being taken from the mass weighted average temperature from the FLUENT directly. So, average of $(T_w - T_f)$has been calculated at different sections along the length direction(here z-axis).Nusselt number is calculated from the following relation.

$$Nu = q / T_w - T_f$$

Then, Colburn factor, $j = Nu / \mathrm{Re}\,\mathrm{Pr}^{1/3}$ ..... .(7.6)

Where Pr= Prandtl number calculated from the thermo physical properties is 0.744

Then Friction factor, $f = d_h \Delta p / 2\rho l w_m^{\ 2}$ .....(7.7)

Where $\Delta p / l =$ Pressure gradient over the length of the duct.

$w_m = 1/A\int VdA$, the area weighted average velocity calculated from FLUENT directly.

Goodness factor=j/f has been calculated to study the relative surface area compactness.

Table 7.3 Calculation of f and j for Sinusoidal Channel where A/L=0.3,L/D=4.5

a=0.3	Re	$\dot{m}$ (kg/s)	ΔP(Pascal/m)	f	Nu	J=Nu/RePr$^{1/3}$	j/f
	50	5.13e-07	1654.74	0.7000	2.2264	0.049141	0.070201
	100	1.0267e-06	3334.405	0.2880	2.3723	0.026181	0.090905
	200	2.0534e-06	6893.941	0.1825	3.3601	0.018541	0.101594
	300	3.08e-06	10761.81	0.1266	4.4772	0.01647	0.130095
	400	4.1068e-06	14894.18	0.0986	5.384	0.014854	0.150653
	500	5.133e-06	19259.24	0.0816	6.0741	0.013407	0.164298
a=0.4	50	5.42e-07	780.8964	0.6663	2.8413	0.062713	0.094121
	100	1.084e-06	1588.828	0.3389	3.083	0.034024	0.100395
	200	2.168e-06	3372.004	0.1798	4.313	0.023799	0.132364
	300	3.252e-06	5351.807	0.1268	5.3897	0.019827	0.156363
	400	4.336e-06	7489.039	0.0998	6.1436	0.01695	0.169841
	500	5.42e-06	9792.178	0.0835	6.6804	0.014745	0.176586
a=0.5	50	5.75e-07	453.8781	0.6335	3.2368	0.071442	0.112774
	100	1.15e-06	936.7745	0.3269	3.676	0.040568	0.1241
	200	2.3e-06	2032.054	0.1773	5.0775	0.028018	0.158023
	300	3.45e-06	3261.509	0.1264	6.0707	0.022332	0.176677
	400	4.6e-06	4606.768	0.1005	6.7177	0.018534	0.184418
	500	5.75e-06	6070.434	0.0847	7.2132	0.015921	0.187968
a=0.6	50	6.1167e-07	302.0664	0.6052	3.6286	0.08009	0.132337
	100	1.223e-06	632.203	0.3168	4.1680	0.045998	0.145195
	200	2.4467e-06	1394.848	0.1747	5.4054	0.029827	0.170732
	300	3.67e-06	2257.01	0.1256	6.1312	0.022555	0.179574
	400	4.894e-06	3206.158	0.1003	6.5974	0.018202	0.181477
	500	6.11678e-06	4244.791	0.0850	7.1230	0.015722	0.184962
a=0.7	50	6.51e-07	220.246	0.5812	3.6297	0.080114	0.137843
	100	1.3e-06	466.8525	0.3089	4.1680	0.045998	0.148908
	200	2.6e-06	1044.585	0.1728	5.4054	0.029827	0.172609
	300	3.9e-06	1697.453	0.1248	6.1349	0.022568	0.180834
	400	5.2e-06	2423.881	0.1002	6.5974	0.018202	0.181658
	500	6.51e-06	3212.199	0.0848	6.9774	0.0154	0.181609

Table 7.4 Calculation of f and j for Sinusoidal Channel where A/L=0.5,L/D=4.5

a=0.3	Re	$\dot{m}$ (kg/s)	ΔP(Pascal/m)	f	Nu	J=Nu/RePr$^{1/3}$	j/f
	50	5.13e-07	4222.501	1.791	2.0472	0.0452	0.025229
	100	1.0267e-06	8509.75	0.9013	2.2976	0.0254	0.028133
	200	2.0534e-06	17513.64	0.4637	3.6092	0.0199	0.042949
	300	3.08e-06	27163.46	0.3278	4.9130	0.0181	0.055135
	400	4.1068e-06	37415.85	0.2477	5.8624	0.0162	0.065298
	500	5.133e-06	48224.43	0.20434	6.5750	0.0145	0.07102
a=0.4	50	5.42e-07	1951.106	1.664	2.5836	0.057	0.03427
	100	1.084e-06	3961.382	0.845	3.1168	0.0344	0.040706
	200	2.168e-06	8301.707	0.4427	4.8088	0.0265	0.059939
	300	3.252e-06	13056.21	0.3094	6.0272	0.0222	0.071661
	400	4.336e-06	18172.22	0.2423	6.8596	0.0189	0.078108
	500	5.42e-06	23658.45	0.2018	7.4749	0.0165	0.081757
a=0.5	50	5.75e-07	1107.634	1.546	3.0796	0.068	0.043967
	100	1.15e-06	2272.834	0.7930	3.7506	0.0414	0.052196
	200	2.3e-06	4846.561	0.4228	5.4698	0.0302	0.071386
	300	3.45e-06	7715.938	0.2992	6.5702	0.0242	0.08078
	400	4.6e-06	10853.16	0.2367	7.3058	0.0202	0.085157
	500	5.75e-06	14244.41	0.1988	7.8520	0.0173	0.087177
a=0.6	50	6.1167e-07	718.7936	1.4400	3.4833	0.0769	0.053391
	100	1.223e-06	1490.109	0.7460	4.2213	0.0466	0.062448
	200	2.4467e-06	3227.877	0.4042	5.8288	0.0322	0.079572
	300	3.67e-06	5193.698	0.2890	6.8288	0.0251	0.086923
	400	4.894e-06	7360.486	0.2300	7.4937	0.0207	0.089891
	500	6.11678e-06	9709.384	0.1945	8.0041	0.0177	0.090831
a=0.7	50	6.51e-07	510.4787	1.347	3.7410	0.0826	0.0613
	100	1.3e-06	1067.829	0.7066	4.5353	0.0501	0.070834
	200	2.6e-06	2347.845	0.3884	6.0342	0.0333	0.085727
	300	3.9e-06	3812.382	0.2800	6.9042	0.0254	0.090708
	400	5.2e-06	5446.026	0.2250	7.4800	0.0206	0.091721
	500	6.51e-06	7212.172	0.1900	7.9251	0.0175	0.092064

7.5.3 Role of Reynolds Number and Geometric Parameters

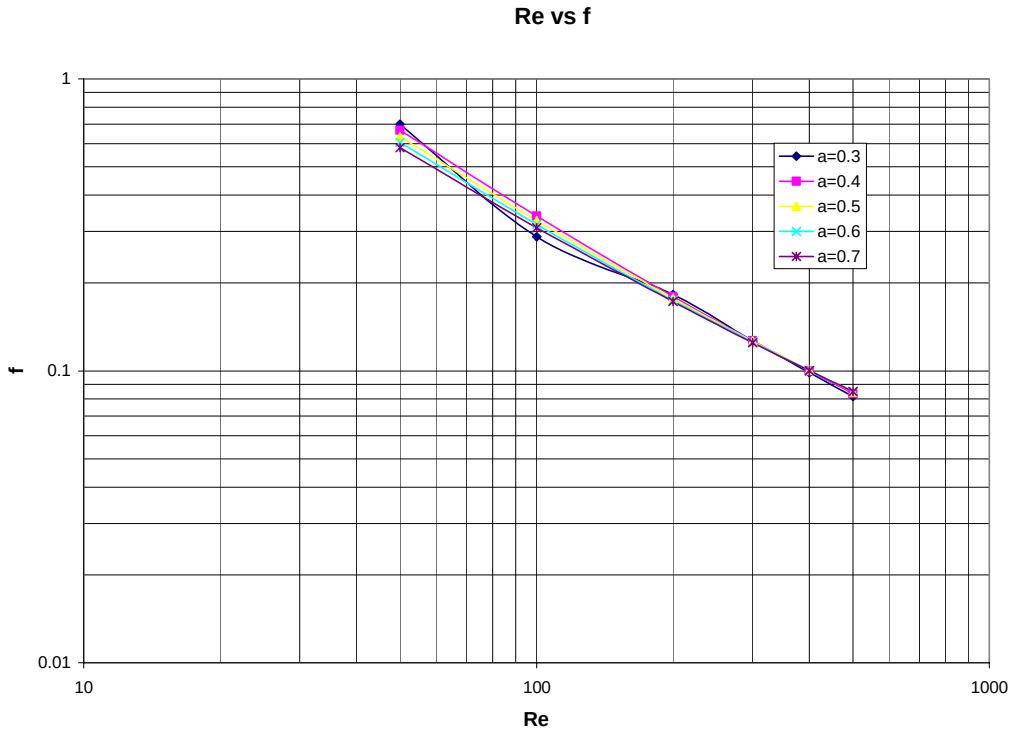

Fig.7.12 Fanning friction factor for periodically developed laminar airflows in sinusoidal wavy channel.(A/L=0.3)

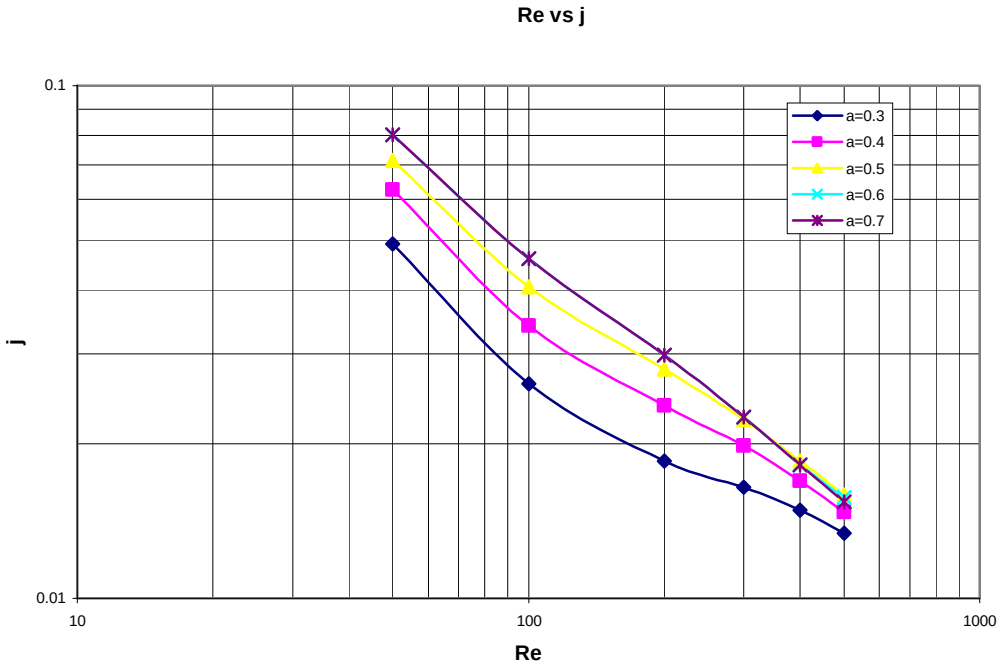

Fig 7.13. Colburn factor for periodically developed laminar airflows in sinusoidal wavy channels (A/L=0.3) with constant heat flux.

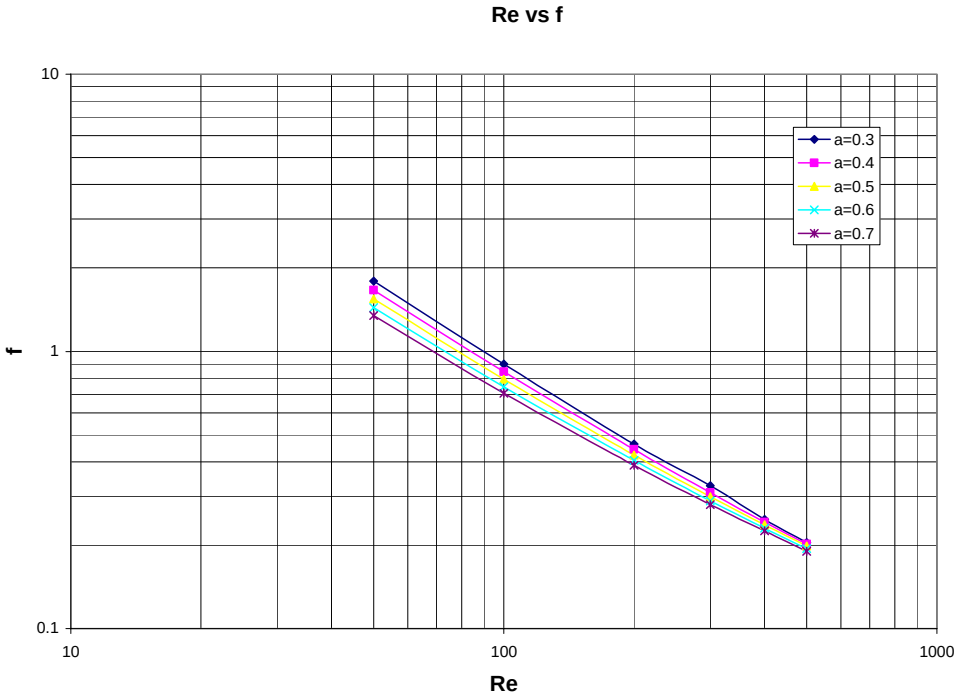

Fig7.14. Fanning friction factor for periodically developed laminar airflows in sinusoidal wavy channel.(A/L=0.5)

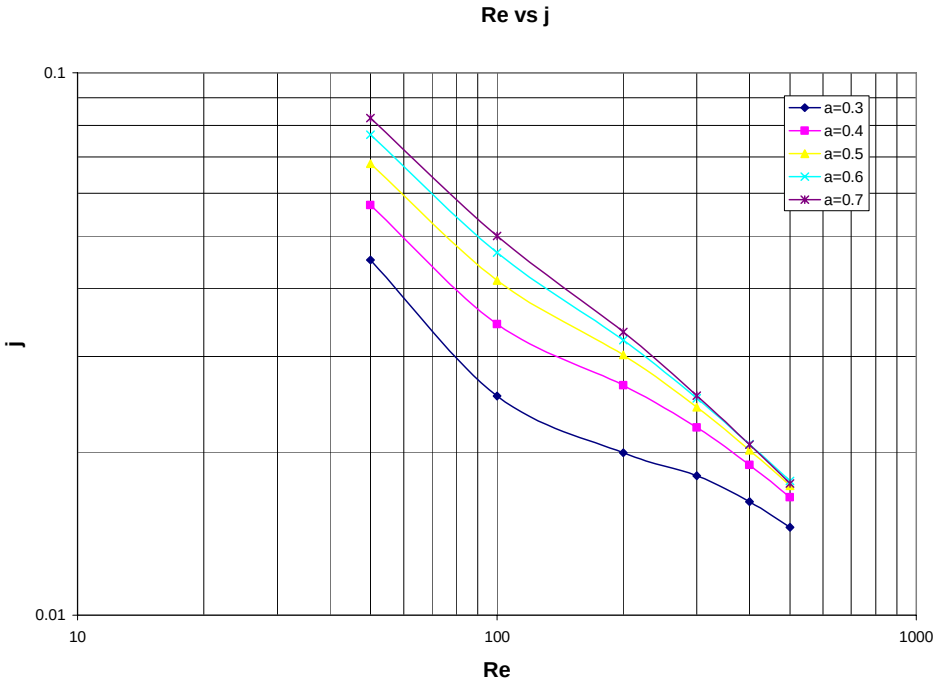

Fig.7.15 Colburn factor for periodically developed laminar airflows in sinusoidal wavy channels (A/L=0.5) with constant heat flux.

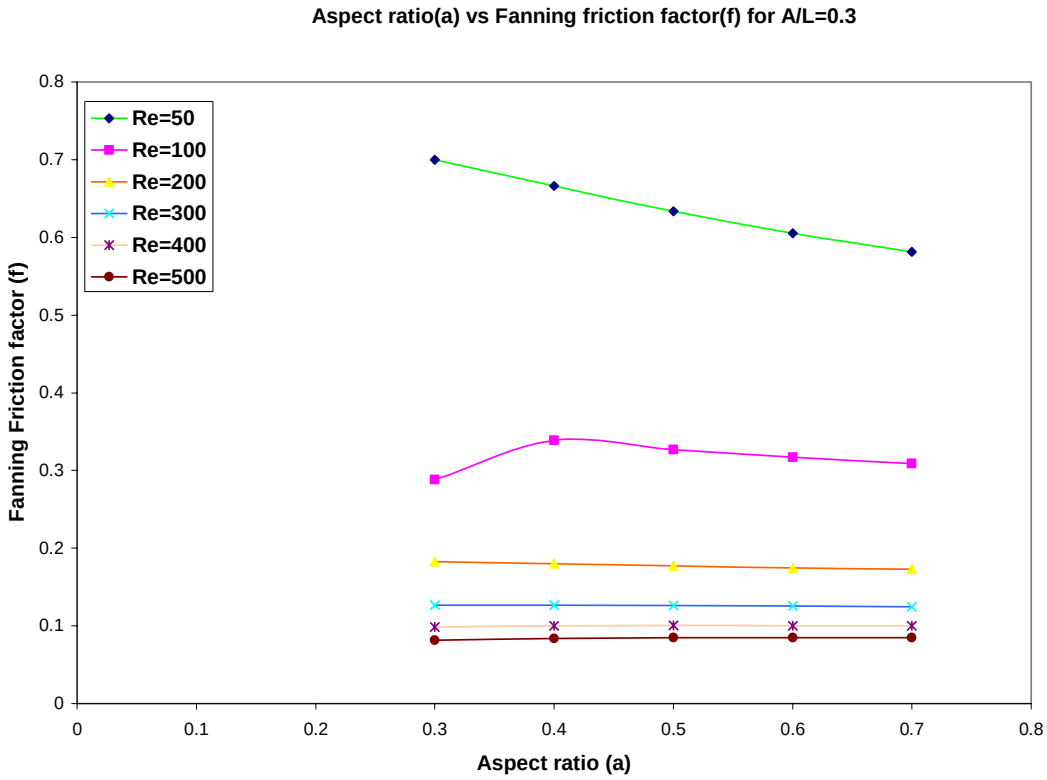

Fig.7.16 Variation of Fanning friction factor (f) with Aspect ratio ,A/L=0.3

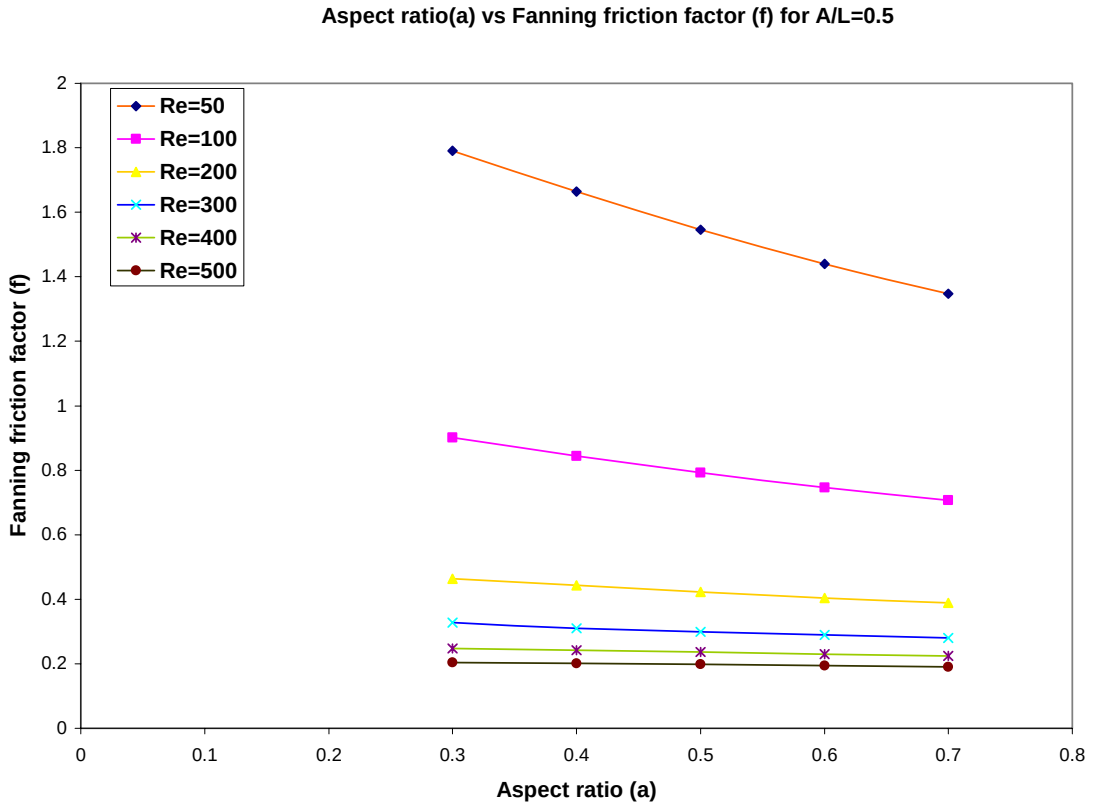

Fig.7.17 Variation of Fanning friction factor (f) with Aspect ratio for A/L=0.5

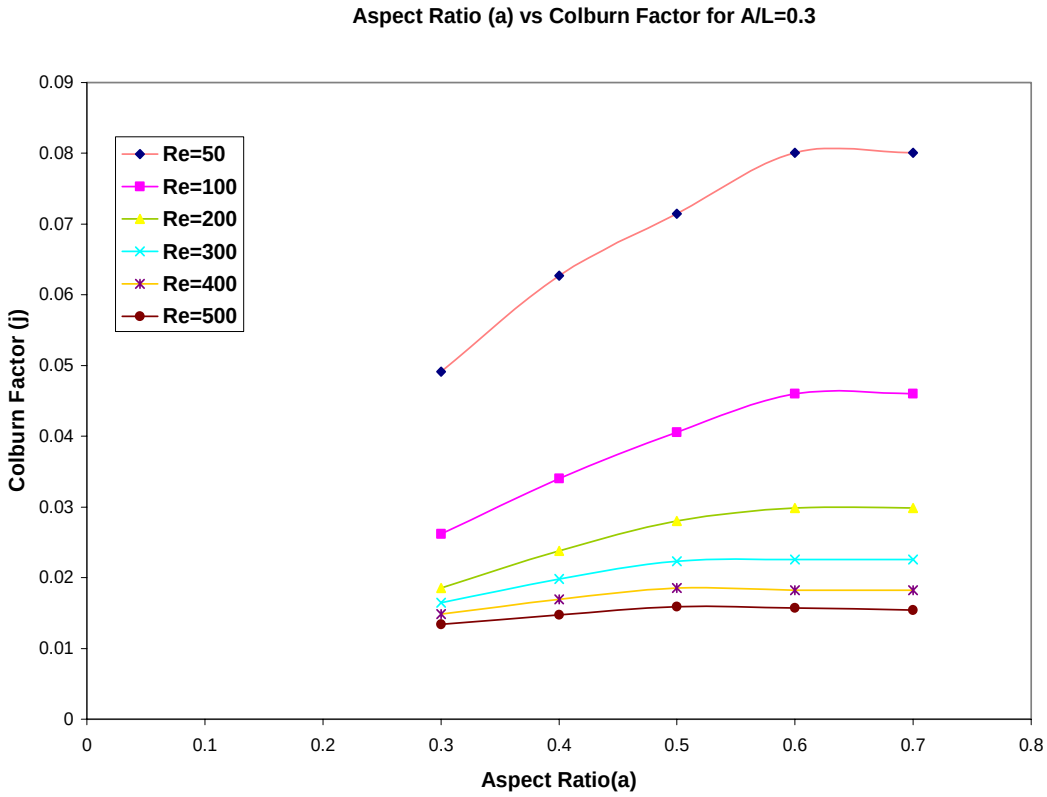

Fig.7.18 Variation of Colburn factor (j) with Aspect ratio, for A/L=0.3

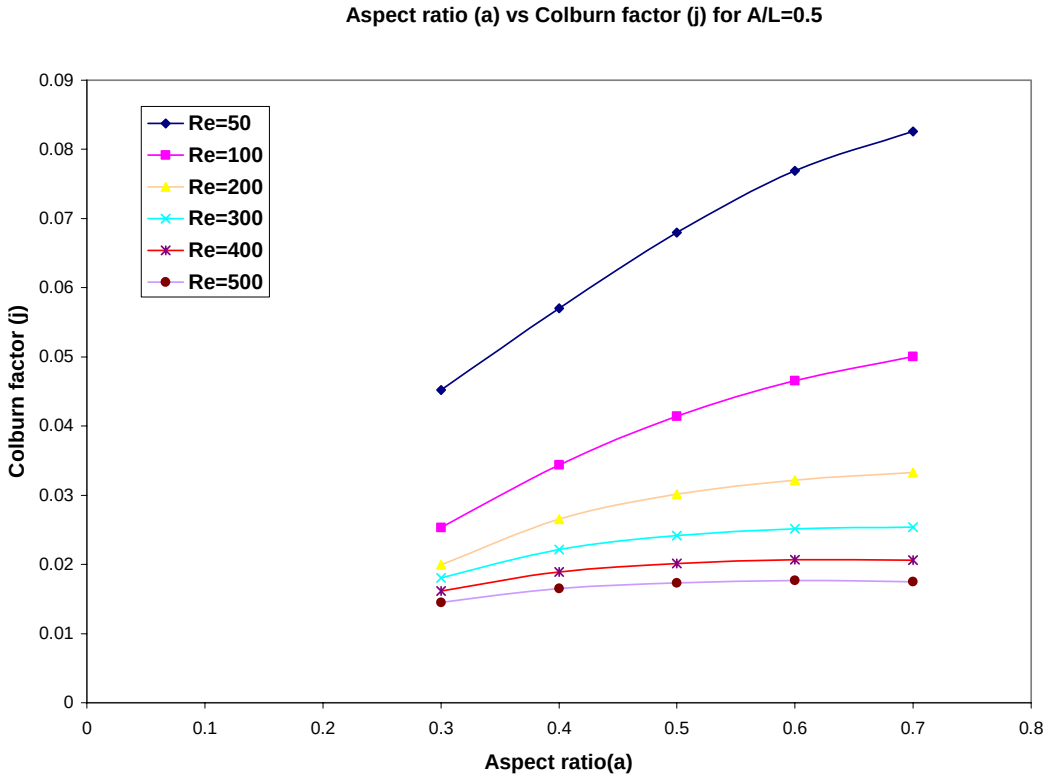

Fig.7.19 Variation of Colburn factor (f) with Aspect ratio (a) for A/L=0.5

7.5.4 Generation of Heat Transfer and Flow Friction Correlations

The correlation for the given geometry at a fixed A/L ratio can be found from the following relation.

f or $j=C\ Re^{K}$……..(7.8)

Firstly the different results have been tabulated .Then the graphs between friction factor and Coburn factor corresponding to different Reynolds number are plotted for various geometry based on different aspect ratios.

Then C and K value have been found from the graphs by fitting to a power law.

Table 7.5 Correlation for the sinusoidal channel A/L=0.3

Aspect Ratio	Correlation between Reynolds Number & Fanning friction	Correlation between Reynolds Number & Colburn factor
a =0.3	$f = 21.183\ Re^{-0.8987}$	$J = 0.3515\ Re^{-0.5358}$
a =0.4	$f = 22.047\ Re^{-0.902}$	$J = 0.6028\ Re^{-0.601}$
a =0.5	$f = 18.705\ Re^{-0.8735}$	$J = 0.7983\ Re^{-0.6303}$
a =0.6	$f = 16.433\ Re^{-0.852}$	$J = 1.1958\ Re^{-0.6979}$
a =0.7	$f = 14.782\ Re^{-0.8347}$	$J = 1.2237\ Re^{-0.7028}$

Table 7.6 Correlation for the sinusoidal channel A/L=0.5

Aspect Ratio	Correlation between Reynolds Number & Fanning friction	Correlation between Reynolds Number & Colburn factor
a =0.3	$f = 69.786\ Re^{-0.9412}$	$J = 0.2389\ Re^{-0.456}$
a =0.4	$f = 58.677\ Re^{-0.9172}$	$J = 0.396 Re^{-0.5102}$
a =0.5	$f = 49.1\ Re^{-0.8915}$	$J = 0.6161\ Re^{-0.5721}$
a =0.6	$f = 41.924\ Re^{-0.8699}$	$J = 0.8602\ Re^{-0.623}$
a =0.7	$f = 36.232\ Re^{-0.8498}$	$J = 1.0905\ Re^{-0.6623}$

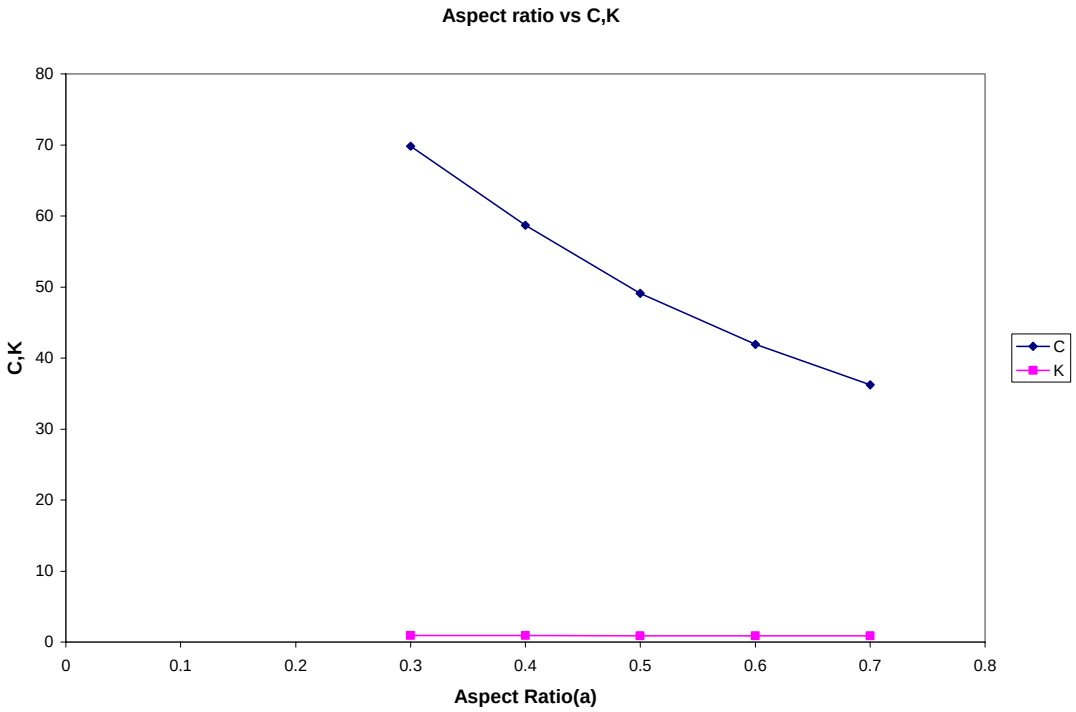

Fig.7.20C,K variation with aspect ratio for calculating Fanning friction factor of a sinusoidal channel where A/L=0.5

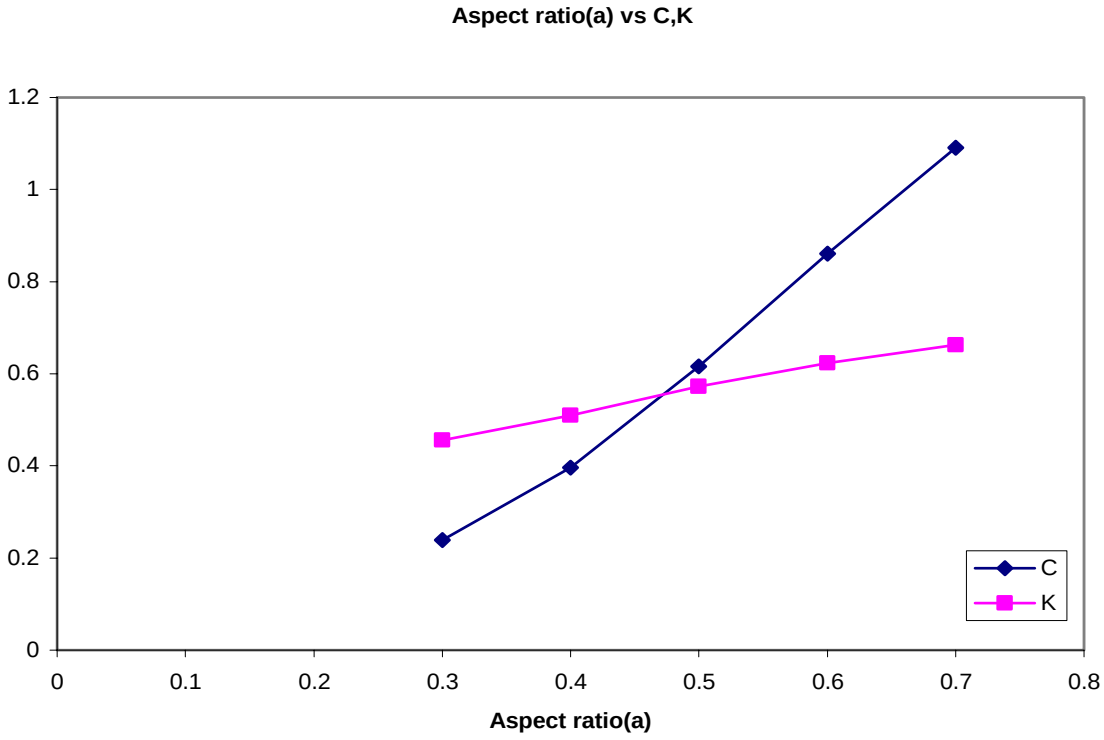

Fig.7.21C,K variation with aspect ratio for calculating Colburn factor of a sinusoidal channel where A/L=0.5

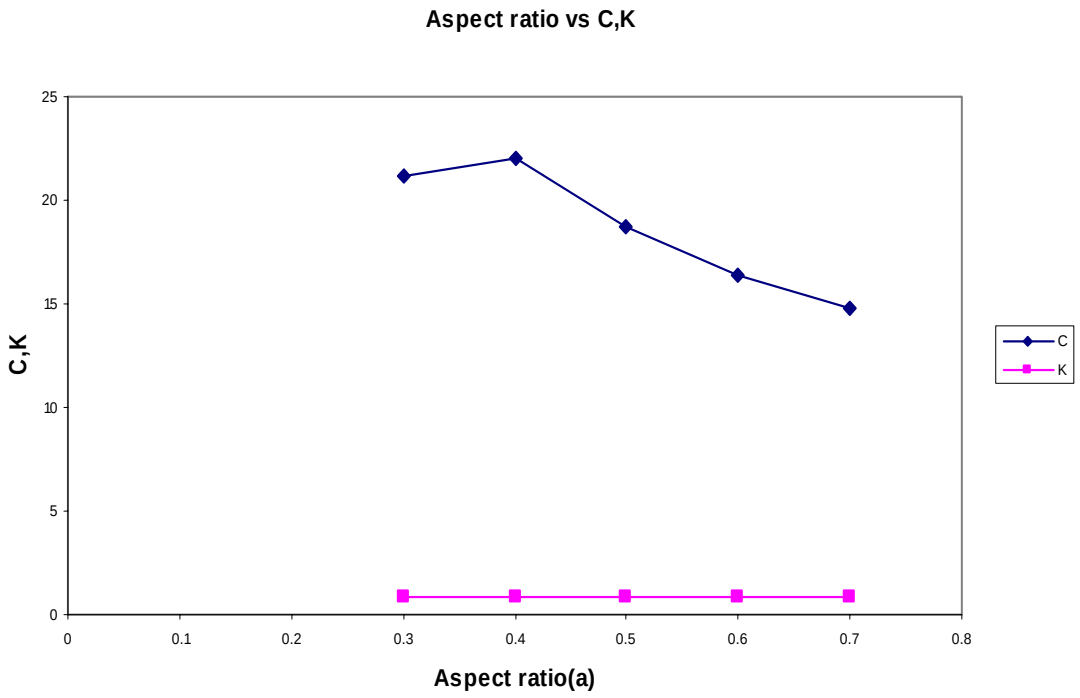

Fig.7.22 C,K variation with aspect ratio for calculating Fanning friction factor of a sinusoidal channel where A/L=0.3

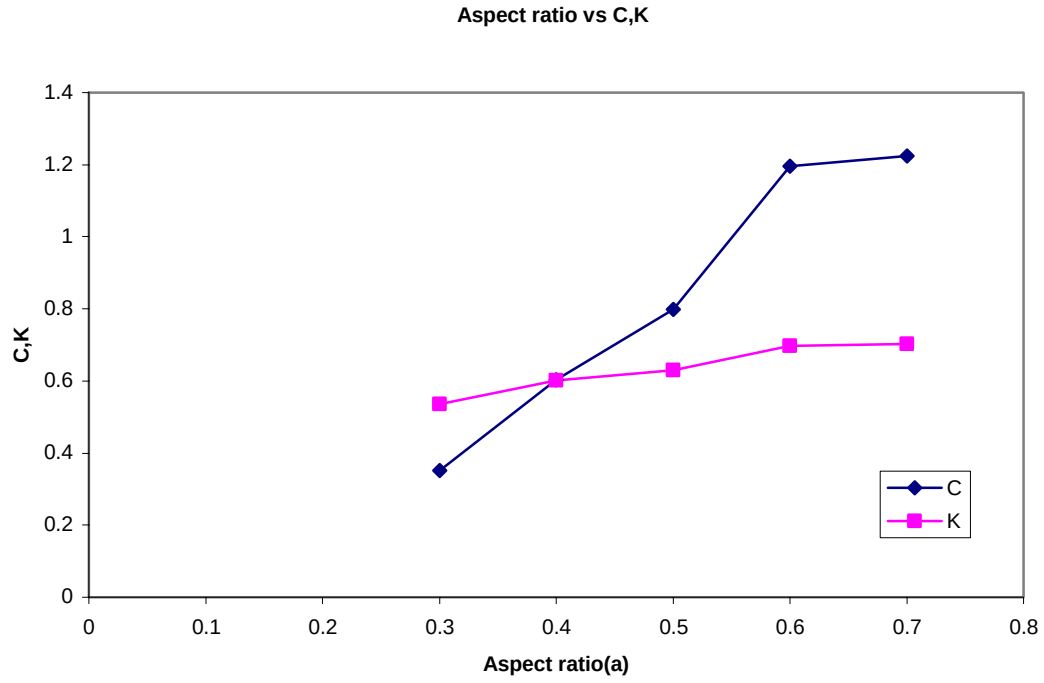

Fig.7.23 C, K variation with aspect ratio for calculating Colburn factor of a sinusoidal channel where A/L=0.3

The final correlation for the sinusoidal channel considering all geometrical parameters like aspect ratio (a) and amplitude-wave length (A/L) will be in the form

$f \text{ or } j = C\, Re^{K} (a)^{P} (A/L)^{Q}$

Here, we have found the correlation by regression analysis.

The **final correlation** is of the form

$$\mathbf{f = 139.805\, Re^{-0.880} (a)^{-0.121} (A/L)^{1.721} \ldots\ldots\ldots\ldots (7.9)}$$

$$\mathbf{R^2 = 0.99}$$

$$\mathbf{j = 1.123\, Re^{-0.612} (a)^{0.508} (A/L)^{0.122} \ldots\ldots\ldots\ldots (7.10)}$$

$$\mathbf{R^2 = 0.99}$$

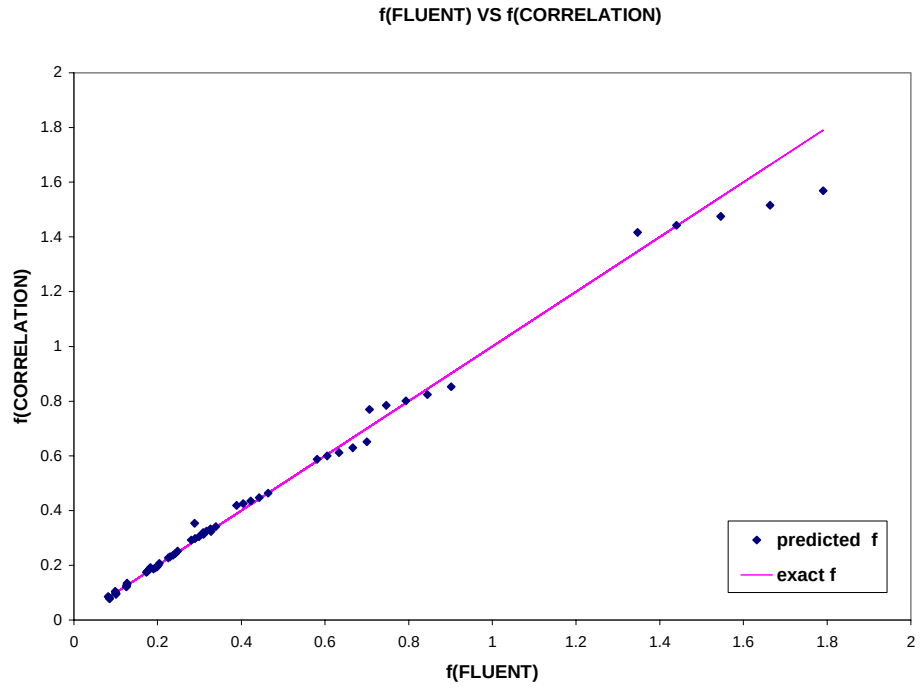

Fig. 7.24 Showing the variation f found from FLUENT and from the Correlation

Red line represents the exact f .

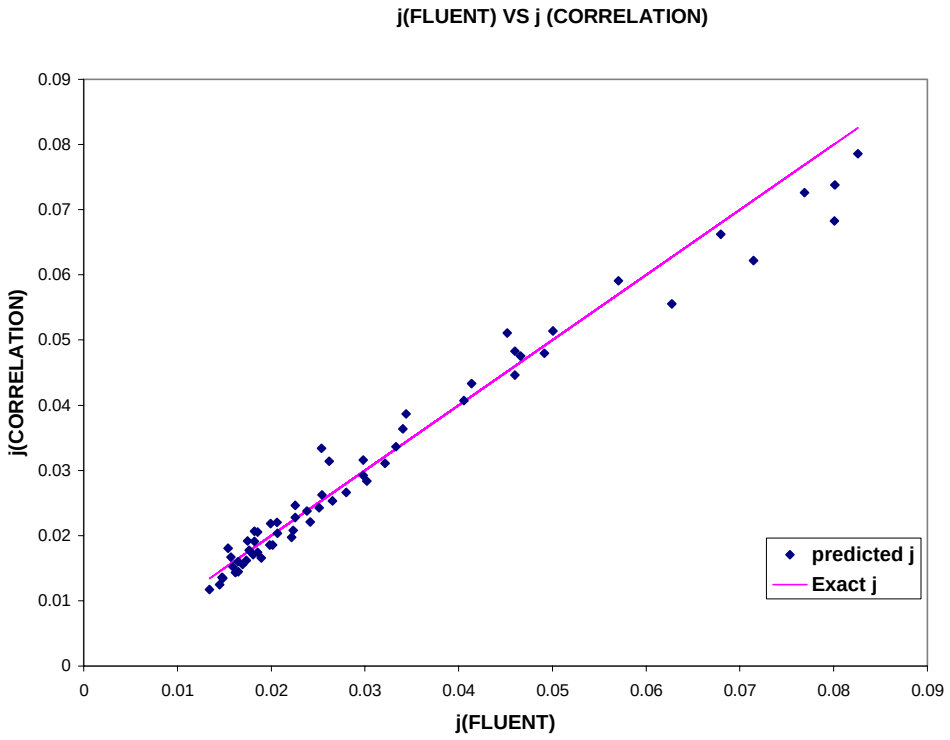

Fig. 7.25 Showing the variation of j found from FLUENT and from the Correlation

Red line represents the exact j.

7.6 DISCUSSIONS

(1)From fig. 7.5 & fig. 7.6 it is clearly shown that as the amplitude to wavelength ratio increases ,the pressure drop increases .This can be explained by the friction generation due to travel of the fluid to a greater height.

(2)For a particular L/D ratio and A/L ratio and at a fixed aspect ratio, as the Reynolds number increases, the rapid mixing of fluid occurs at the core and the transition of temperature from the wall to the core of the fluid becomes faster.

(3)From fig 7.12 & 7.14 for a particular aspect ratio, fanning friction factor decreases as the Reynolds number increases For a given Reynolds number, friction factor is lowest for aspect ratio=0.3 irrespective of L/D ratio. Change of friction factor becomes independent of aspect ratio after Reynolds number=200 for A/L=0.3 which is not in case of A/L=0.5

(4) Plot of Re vs. j factor (fig.7.13 & 7.15) shows that j decrease as Re increases for a fixed aspect ratio. At a fixed aspect ratio, the geometry having aspect ratio 0.7 gives the highest value of j.

(5)From fig. 7, 16 and fig. 7.17, it is clear that as the Reynolds number increases, the fanning friction factor curve becomes flatter and flatter which indicates that it is no more dependent upon the aspect ratio. The same trend is seen in fig. 7.18 and fig. 7.19 for colburn factor.

(6) For Fanning friction factor correlation graph shown by fig.7.20 & 7.22, the indices K value is remaining constant for all aspect ratios and different amplitude-wavelength ratios.

(6)There is linear variation of C value with respect to aspect ratio for correlation of fanning friction factor.

(7)For the correlation of colburn factor shown by fig7.21 and fig. 7.23, the C and K value variation is linear with respect ratio to aspect ratios.

(8) Fig. 7.24 and fig. 7.25 concludes that the correlation for f and j found from the regression analysis gives the nearly same value of f and j from FLUENT.

Chapter 8

CONCLUSION

- **Contribution of this thesis**
- **Future Scope**

8.1 CONTRIBUTION OF THIS THESIS

The flow behavior and heat transfer characteristics of semi elliptical straight and sinusoidal channels have been studied successfully using FLUENT. To get the best heat transfer enhancement with low pressure drop usually indicated by the goodness factor (j/f), we have to increase the aspect ratio of the channel cross sections. The aspect ratio 0.7 is preferred.

Different correlations have been found to analyze the geometries used in PCHE.

Table 8.2 Correlation of the geometries

Geometry	Correlation
Semi elliptical Straight Duct (Entrance Region)	$f = 11.934\ Re^{-0.948}(a)^{-0.067}$ $R^2 = 1$ $j = 2.785\ Re^{-0.908}\ (a)^{0.292}$ $R^2 = 1$
Semi elliptical Straight Duct (Fully Developed Flow)	$f = 14.183\ Re^{-0.997}\ (a)^{-0.121}$ $R^2 = 1$ $j = 4.557\ Re^{-0.866}\ (\ a\ )^{1.142}$ $R^2 = 0.96$
Sinusoidal Duct(Fully Developed Flow)	$f = 139.805\ Re^{-0.880}(a)^{-0.121}(A/L)^{1.721}$ $R^2 = 0.99$ $j = 1.123\ Re^{-0.612}\ (a)^{0.508}\ (A/L)^{0.122}$ $R^2 = 0.99$

8.2 FUTURE SCOPE

1. Flow behavior and heat transfer characteristics of zigzag channel with semi elliptical Cross section should be studied using FLUENT.

2. Conduction effect can be considered for straight, sinusoidal and zigzag channel while Using FLUENT.

3. Viscous fluid used in heat exchanger industry can be taken in place of air and the flow behavior and heat transfer characteristics can be studied.

4. More detail study should concentrate on evaluating the potential of zigzag channels, Sinusoidal channel collecting experimental data for comparison with theoretical and simulation based calculation.

5. Future attention should also focus on Heatric‘s new multi-ported (MP) configuration.

6 Research would also shed light on the applicability of PCHES to even more extreme design conditions i.e. those with very steep temperature gradients.

7. Transient Analysis is needed to elucidate the material behavior with particular emphasis on of thermal stress.

8. PCHE performance and behavior with liquid metals and molten salts is a relatively unexplored field which must be investigated further since most advanced nuclear reactor designs employ such coolants.

REFERENCES

[1] Doty, D.F., The Micro tube Strip Heat Exchanger, Heat Transfer Engineering,Vol 12.

No.3, 1991.

[2] Gezelius, K.et al .,Design of a Shell and Tube Heat Exchanger for the S-CO $_2$Cycle & Laminar Flow in Micro channel Heat Exchangers, Report # MIT-GFR-004,Massachusetts Institute of Technology(MIT),Cambridge:MA,2003

[3]Hesselgreaves,J.E.,Compact Heat Exchangers,Pergamon Press, New York:NY,2001.

[4] Heatic^{TM} Homepage. Available online at http://www.heatric.com

[5]Gezelius,Knot.,Design of Compact Intermediate Heat Exchangers for Gas Cooled Fast reactors, Report # Massachusetts Institute of Technology(MIT),Cambridge:MA,2004

[6] Hong, S. W. and Bergles, A. E. 1976. Laminar flow heat transfer in the entrance region of semi-circular tubes with uniform heat flux. Int. J. Heat Mass Transfer, 19, 123-124

[7] Shah, R. K. and London, A. L. 1978. Laminar Flow-Forced Convection in Ducts. Academic Press, New York

[8] Manglik, R. M. and Bergles, A. E. 1988. Laminar flow heat transfer in a semi-circular tube with uniform wall temperature. Int. J. Heat Mass Transfer. 31, 625-636

[9] Lei, Q. M. and Trupp, A. C. 1989a. Maximum velocity location and pressure drop of fully developed laminar flow in circular sector ducts. J. Heat Transfer, 111, 1085-1087

[10]Lei, Q. M. and Trupp, A. C. 1989b. Further analyses of laminar flow heat transfer in circular sector ducts. J. Hear Transfer, 111, 1088-1089

[11]Ben-Ali, T. M., Soliman, H. M. and Zariffeh, E. K. 1989. Further results for laminar heat transfer in annular sector and circular sector ducts. J. Heat Transfer, 111, 1089-1093

[12] Bhatti, M. S. 1983. Laminar flow in the entrance region of elliptical ducts. J. Fluids Eng., 105, 29s-296

[13]Bhatti, M. S. 1984. Heat transfer in the fully developed region of elliptical ducts with uniform wall heat flux. J. Heat Transfer, 106, 895-898

[14] Abdel-Wahed, R. M., Attia, A. E. and Hifni, M. A. 1984. Experiments on laminar flow and heat transfer in an elliptical duct. Int. J. Heat Mass Transfer, 27, 2397-2413

[15]Dong, Z. F. and Ebadian, M. A. 1991. Numerical analysis of laminar flow in curved elliptic ducts. J. Fluids Eng., 113, 555-562

[16]Dong, Z. F. and Ebadian, M. A. 1992a. Effects of buoyancy on laminar flow in curved elliptic ducts. J. Hear Transfer, 114, 936943

[17]Dong, Z. F. and Ebadian, M. A. 1992b. Convective and radiative heat transfer in the entrance region of an elliptic duct with fins, Num. Hear Transfer. 2lA, 91-107

[18]Ebadian, M. A., Topakoglu, H. C. and Arnas, O. A. 1986. On the convective heat transfer in a tube of elliptic cross-section maintained under constant wall temperature. J Heat Transfer, 108, 33-39

[19]Garg, V. K. and Velusamy, K. 1989. Developing flow in an elliptical duct. Int. J. Eng. Fluid Mech., 2, 177-196

[20] Eckert, E. R. G. et al. 1992. Heat transfer-A review of 1991 literature. Int. J. Heat Mass Transfer, 35, 3153-3235

[21]Rosaguti, N.R., Fletcher, D.F., Haynes, B.S., 2005. Low-Reynolds number heat transfer enhancement in sinusoidal channels. Chemical Engineering Science 62(2007) 694-702

[22]Manglik, R.M., Zhang, J., Muley, A., 2005. Low Reynolds number forced convection in three-dimensional wavy-plate-fin compact channels: fin density effects. International journal of Heat and Mass Transfer 48 (8), 1439–1449.

[23]Harms, T.M., Jog, M.A., Manglik, R.M. Effects of temperature dependent viscosity variations and boundary Conditions on fully developed laminar forced convection in a semicircular duct. ASME Journal of Heat Transfer, Vol. 120,1998, pp.600-605

[24]Vijay, K. Garg, Vijay. K., Vaidyanathan G, Fully developed flow and heat transfer in semi-elliptical ducts, International journal of Heat and Fluid Flow, Vol.16.No. 2, 1995, pp 147-152

[25] Rosaguti, N.R., Fletcher, D.F., Haynes, B.S., 2006. Laminar flow and heat transfer in a periodic serpentine channel with semi-circular cross-section. International Journal of Heat and Mass Transfer 49 (17–18), 2912–2923

[26] Zhang, J., Kundu, J., Manglik, R.M., 2004. Effect of fin waviness and spacing on the lateral vortex structure and laminar heat transfer in wavy-plate-fin cores. International Journal of Heat and Mass Transfer 47 (8–9), 1719–1730

[27] Rush, T.A., Newell, T.A., Jacobi, A.M., 1999. An experimental study of flow and heat transfer in sinusoidal wavy passages. International Journal of Heat and Mass Transfer 42 (9), 1541–1553.

[28] Paul E. Geyer, Nathan R. Rosaguti David F. Fletcher & Brian S. Haynes Thermo hydraulics of square-section micro channels following a serpentine path .Micro fluid Nanofluid (2006) 2: 195–204

[29] Kalb CE, Seader JD (1972) Heat and mass transfer phenomena for viscous flow in curved circular tubes. Int J Heat Mass Transfer 15(4):801–817

[30] Bolinder CJ, Sunde´ n B (1996) Numerical prediction of laminar flow and forced convective heat transfer in a helical square duct with a finite pitch. Int J Heat Mass Transfer 39(15):3101–3115

[31] Dean WR (1928) Fluid motion in a curved channel. Proc R Soc LindserA121 (787):402–420

[32]]Kakac, S., Heat Exchangers-Selection, Rating, and Thermal Design, 2nd Ed., CRC Press, New York: NY, 2002

[33]Fluent INC. 2003. FLUENT 6.1 User Manual

[34]www.cfd-online.com